Electronic Supporting Information for

Mechanically Robust and Reprocessable Imine Exchange Networks from Modular Polyester Pre-Polymers

Rachel L. Snyder[‡,a], Claire A. Lidston[‡,a], Guilhem X. De Hoe[†,b], Maria J. S. Parvulescu[†,a], Marc A. Hillmyer[b,*], Geoffrey W. Coates[a,*]

[a]*Department of Chemistry and Chemical Biology, Baker Laboratory, Cornell University, Ithaca, New York 14853, United States*

[b]*Department of Chemistry, University of Minnesota, 207 Pleasant Street SE, Minneapolis, Minnesota 55455, United States*

1. Characterization Techniques

All manipulations of air and water sensitive compounds were carried out under nitrogen in an MBraun Labmaster glovebox or using standard Schlenk line techniques. ^{1}H and ^{13}C Nuclear Magnetic Resonance (NMR) spectra were recorded on a Bruker AV III HD (^{1}H, 500 MHz and ^{13}C, 125 MHz) spectrometer with a broad band Prodigy cryoprobe or Varian INOVA 400 (^{1}H, 400 MHz) spectrometer. Chemical shifts (δ) for ^{1}H and ^{13}C NMR spectra were referenced to the residual solvent for ^{1}H and deuterated solvent itself for ^{13}C NMR. High-resolution mass spectrometry (HRMS) was performed on a Thermo Scientific Exactive Orbitrap MS system equipped with an Ion Sense DART ion source.

Gel permeation chromatography (GPC) analyses were carried out using an Agilent 1260 Infinity GPC System equipped with an Agilent 1260 Infinity autosampler and refractive index detector. The Agilent GPC system was equipped with two Agilent PolyPore columns (5 micron, 4.6 mm ID), which were eluted with THF at 30 °C at 0.3 mL/min and calibrated using monodisperse polystyrene standards. Flash column chromatography was performed using silica gel (particle size 40–64 μm, 230–400 mesh).

Uniaxial extension experiments were performed on a Shimadzu Autograph AGS-X series instrument using dogbone-shaped samples (ca. 0.8 mm (T) × 3.5 mm (W) × 27 mm (L) with a gauge length of ca. 15 mm, Figure S4 and Figure S12–Figure S21) at 22 °C. Metal grips were used for tensile testing at 0.4–0.5 MPa of pressure, and the ramp speed was set to 5 mm/min. Extension to break tests were performed with 5 replicates per material to report average values and standard deviations for each set. *Trapezium* software was used to analyze the resulting data. The Young's modulus was calculated using the slope of the stress-strain curve from 0 to 0.1% strain.

Dynamic mechanical thermal analysis (DMTA) was performed on a TA Instruments RSA-G2 analyzer (New Castle, DE) using dogbone specimens (Figure S4 and Figure S12–Figure S21) in tensile geometry with an initial gauge length of 7.0 mm. The transducer was set to spring mode. The sample was initially equilibrated to 30 °C for 10 min, and the axial force was continuously adjusted to 5.0 ± 2.0 g prior to the test to ensure the sample remained in tension and did not buckle. Force tracking mode was selected to maintain an axial force at least 100% greater than the dynamic oscillatory force. A strain adjust of 30% was set with a minimum strain value of 0.01% and a maximum strain value of 5.0%. Minimum and maximum forces were set to 1.0 g and 20.0 g, respectively, such that the sample remained in the specified strain range. The sample was heated from 35 °C to 130, 150, or 180 °C at 5 °C/min with an oscillating strain of 0.05% at an angular frequency of 1 Hz (6.28 rad/s). During the experiments, the low viscosity of the gradient samples caused significant extension in the instrument (200–300% of the initial gauge length). The instrument baffle was placed outside the heating chamber to allow full extension, and the maximum gap was set to 30 mm. The glass transition temperature (T_g) was determined from the maximum value of tanδ.

Equation S1 was used to calculate the effective molar mass between cross-links ($M_{x,eff}$), where E' is the tensile storage modulus and G' is the shear storage modulus at a given temperature (T) in the rubbery plateau region, R is the universal gas constant, ν_e is the effective cross-linking density, and ρ is the density of the pristine samples. Density was determined by weighing a disc of polymer with a known volume. The dimensions and mass were measured in triplicate, and the average values were used to determine cross-linking density with Equation S1.

$$E'(T) = 3G'(T) = 3RT\nu_e = \frac{3\rho RT}{M_{x,eff}} \qquad \text{Equation S1}$$

Fourier-transform infrared (FT-IR) spectra for all materials were obtained on either a Bruker Alpha Platinum spectrometer or Bruker Tensor II Infrared Spectrometer, both of which were equipped with a diamond crystal. Data were collected in attenuated total reflection (ATR) mode at a resolution of 4 cm^{-1} over 32 scans.

Gel fractions were measured by swelling a 100–150 mg polymer sample in 15 mL of anhydrous THF at 10 °C for 4 days. The swollen sample was isolated from the solvent and dried under high vacuum first at 22 °C for 12 h and then at 90 °C for 6 h to ensure full removal of THF.

Thermal gravimetric analysis was obtained using a TA Instruments Q500 Analyzer. Analysis was performed on ~10 mg of sample at a heating rate of 10 °C/min from 22 to 550 °C under nitrogen.

Differential scanning calorimetry (DSC) was performed on a TA Instruments Q1000 Modulated Differential Scanning Calorimeter using 4–6 mg samples. The sample was first heated to 130 °C at a rate of 10 °C/min and held for 5 min to erase the thermal history. Then, the sample was cooled to –80 °C at 10 °C/min, held for 10 min to equilibrate, and heated again to 150 °C. The T_g value was determined from the second heat ramp using the maximum value of the derivative of heat flow with respect to temperature.

Stress Relaxation Analysis (SRA) was performed on **GG$_{43\%}$-*stat*** using a TA Instruments DHR3 Rheometer with a steel parallel plate geometry (diameter = 8 mm) in an environmental test chamber under air flow. The sample discs (8 mm (D) × 0.6–1.0 mm (T)) were first equilibrated at a given temperature (55–125 °C) for 10 min. Then, a constant axial normal force of 5.0 ± 2.0 g was applied to ensure the sample was compressed between the plates. A strain sweep was first performed from 0.01–10% strain at a frequency of 1 Hz at 100 °C to identify the linear viscoelastic regime. These dynamic imine polyester materials exhibited a surprisingly small linear viscoelastic

region (0.01–1%), and all measurements were conducted with 0.05% strain. For SRA experiments at a given temperature, an instantaneous step strain of 0.05% was applied to the sample, and the resultant stress was allowed to decay for the appropriate time (5 s–10 min). This experiment was repeated in triplicate for each sample at a given temperature. Samples were soaked at a given temperature (75, 85, 90, 95, 100, 105, 110, 115, 120, 125, 130 °C) for 1–3 min between each run to minimize residual stress from prior experiments. All stress relaxation data were normalized to the observed shear storage modulus (G') at 0.02 s. The characteristic value $\tau*$ was recorded when the normalized stress relaxed to 37% (1/e) of its initial value. Activation energy (E_a) was determined using previously reported methodology and Equation S2.[1,2]

$$\tau^*(T) = \tau_0 \times e^{E_a/RT} \qquad \text{Equation S2}$$

Equation S3 was used to calculate the topology freezing transition temperature, T_v, which is defined as the point where the viscosity equals 10^{12} Pa·s (*i.e.* the liquid to solid transition viscosity), where η is the complex viscosity, and E' is the rubbery storage modulus above the T_g.

$$\eta = \frac{1}{3} E' \times \tau^* \qquad \text{Equation S3}$$

In this equation, $\tau*$ represents the characteristic relaxation time at T_v, which can be extrapolated using the Arrhenius activation energy equation (Equation S2) as determined by stress relaxation analysis. Because the rubbery storage modulus above T_g was not constant for **PO$_{23\%}$-*grad***, **PO$_{42\%}$-*grad***, or **PO$_{62\%}$-*grad***, the Arrhenius activation energy and T_v were not calculated for these samples.

2. Materials

2.1. General Materials

Solvents for air sensitive reactions were purchased from Fisher Scientific, sparged with ultrahigh purity grade nitrogen, and either passed through two columns containing reduced copper (Q-5) and alumina (hexanes, toluene, and tetrahydrofuran) or passed through two columns of alumina (dichloromethane). These solvents were dispensed into an oven-dried Straus flask, degassed over three freeze-pump-thaw cycles, and vacuum transferred before use. Otherwise, solvents (ethyl acetate, diethyl ether, hexanes, methanol, ethanol, chloroform, dimethylformamide, pentane, heptane) were used as received. Triethylamine was dried over calcium hydride for three days, vacuum transferred to an oven-dried Schlenk flask, degassed by three freeze-pump-thaw cycles, and stored under nitrogen. Deuterated acetonitrile (CD_3CN) was degassed by three freeze-pump-thaw cycles and stored over 3 Å molecular sieves under nitrogen. All other chemicals and reagents, except for polymerization materials (*vide infra*), were purchased from commercial sources (Aldrich, Oakwood Chemical, Strem, TCI, Alfa Aesar, Acros, and Fisher Scientific) and used without further purification.

2.2. Polymerization Materials

Phthalic anhydride (**PA**; Aldrich ≥99%) was sublimed at 60 °C under dynamic vacuum. **PA** was stored at 22 °C in a glovebox under nitrogen atmosphere. Propylene oxide (**PO**; Aldrich ≥99%) was stirred over calcium hydride for at least three days, vacuum transferred to an oven-dried Straus flask, degassed by three freeze-pump-thaw cycles, and stored in a glovebox under nitrogen atmosphere.

3. Pre-Polymer and Network Synthesis

3.1. Monomer Synthesis

Vanillin Glycidyl Ether (VG)

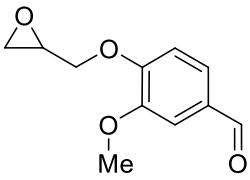

Vanillin (38 g, 0.25 mol, 1.0 equiv) and benzyltriethylammonium chloride (5.7 g, 0.025 mol, 0.10 equiv) were dissolved in epichlorohydrin (200 mL, 2.55 mol, 5.1 equiv). The reaction mixture was heated to 70 °C while stirring for 1–6 h, monitoring conversion by TLC. Upon full consumption of the starting material, the reaction mixture was cooled to 22 °C, and ground sodium hydroxide (4.0 g, 0.10 mol, 0.40 equiv) was added. After stirring 1 h at 22 °C, the reaction mixture was filtered to afford a pale yellow powder that was triturated with 60:40 hexanes:EtOAc (3 × 150 mL) and filtered. Recrystallization from saturated EtOAc at 7 °C afforded pale yellow crystals that were first dried in vacuo at 22 °C for 16 h. Subsequent sublimation under dynamic vacuum at 95 °C afforded a white crystalline solid (27 g, 51% yield). **^{1}H NMR** (400 MHz, $CDCl_3$): δ 9.85 (s, 1H), 7.45–7.42 (m, *J* = 8.51, 10.41 Hz, 2H), 7.03 (d, *J* = 8.01, 1H), 4.38 (dd, *J* = 3.04, 11.55 Hz, 1H), 4.10 (dd, *J* = 5.65, 11.51 Hz, 1H), 3.93 (s, 3H), 3.42 (m, 1H), 2.93 (dd, *J* = 4.35, 4.58 Hz, 1H), 2.78 (dd, *J* = 2.61, 4.76 Hz, 1H) ppm. **^{13}C NMR** (125 MHz, $CDCl_3$): δ 190.84, 153.38, 149.96, 130.67, 126.47, 112.27, 109.50, 69.92, 55.01, 49.87, 44.74 ppm. Characterization data were consistent with literature reports.[3]

Guaiacol Glycidyl Ether (GG)

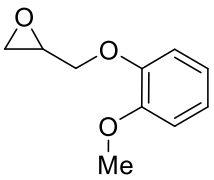

Guaiacol (31 g, 0.25 mol, 1.0 equiv) and benzyltriethylammonium chloride (5.7 g, 25 mmol, 0.10 equiv) were dissolved in epichlorohydrin (200 mL, 2.55 mol, 10.2 equiv) in a 500 mL round-bottom flask and stirred at 80 °C for 16 h. Upon cooling the reaction mixture to 22 °C, aqueous sodium hydroxide (5 M, 200 mL) was added, and the biphasic mixture stirred for 30 min at 22 °C. The aqueous layer was separated and extracted

with EtOAc (3 × 150 mL). The combined organic extracts were washed with saturated brine, dried over $MgSO_4$, filtered, and concentrated to afford a pale yellow oil. Purification by silica column chromatography (gradient from hexanes to 70:30 hexanes:EtOAc) afforded the product as colorless oil which was degassed and dried over molecular sieves under nitrogen for 8 h (37.3 g, 83% yield). **^{1}H NMR** (400 MHz, $CDCl_3$): 7.00–6.86 (m, 4H), 4.24 (dd, *J* = 3.60, 11.37 Hz, 1H), 4.05 (dd, *J* = 5.35, 11.34 Hz, 1H), 3.87 (s, 3H), 3.40 (m, 1H), 2.90 (dd, *J* = 4.67, 4.67, 1H), 2.74 (dd, *J* = 2.62, 4.91, 1H) ppm. **^{13}C NMR** (125 MHz, $CDCl_3$): δ 149.52, 147.85, 121.76, 120.66, 114.21, 111.87, 70.07, 55.66, 49.99, 44.62 ppm. Characterization data were consistent with literature reports.[4]

3.2. Catalyst Synthesis

Bifunctional Aluminum Catalyst

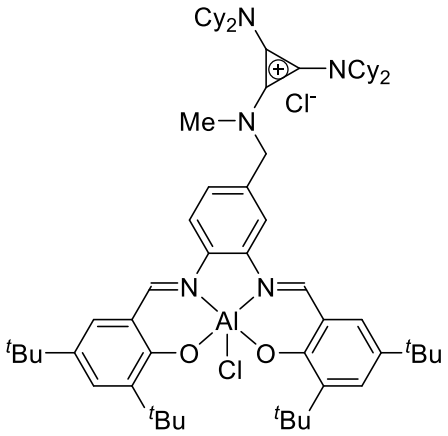

The aminocyclopropenium salen ligand was synthesized and metalated with diethyl aluminium chloride according to a reported procedure.[5] The resulting orange-yellow powder was dried in vacuo for 16 h at 22 °C (2.20 g, 97% yield). **^{1}H NMR** (500 MHz, $CDCl_3$): δ 9.42 (s, 1H), 9.07 (s, 1H), 8.33 (s, 1H), 7.89 (d, *J* = 8.5 Hz, 1H), 7.64 (d, *J* = 2.1 Hz, 2H), 7.56 (s, 1H), 7.35 (d, *J* = 8.5 Hz, 1H), 7.33 (d, *J* = 1.9 Hz, 1H), 5.07 (s, 2H), 3.42–3.34 (m, 4H), 3.34 (s, 3H), 1.93–1.79 (m, 16H) 1.67–1.59 (m, 12H), 1.58 (s, 18H), 1.34 (s, 9H), 1.33 (s, 9H), 1.24 1.30–1.18 (m, 8H), 1.06 (q, *J* = 12.4, 12.0 Hz, 4H) ppm. **^{13}C NMR** (125 MHz, $CDCl_3$): δ 164.50, 164.42, 164.40, 162.81, 141.56, 141.14, 139.81, 139.73, 138.73, 137.60, 135.78, 133.21, 133.09, 129.40, 128.51, 126.09, 119.97, 119.05, 118.71, 118.60, 116.58, 116.27, 60.89, 57.86,

40.28, 35.78, 35.75, 34.31, 34.26, 32.30, 31.46, 31.40, 29.99, 29.96, 25.82, 24.76 ppm. Characterization data were consistent with literature reports.[5]

3.3. Pre-Polymer Synthesis

General Procedure

In a glovebox, the appropriate amount of bifunctional aluminum catalyst (1 equiv) was weighed into an oven-dried 50 mL Schlenk flask. Phthalic anhydride (400 equiv) and vanillin glycidyl ether (x equiv) were then weighed into the flask. THF and propylene oxide or guaiacol glycidyl ether (y equiv) were added sequentially by volume (where x + y = 400). The Schlenk flask was sealed and secured with Teflon and electrical tape before removing from the glovebox and placing in a preheated oil bath. Conversion was monitored by cooling the reaction mixture to 22 °C, placing the flask under positive pressure of nitrogen, and removing a small aliquot via syringe for ^{1}H NMR analysis. Pre-polymer was purified by dissolving in minimal DCM and precipitating into MeOH to remove monomer, then filtering through silica gel to remove catalyst residue. ^{1}H NMR spectroscopic analysis was performed to quantify the relative incorporation of **VG** and **PO** or **GG**. GPC was performed to determine the molecular weight and dispersity of the pre-polymer. As is common for anionic ring-opening copolymerizations, GPC traces of the pre-polymers revealed bimodal molecular weight distributions consistent with the presence of adventitious water, diol, or diacid (Figure S2).

Pre-PO$_{62\%}$-*grad* Pre-Polymer

In a glovebox, **VG** (5.4 g, 26 mmol, 160 equiv), bifunctional aluminium catalyst (174 mg, 0.161 mmol, 1.00 equiv), adamantane carboxylic acid (59 mg, 0.32 mmol, 2.0 equiv), and **PA** (9.56 g, 64.8 mmol, 400 equiv) were combined in an oven-dried Schlenk flask equipped with a Teflon-coated stir bar. THF (21 mL) and **PO** (2.73 mL, 38.9 mmol, 240 equiv) were added

sequentially, before sealing the flask and removing it from the glovebox. The reaction mixture was stirred at 80 °C for 16 h. At 23 h, an aliquot analyzed by ^{1}H NMR spectroscopy showed 90% consumption of **VG** and residual unreacted phthalic anhydride. Allowing that significant **PO** (b.p. = 34 °C) may occupy the headspace at 80 °C, the flask was taken back into the glovebox and excess **PO** (5 mL) was added to drive the polymerization to full conversion of **PA**. The reaction mixture was then removed from the box and heated at 80 °C for 16 h. Full consumption of **PA** was confirmed by ^{1}H NMR, and the pre-polymer was purified by precipitating into MeOH (300 mL). The precipitate was then dissolved in minimal DCM and filtered through silica gel (220 mL) to remove catalyst residue. The filtrate was concentrated in vacuo to afford **pre-PO$_{62\%}$-*grad*** as a glassy yellow solid (17.0 g, 98% yield). **^{1}H NMR** (500 MHz, $CDCl_3$): δ 9.76 (m), 7.70 (d), 7.47 (bs), 7.32 (m), 6.98 (m), 5.57 (bs), 5.40 (bs), 4.66 (m), 4.37 (m), 3.79 (s), 1.35 (s) ppm. **^{13}C NMR** (125 MHz, $CDCl_3$): δ 190.75, 166.80–166.43, 153.08, 150.06, 132.16–130.75, 129.12–128.83, 126.19, 112.77, 109.70, 70.63, 69.55, 66.87, 63.33, 55.79, 16.25 ppm. **GPC**: M_n = 6.0 kDa, $Đ$ = 1.38.

Pre-PO$_{62\%}$-*grad*, ^{1}H NMR Spectrum (500 MHz, CDCl$_3$)

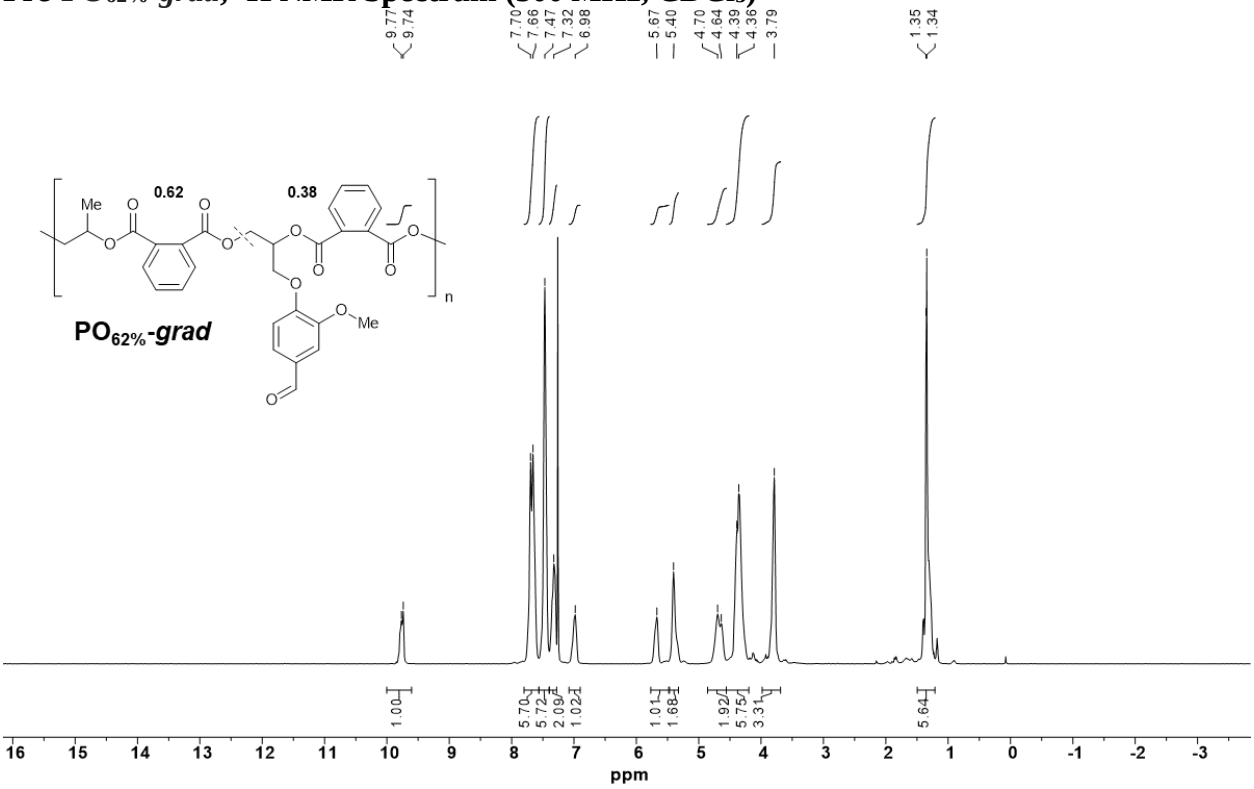

Pre-PO$_{62\%}$-*grad*, ^{13}C NMR Spectrum (125 MHz, CDCl$_3$)

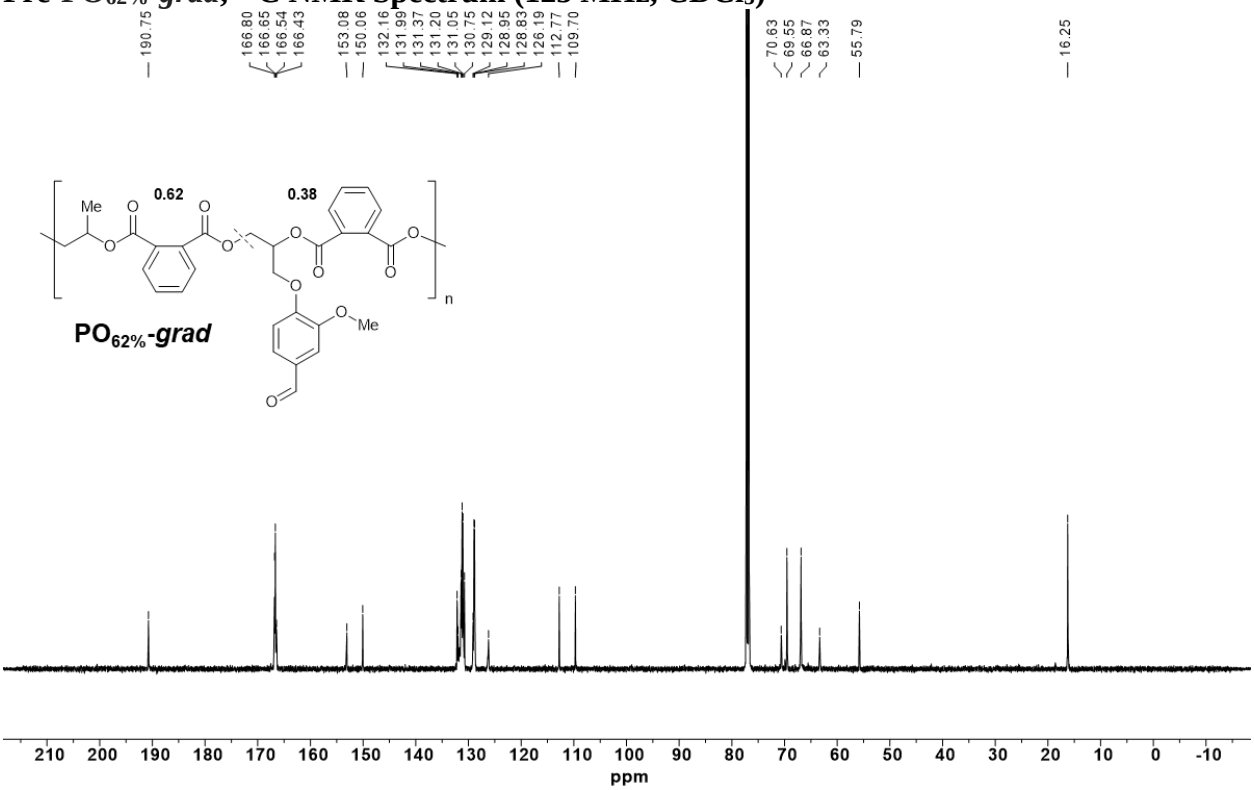

Pre-PO$_{42\%}$-*grad* Pre-Polymer

In a glovebox, **VG** (5.83 g, 28.0 mmol, 240 equiv), bifunctional aluminium catalyst (128 mg, 0.120 mmol, 1.00 equiv), adamantane carboxylic acid (44 mg, 0.24 mmol, 2.0 equiv), and **PA** (7.05 g, 47.0 mmol, 400 equiv) were combined in an oven-dried Schlenk flask equipped with a Teflon-coated stir bar. THF (16 mL) and **PO** (1.34 mL, 19.0 mmol, 160 equiv) were added sequentially before sealing the flask and removing it from the glovebox. The reaction mixture was stirred at 80 °C for 16 h. At 22 h, an aliquot analyzed by ^{1}H NMR spectroscopy showed 95% consumption of **VG** and residual unreacted phthalic anhydride. Allowing that significant **PO** (b.p. 34 °C) may occupy the headspace at 80 °C, the flask was taken back into the glovebox and excess **PO** (5 mL) was added to drive the polymerization to full conversion of **PA**. The reaction mixture was then removed from the box and heated at 80 °C for 16 h. Full consumption of **PA** was confirmed by ^{1}H NMR, and the pre-polymer was purified by precipitating into MeOH (300 mL). The precipitate was then dissolved in minimal DCM and filtered through silica gel (150 mL) to remove catalyst residue. The filtrate was concentrated in vacuo to afford **pre-PO$_{42\%}$-*grad*** as a glassy yellow solid (12 g, 86% yield). **^{1}H NMR** (500 MHz, $CDCl_3$): δ 9.76 (m), 7.66 (m), 7.45 (s), 7.32 (m), 6.98 (m), 5.67 (s), 5.36 (m), 4.67 (d), 4.34 (s), 3.79 (m), 1.30 (m) ppm. **^{13}C NMR** (125 MHz, $CDCl_3$): δ 190.81, 166.72, 166.48, 153.16, 150.09, 131.97–130.77, 129.15, 128.93, 126.27, 112.79, 109.74, 70.65, 69.56, 66.92, 63.37, 55.83, 16.23 ppm. **GPC**: M_n = 3.8 kDa, $Đ$ = 1.12.

Pre-PO$_{42\%}$-*grad*, ^{1}H NMR Spectrum (500 MHz, CDCl$_3$)

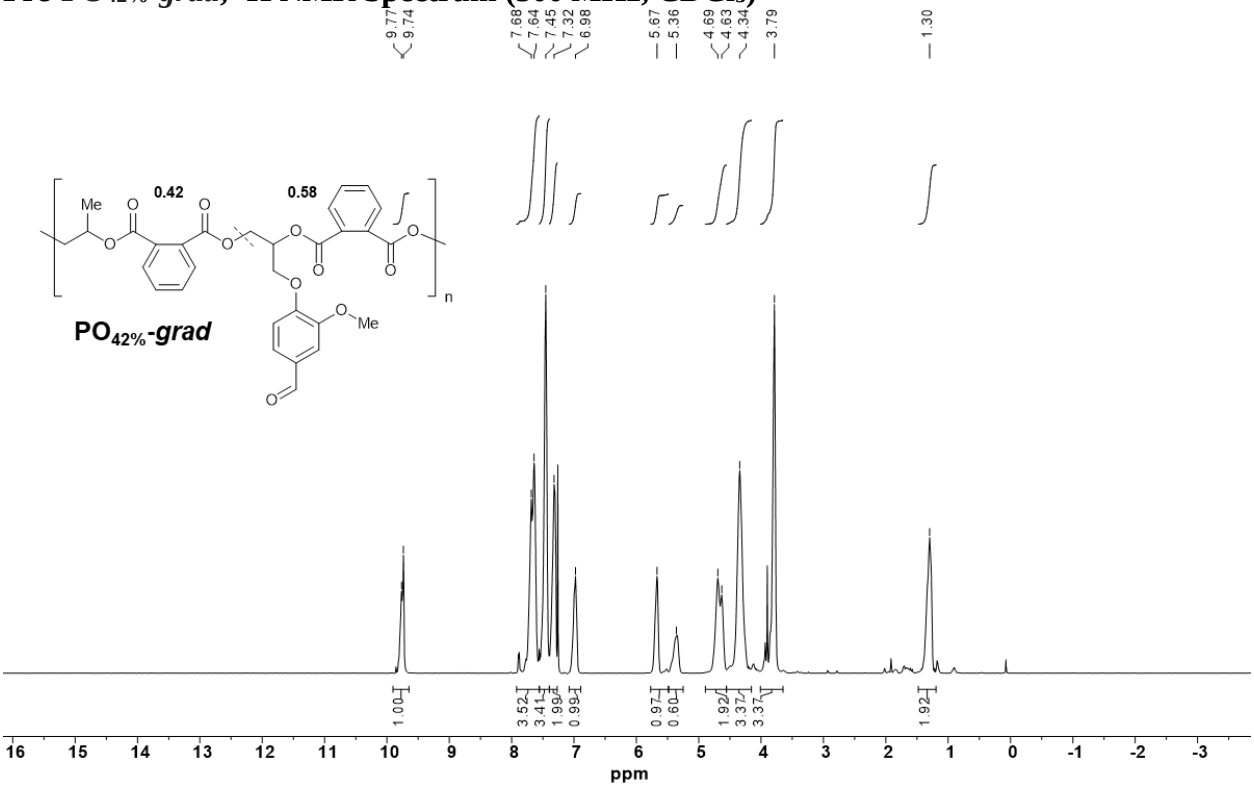

Pre-PO$_{42\%}$-*grad*, ^{13}C NMR Spectrum (125 MHz, CDCl$_3$)

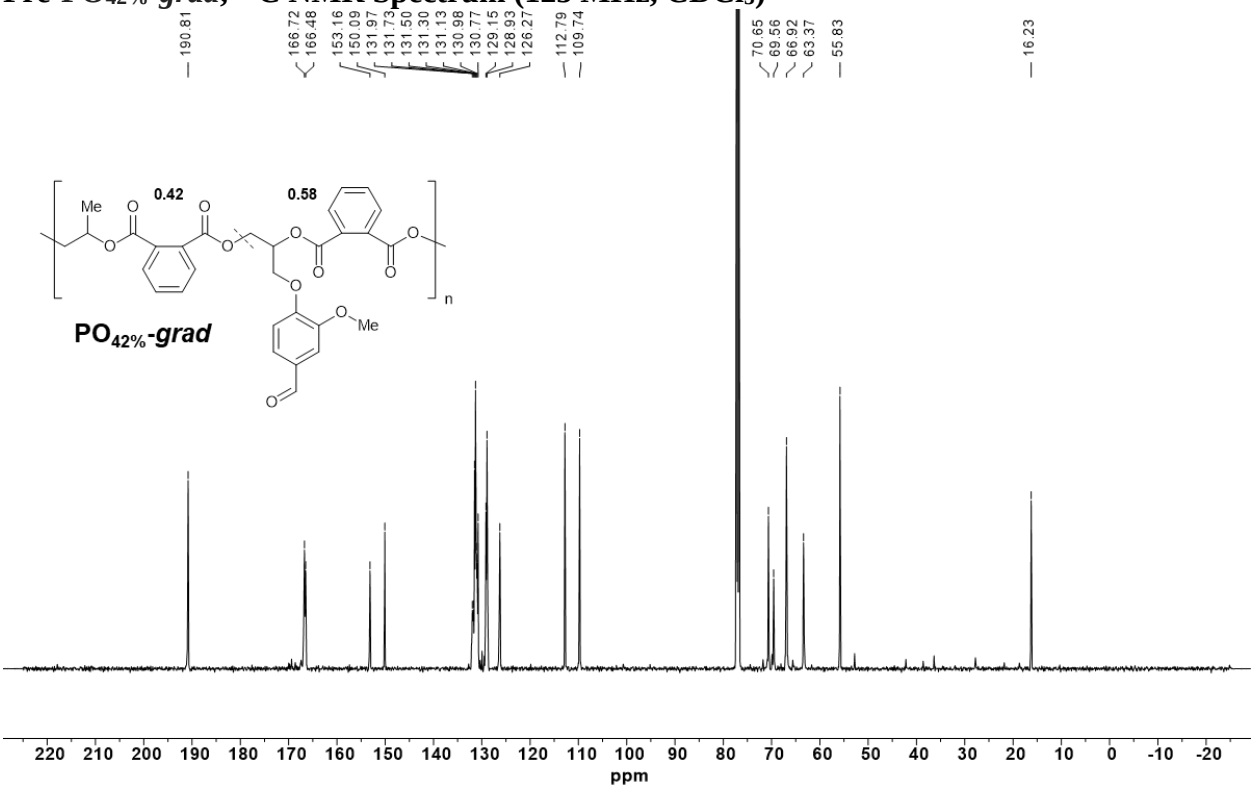

Pre-PO$_{23\%}$-*grad* Pre-Polymer

In a glovebox, **VG** (5.72 g, 27.5 mmol, 320 equiv), bifunctional aluminium catalyst (88 mg, 0.081 mmol, 1.0 equiv), and **PA** (5.18 g, 35.0 mmol, 400 equiv) were combined in an oven-dried Schlenk flask equipped with a Teflon-coated stir bar. THF (11 mL) and **PO** (0.50 mL, 7.1 mmol, 80 equiv) were added sequentially, before sealing the flask and removing it from the glovebox. The reaction mixture was stirred at 80 °C for 48 h, monitoring polymerization progress by ^{1}H NMR spectroscopy. At full conversion, the pre-polymer was precipitated into MeOH (200 mL) to remove monomer then dissolved in minimal DCM and filtered through silica gel (110 mL). The filtrate was concentrated in vacuo to afford **pre-PO$_{23\%}$-*grad*** as a glassy pale yellow solid that was further dried in vacuo at 22 °C for 16 h (4.7 g, 43% yield). **^{1}H NMR** (500 MHz, $CDCl_3$): δ 9.73 (m), 7.65 (d), 7.45 (m), 7.29 (m), 6.96 (m), 5.66 (bs), 5.38 (bs), 4.65 (d), 4.31 (m), 3.77 (s), 1.30 (m) ppm. **^{13}C NMR** (125 MHz, $CDCl_3$): δ 190.72, 166.67, 166.44, 153.09, 150.05, 131.72–130.78, 129.12, 128.90, 126.19, 112.78, 109.74, 70.64, 69.53, 66.92, 63.35, 55.80, 16.23 ppm. **GPC**: M_n = 3.1 kDa, $Đ$ = 1.23.

Pre-PO$_{23\%}$-*grad*, ^{1}H NMR Spectrum (500 MHz, CDCl$_3$)

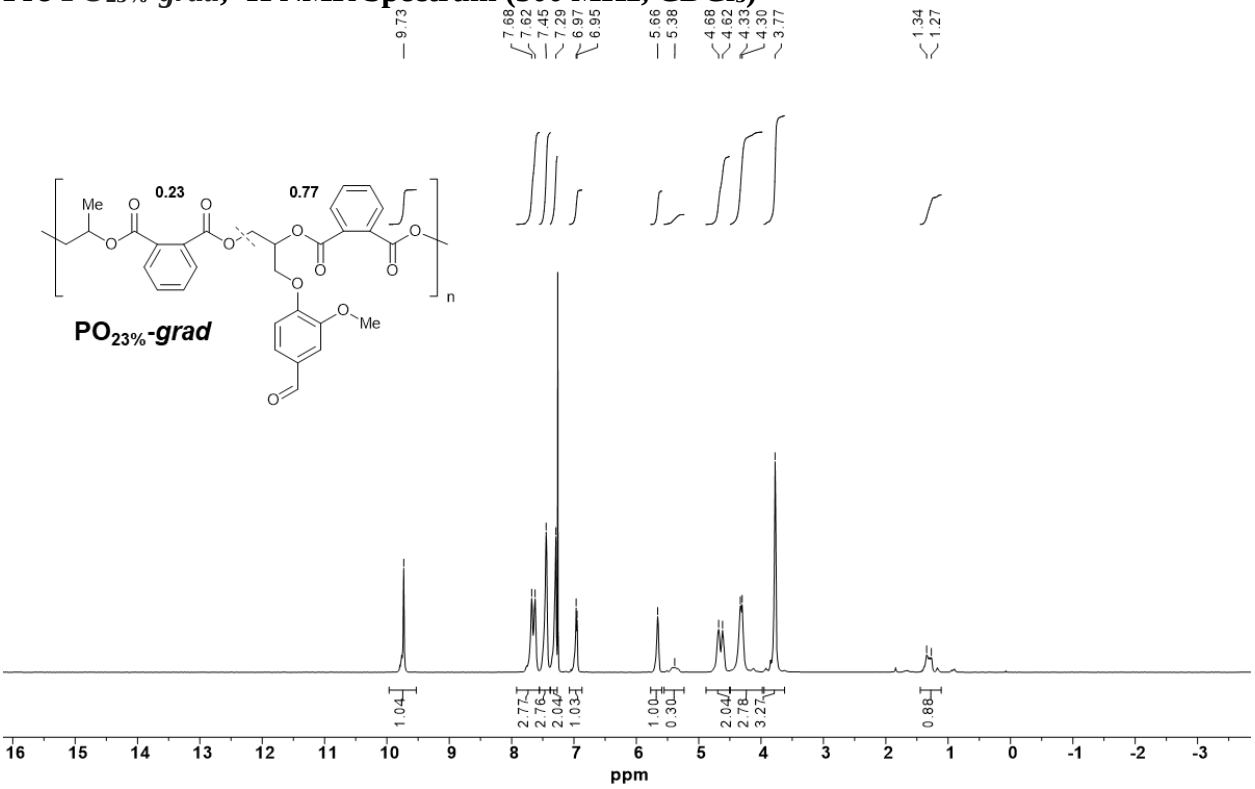

Pre-PO$_{23\%}$-*grad*, ^{13}C NMR Spectrum (125 MHz, CDCl$_3$)

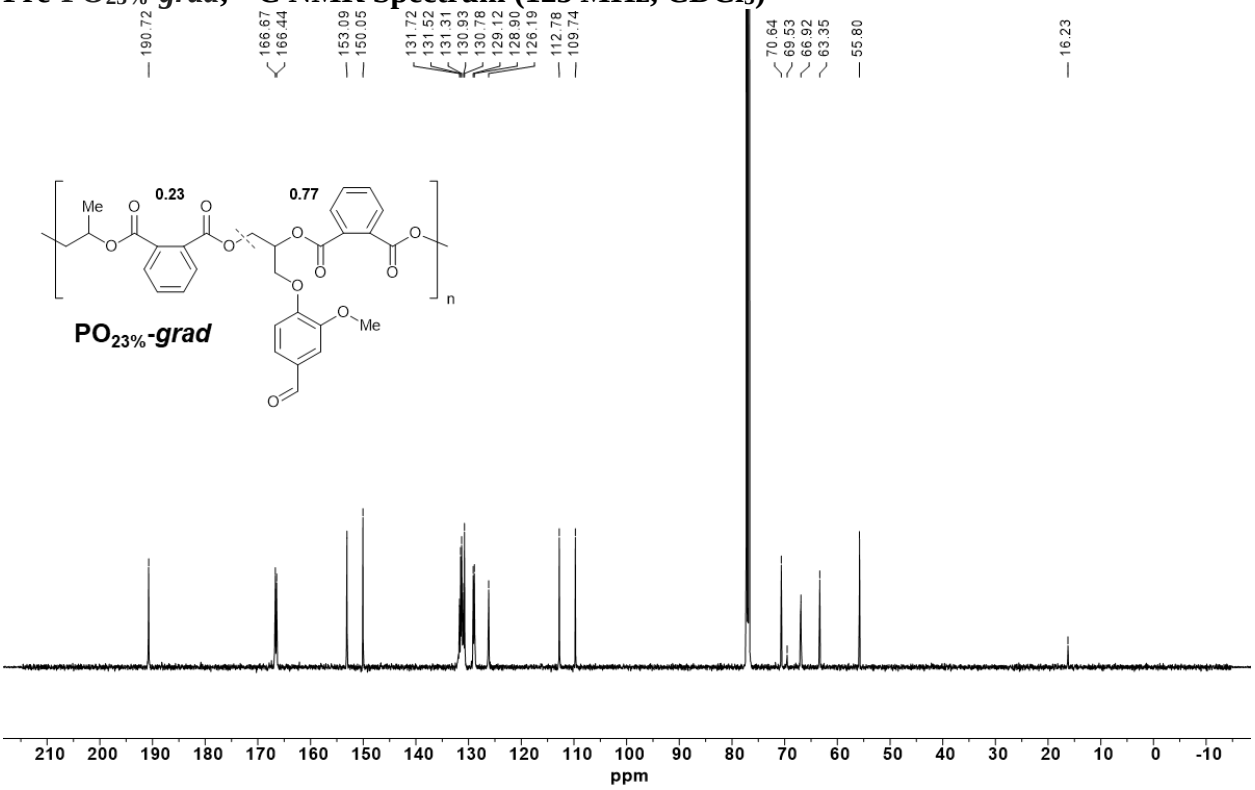

Pre-PO$_{35\%}$-*stat* Pre-Polymer

In a glovebox, **VG** (5.83 g, 28.0 mmol, 240 equiv), bifunctional aluminium catalyst (128 mg, 0.118 mmol, 1 equiv), and **PA** (7.05 g, 47.6 mmol, 400 equiv) were combined in an oven-dried Schlenk flask equipped with a Teflon-coated stir bar. THF (15 mL) and **PO** (1.34 mL, 19.1 mmol, 160 equiv) were added sequentially before sealing the flask and removing it from the glovebox. The reaction mixture was stirred at 60 °C for 60 h, monitoring polymerization progress by ^{1}H NMR spectroscopy. The pre-polymer was purified by precipitating repeatedly into MeOH (5 × 300 mL). Redissolution in DCM, followed by concentrating and drying in vacuo afforded **pre-PO$_{35\%}$-*stat*** as a glassy yellow solid (8.97 g, 64% yield). **^{1}H NMR** (500 MHz, $CDCl_3$): δ 9.75 (m), 7.66 (d), 7.45 (bs), 7.32 (m), 6.98 (m), 5.67 (bs), 5.34 (bs), 4.66 (d), 4.34 (bs), 3.79 (s), 1.29 (s) ppm. **^{13}C NMR** (125 MHz, $CDCl_3$): δ 190.76, 166.69, 166.45, 153.15, 150.07, 131.97–130.77, 129.13, 128.92, 126.22, 112.78, 109.72, 70.64, 69.54, 66.91, 63.35, 55.81, 16.22 ppm. **GPC**: M_n = 5.1 kDa, $Đ$ = 1.13.

Pre-PO$_{35\%}$-*stat*, ^{1}H NMR Spectrum (500 MHz, CDCl$_3$)

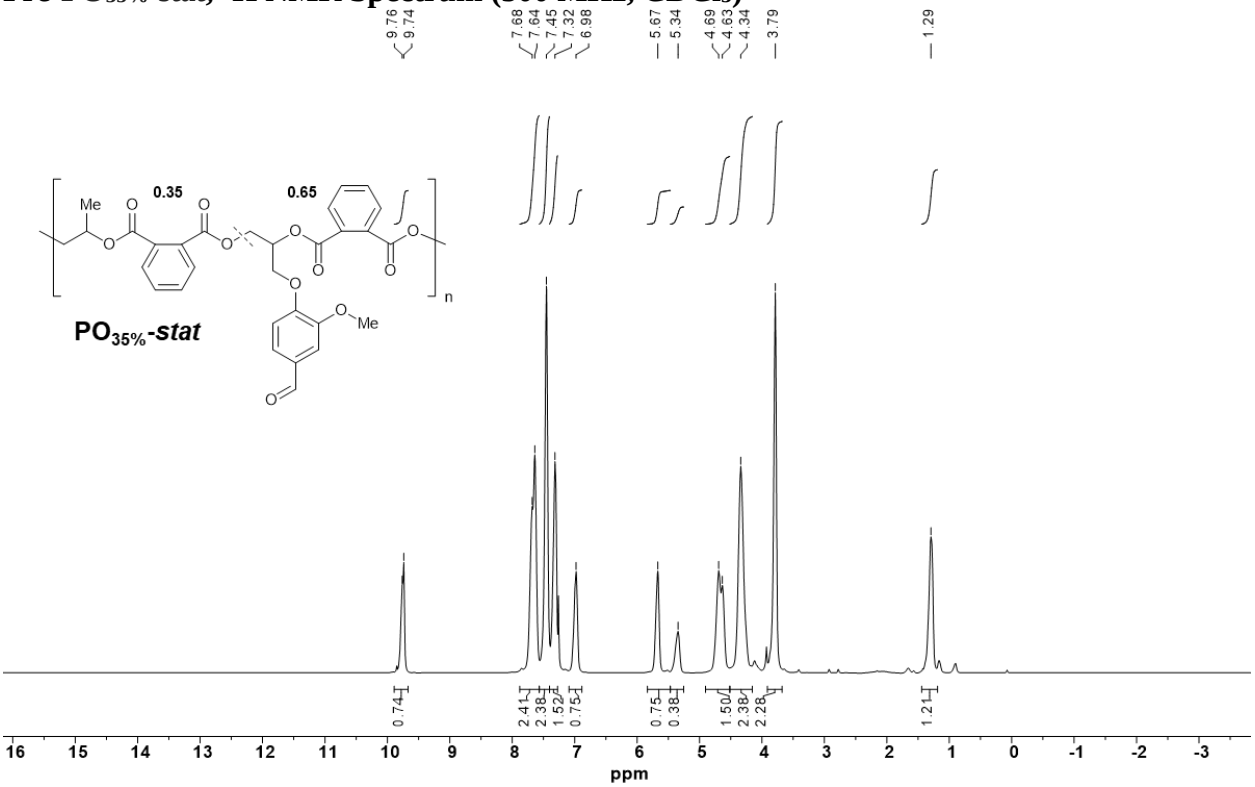

Pre-PO$_{35\%}$-*stat*, ^{13}C NMR Spectrum (125 MHz, CDCl$_3$)

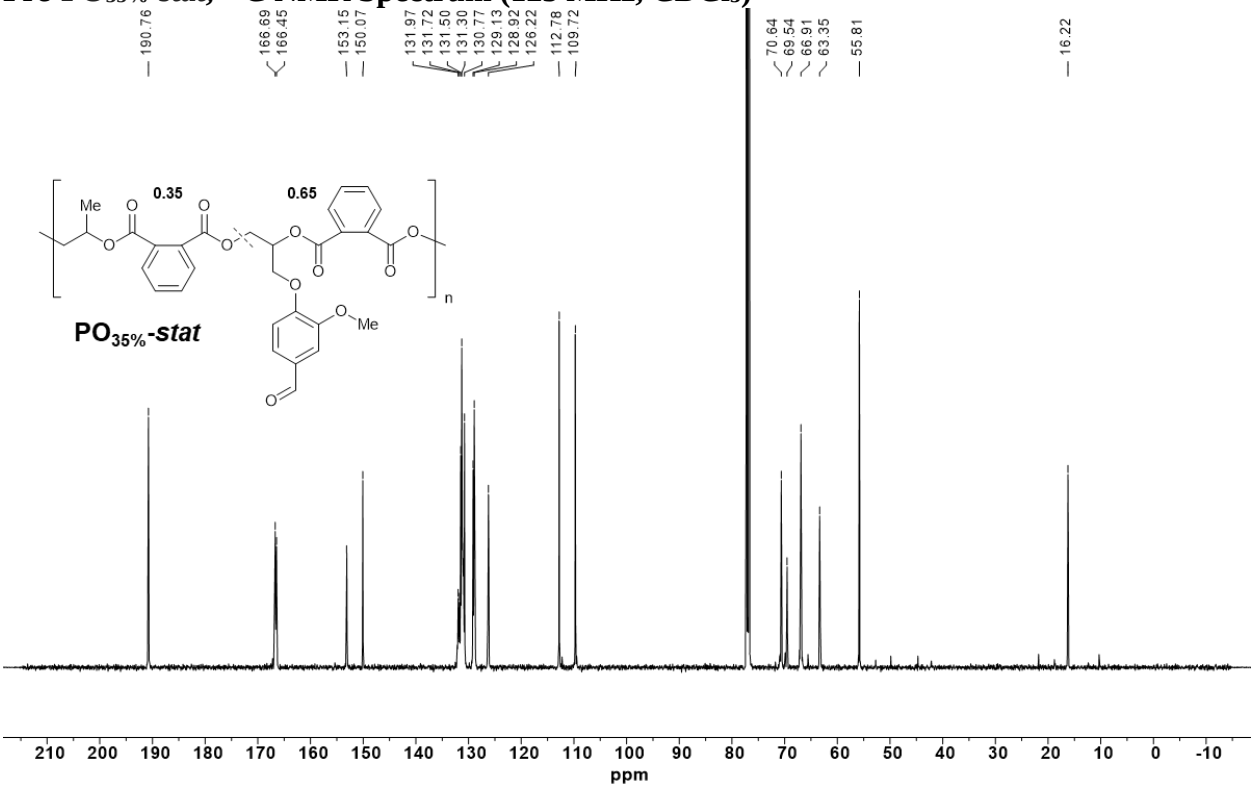

Pre-GG$_{43\%}$-*stat* Pre-Polymer

In a glovebox, **VG** (5.83 g, 28.0 mmol, 240 equiv), bifunctional aluminium catalyst (128 mg, 0.118 mmol, 1.00 equiv), and **PA** (7.05 g, 47.6 mmol, 400 equiv) were combined in an oven-dried Schlenk flask equipped with a Teflon-coated stir bar. THF (15 mL) and **GG** (3.38 g, 18.7 mmol, 160 equiv) were added sequentially, before sealing the flask and removing it from the glovebox. The reaction mixture was stirred at 60 °C for 18 h, and the polymerization progress was monitored by ^{1}H NMR spectroscopy. The pre-polymer was purified by precipitating into MeOH (300 mL), then dissolved in minimal DCM and filtered through silica gel (160 mL). The filtrate was concentrated in vacuo to afford **pre-GG$_{43\%}$-*stat*** as a glassy pale yellow solid which was further dried in vacuo at 22 °C for 16 h (9.5 g, 58% yield). **^{1}H NMR** (500 MHz, $CDCl_3$): δ 9.76 (m), 7.69 (d), 7.46 (bs), 7.32 (s), 6.91 (m), 5.69–5.46 (m), 4.68 (d), 4.31 (m), 3.80–3.74 (m) ppm. **^{13}C NMR** (125 MHz, $CDCl_3$): δ 190.74, 166.65, 166.41, 153.13, 150.03, 147.86, 131.90–130.75, 129.08–128.87, 126.19, 122.35, 120.86, 115.38, 112.75, 112.34, 109.85, 71.08, 70.61, 67.62, 66.91, 63.64, 63.32, 55.77 ppm. **GPC**: M_n = 3.7 kDa, $Đ$ = 1.41.

Pre-GG$_{43\%}$-*stat*, ^{1}H NMR Spectrum (500 MHz, CDCl$_3$)

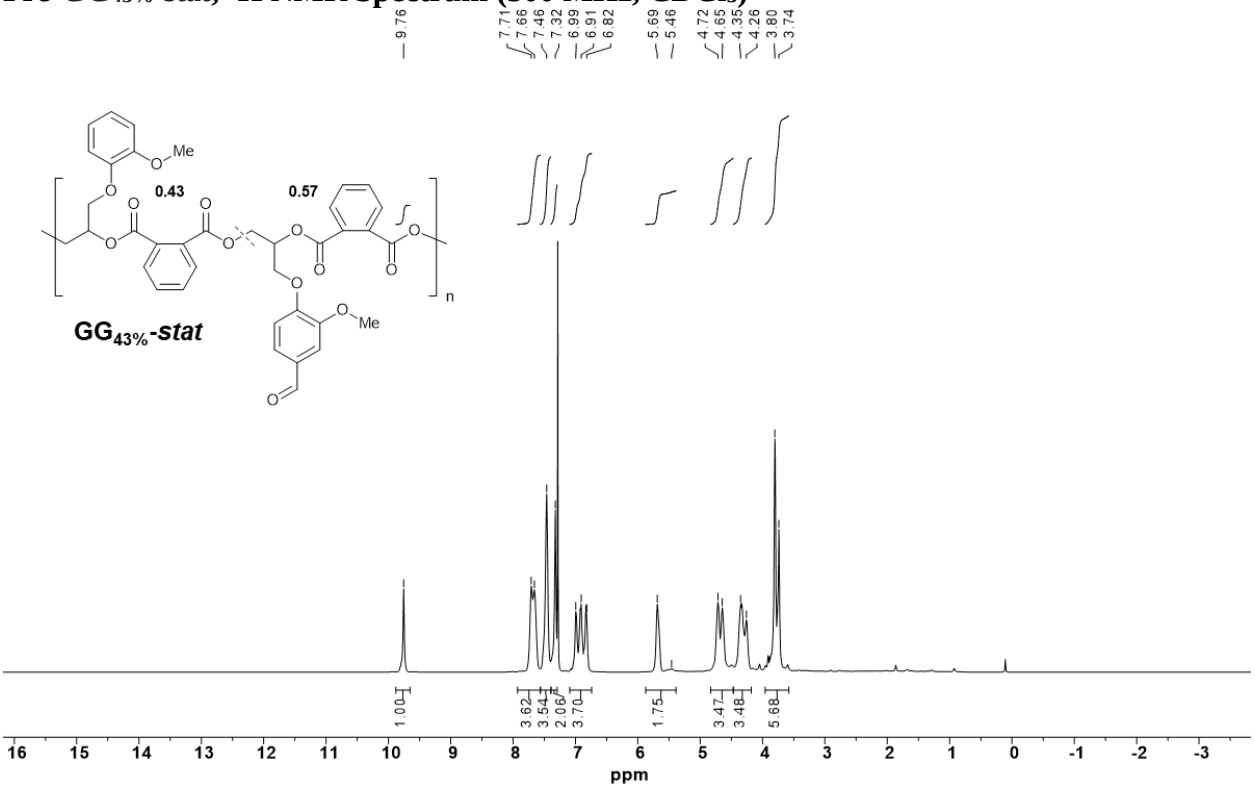

Pre-GG$_{43\%}$-*stat*, ^{13}C NMR Spectrum (125 MHz, CDCl$_3$)

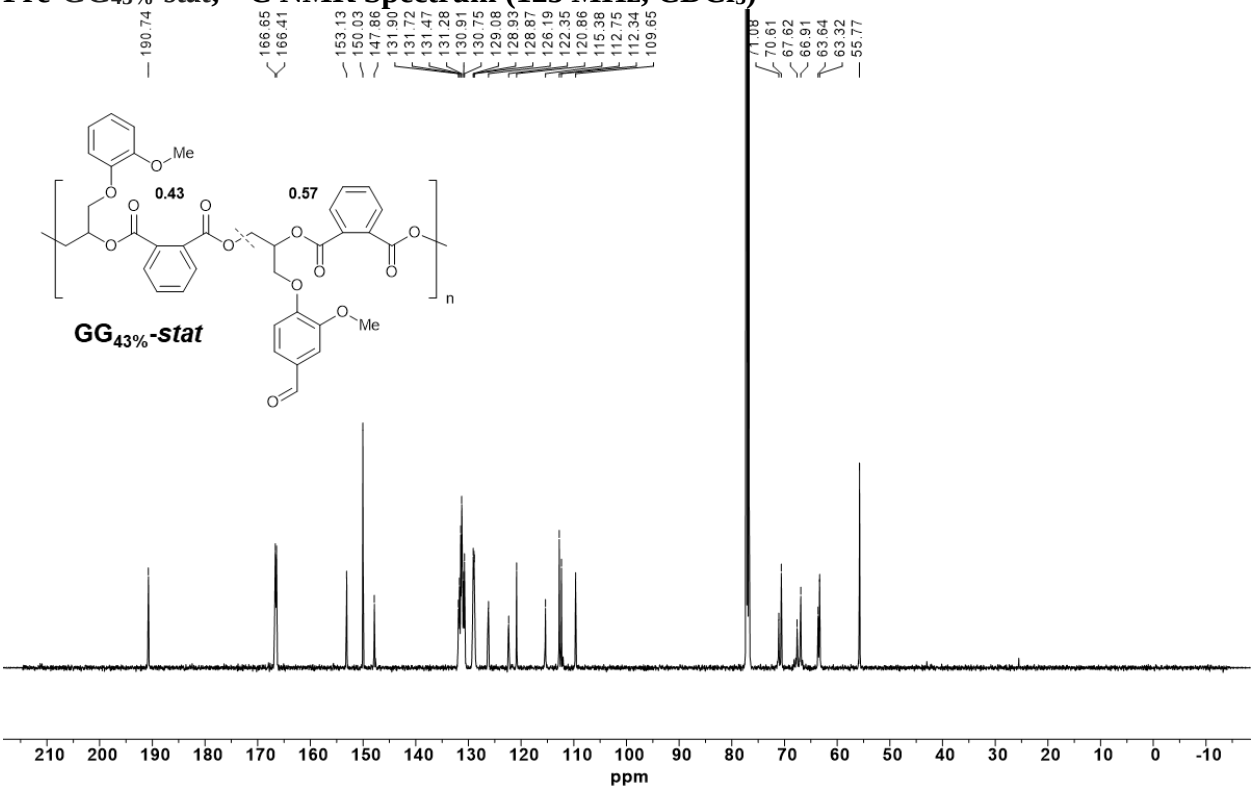

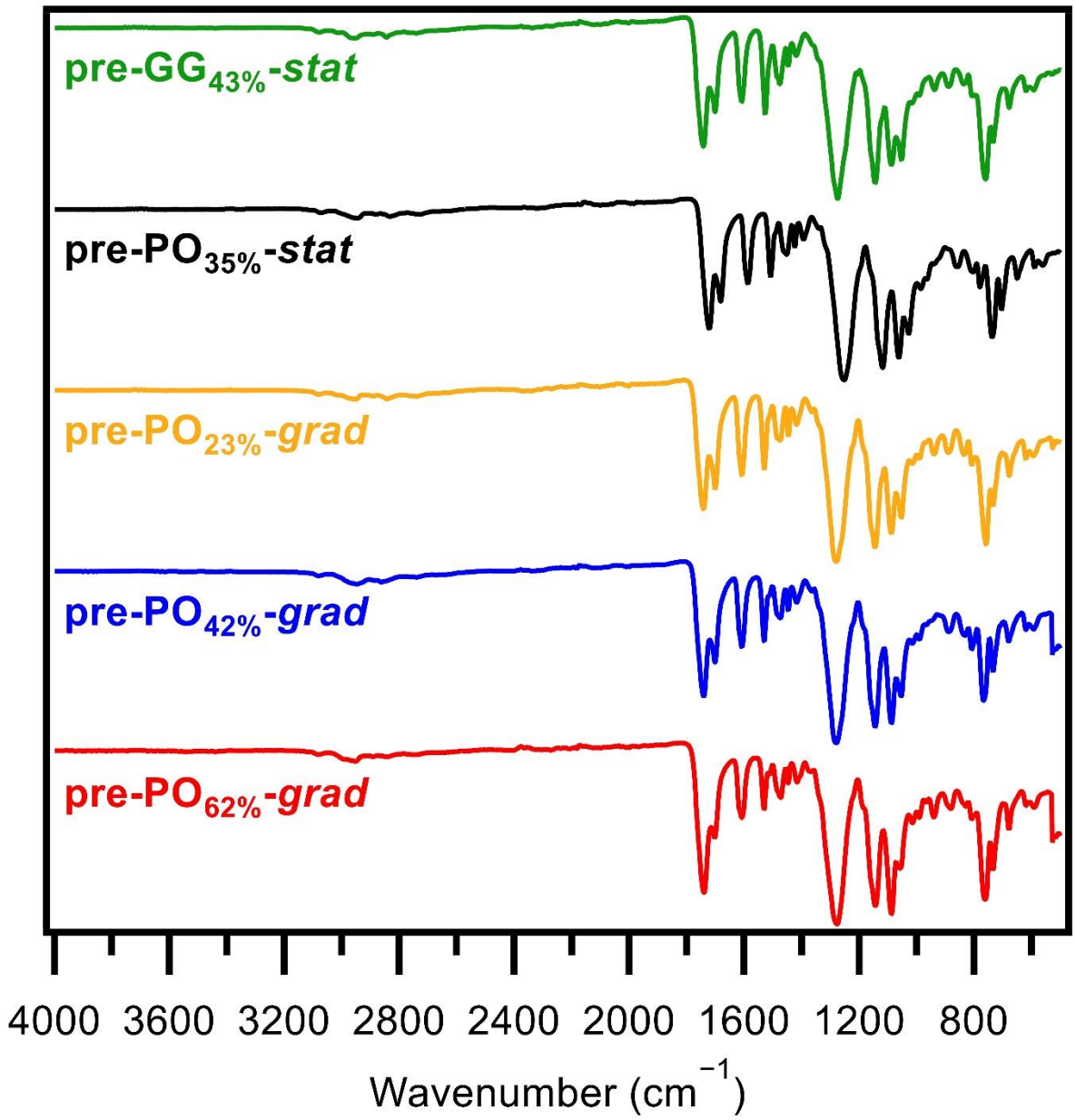

Figure S1. Normalized Fourier transform infrared spectra of polyester pre-polymers. The relative intensity of the aldehyde stretching mode at 1681 cm^{-1} to the ester carbonyl stretching frequency at 1722 cm^{-1} varies as expected with changes in **VG** content.

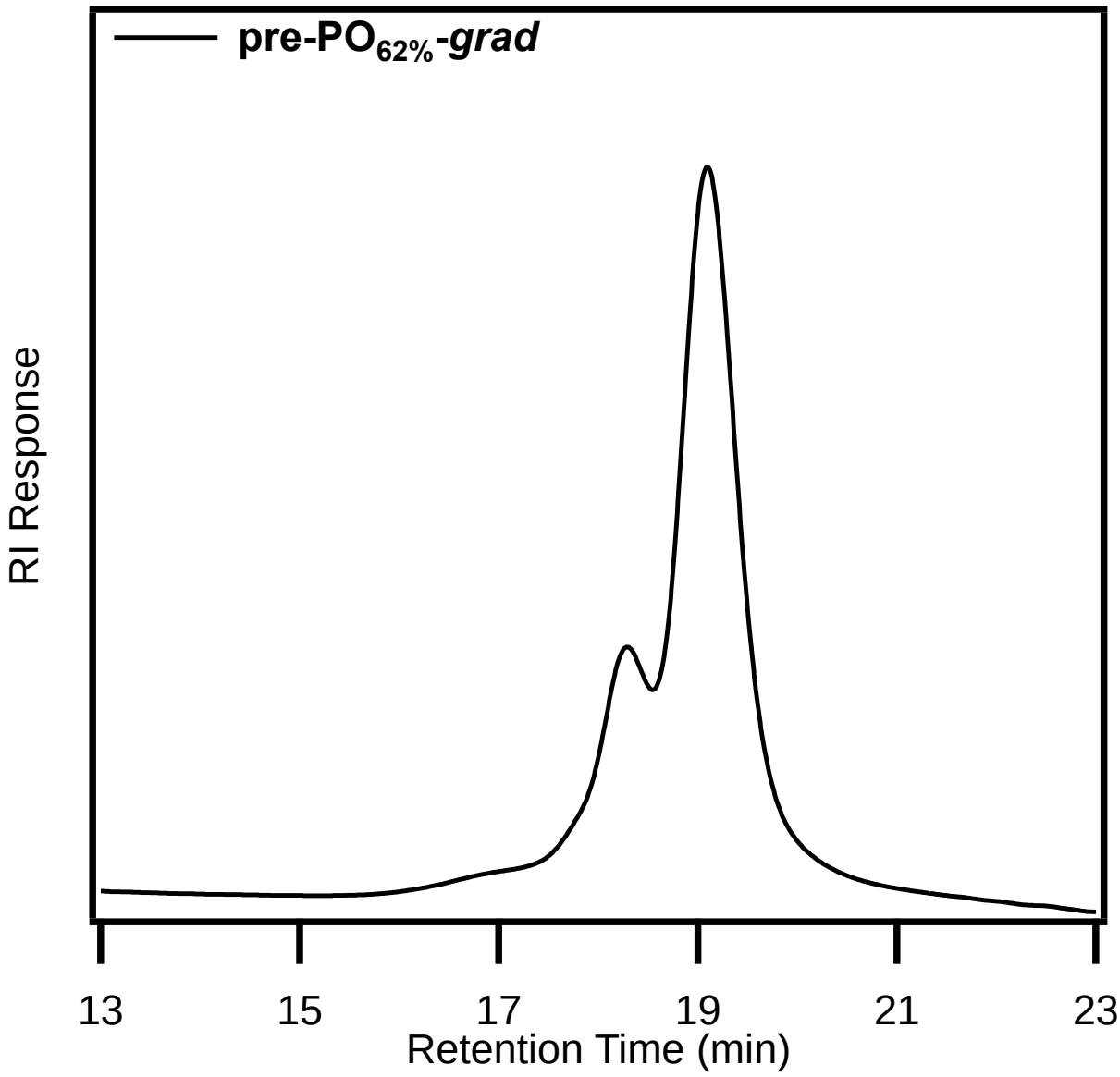

Figure S2. Representative GPC trace of pre-polymer material **pre-PO$_{62\%}$-*grad*** with a primary peak from catalyst-derived chloride initiators and a high molecular weight peak from adventitious bifunctional initiators (i.e. water, diol, diacid).

3.4. Characterization of Pre-Polymer Structure

Pre-polymer structure for **PO**- and **GG**-derived materials was modelled by monitoring **VG** incorporation as a function of conversion from a 50:50 mixture of **VG** and epoxide comonomer with **PA**. In a glovebox, aluminum catalyst was weighed into an oven-dried 4 mL vial with an oven-dried Teflon-coated stir bar, followed by **PA** (0.225 g, 1.51 mmol, 400 equiv) and **VG** (0.158

g, 0.759 mmol, 200 equiv). THF (0.5 mL) was added by volume, followed by **PO** (83 μL, 0.76 mmol, 200 equiv) or **GG** (0.134 g, 0.759 mmol, 200 equiv). The vials were sealed with a Teflon-lined cap, removed from the glovebox, and stirred at 60 °C. Five replicates of each copolymerization were performed, and each was quenched at a different timepoint and analyzed by ^{1}H NMR spectroscopy to determine **VG** incorporation as the reaction progressed. Integration of the **VG** monomer and polymer aldehyde peaks relative to the polymer methine peaks were used to determine the relative incorporation of **VG** and epoxide comonomer. **VG** is preferentially incorporated over **PO** early in the reaction period, producing a tapered structure from ~70:30 **VG**:**PO** to ~50:50 **VG**:**PO** (Figure S3). By contrast, structurally similar comonomers **VG** and **GG** are incorporated at similar rates throughout the polymerization, affording a statistical copolymer (Figure S3).

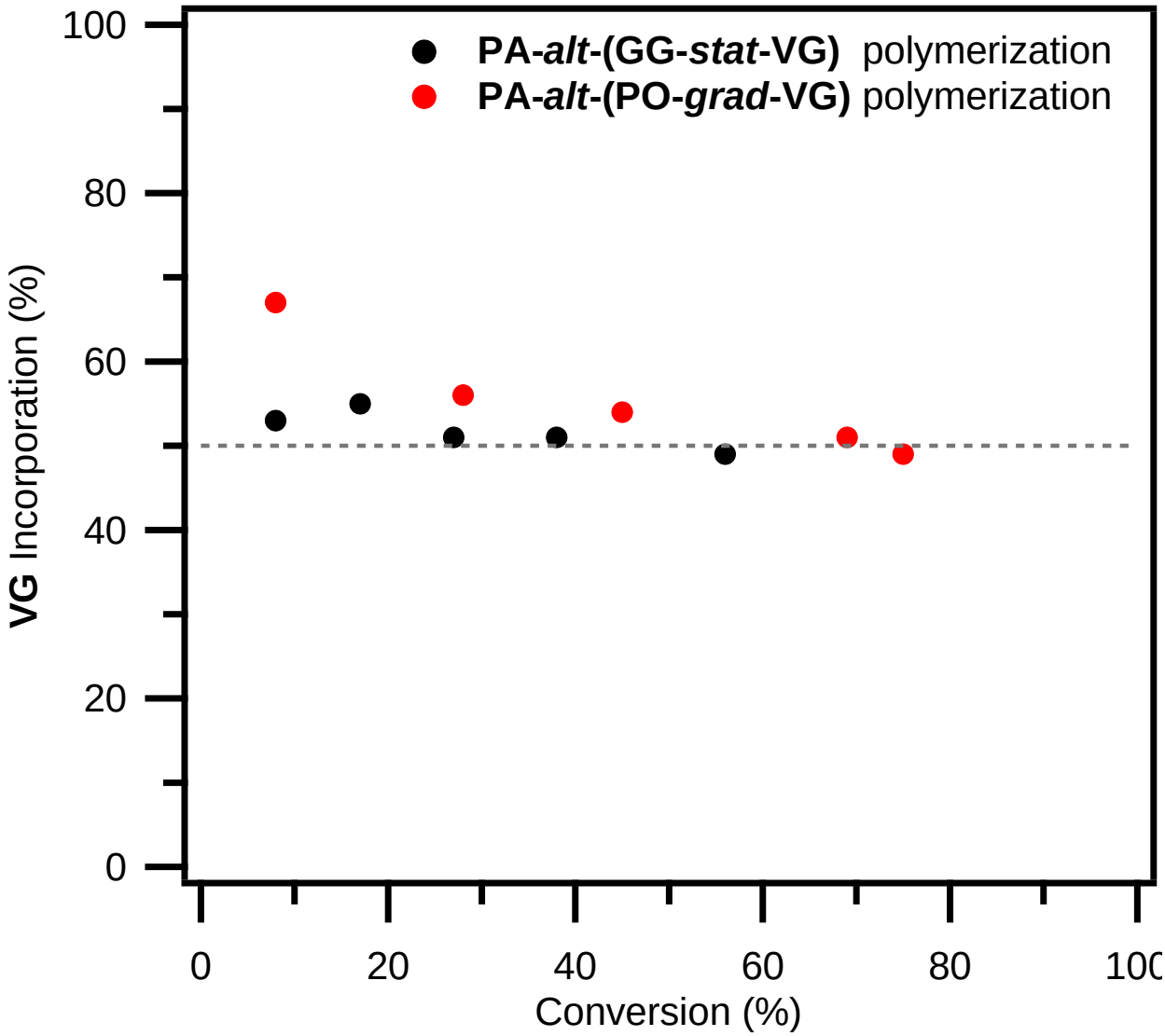

Figure S3. VG incorporation as a function of **PA** conversion from a 50:50 **VG**:epoxide comonomer feed with **PA**.

3.5. Network Synthesis

General Procedure

A given pre-polymer was dissolved in anhydrous THF in a scintillation vial. Using a microliter syringe, 2,2′-(ethylenedioxy)bis(ethylamine) was added to the vial, which was then quickly capped and shaken vigorously for 10 s. The yellow solution was poured into the appropriately sized crystallization dish (see Table S1) and sonicated for 10 s to remove air bubbles.

The mold was left undisturbed under ambient conditions for 1 hour to prevent bubbles from nucleating in the gels. For most samples, gelation was observed after ~5–10 min, and the gel became cloudy due to THF uptake during gelation. The sample was then placed in a vacuum chamber under nitrogen flow and heated to 45 °C for 6 h. Then, the heat was gradually increased to 100 °C over 2 h, as slow evaporation of the solvent limited the formation of bubbles in the films. After curing at 100 °C for 1 h, the nitrogen flow was switched to high vacuum, and the films were cured at 100 °C under high vacuum for 12 h.

Films were then removed from the mold and cooled to 22 °C. The pristine films were initially processed by pressing in a Carver press at 90 °C with 3–4 metric tons of pressure for 30 min to give 0.5–1.0 mm thick smooth, homogenous materials. Dogbones for tensile testing and dynamic mechanical thermal analysis were cut using a custom-made cutting die to the dimensions described in Figure S4. Discs were cut using a circular cutting die with an 8 mm diameter. Materials were stored in a desiccator or under ambient conditions. Percent conversion required to reach the gel point was determined using Flory-Stockmayer gelation theory.[6] Calculated amine conversions of 31–40% were required for the formation of an infinite network.

Table S1. Mold size and amounts of pre-polymer, THF, and diamine cross-linker used for network synthesis.

Network	Dish Diameter [a]	Pre-Polymer (g) [b]	THF (mL)	Diamine Cross-Linker (μL)
PO$_{62\%}$-*grad*	90 mm	2.5	7.2	258
PO$_{42\%}$-*grad*	90 mm	2.5	9.5	354
PO$_{23\%}$-*grad*	90 mm	2.5	12.1	432
GG$_{42\%}$-*stat*	85 mm	2.0	6.7	241
PO$_{35\%}$-*stat*	85 mm	2.0	8.6	306

[a] Pan diameter was selected based on equipment availability. [b] Pre-polymer amounts were adjusted to give ~1 mm thick films.

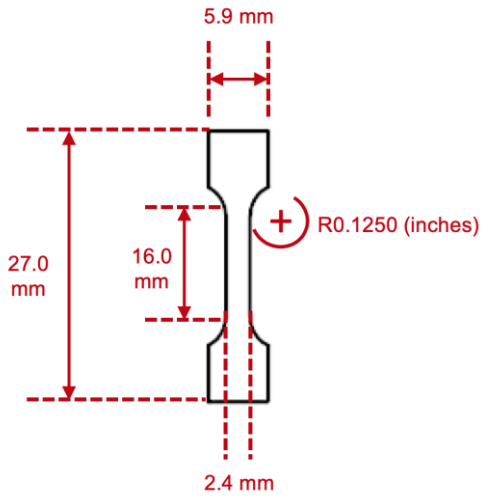

Figure S4. Dogbone dimensions.

3.6. Synthesis of Control Copolymers

PA-*alt*-PO Copolymer

In a glovebox, catalyst (4.1 mg, 0.0038 mmol, 1 equiv) was weighed into an oven-dried 4 mL vial equipped with an oven-dried Teflon-coated stir bar. **PA** (0.225 g, 1.52 mmol, 400 equiv) was then weighed into the vial, and **PO** (0.53 mL, 7.6 mmol, 2000 equiv) was added by volume. The vial was sealed with a Teflon-lined cap, removed from the glovebox, and placed in an oil bath preheated to 60 °C. Upon a color change from yellow to red signifying full conversion, the polymer was precipitated into MeOH (15 mL) and dried in vacuo at 22 °C for 16 h to afford a glassy, pale yellow solid. **^{1}H NMR** (500 MHz, $CDCl_3$): δ 7.71 (m, 2H), 7.75 (d, 2H), 5.41 (s, 1H), 4.38 (m, 2H), 1.35 (d, 3H) ppm. **^{13}C NMR** (125 MHz, $CDCl_3$): δ 166.82, 166.68, 132.18, 131.40, 131.22, 131.06, 128.97, 128.85, 69.57, 66.89, 16.27 ppm. **GPC**: M_n = 31.7, $Đ$ = 1.09. **DSC**: T_g = 52 °C.

PA-*alt*-PO Copolymer, ^{1}H NMR Spectrum (500 MHz, $CDCl_3$)

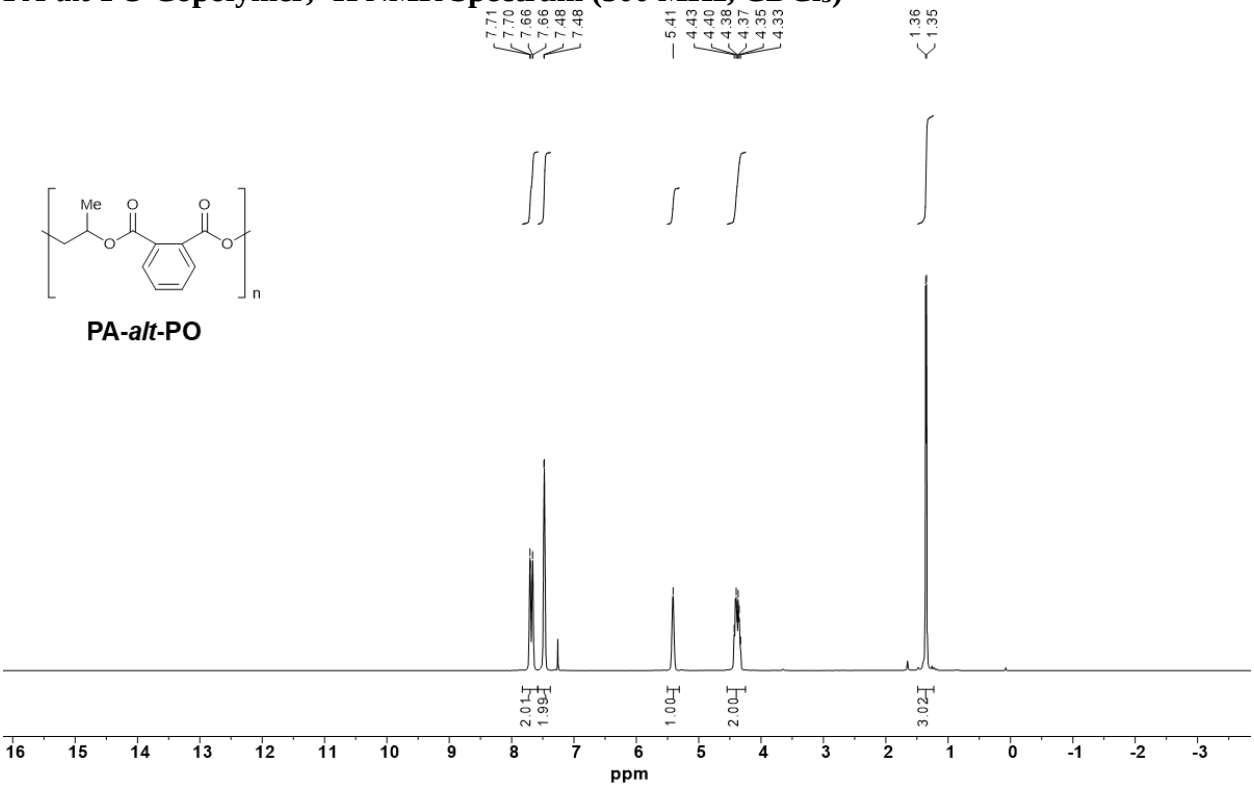

PA-*alt*-PO Copolymer, ^{13}C NMR Spectrum (125 MHz, $CDCl_3$)

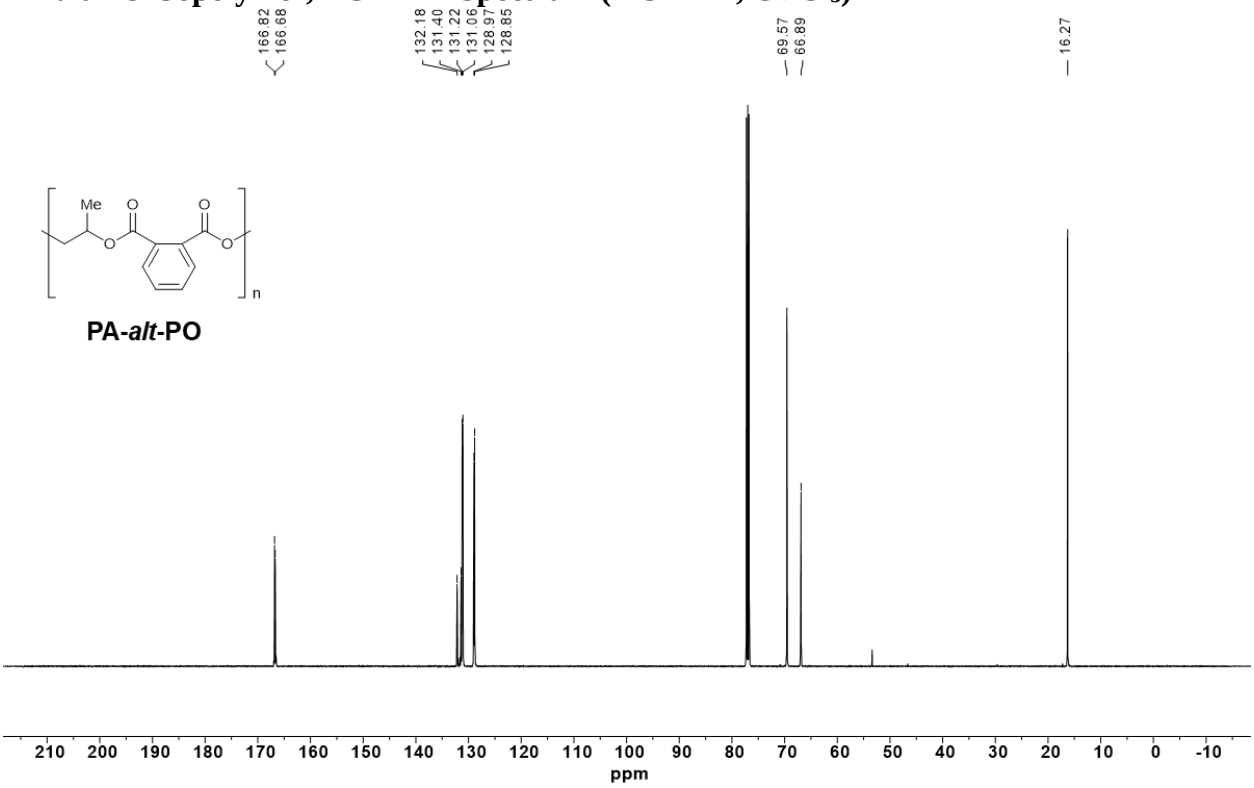

PA-*alt*-VG Copolymer

In a glovebox, catalyst (4.1 mg, 0.0038 mmol, 1 equiv) was weighed into an oven-dried 4 mL vial equipped with an oven-dried Teflon-coated stir bar. **PA** (0.225 g, 1.52 mmol, 400 equiv) was then weighed into the vial followed by **VG** (0.351 g, 1.52 mmol, 400 equiv). Dry, degassed THF (4 mL) was added to dissolve the solids. The vial was sealed with a Teflon-lined cap, removed from the glovebox, and placed in an oil bath preheated to 60 °C for 2 days. After cooling to room temperature, the polymer was precipitated into MeOH (15 mL) and dried in vacuo at 22 °C for 16 h to afford a glassy, pale yellow solid. **^{1}H NMR** (500 MHz, $CDCl_3$): δ 9.73 (m, 1H), 7.65 (d, 2H), 7.44 (m, 2H), 7.29 (m, 2H), 6.95 (d, 1H), 5.65 (s, 1H), 4.65 (m, 2H), 4.31 (m, 2H), 3.76 (m, 3H) ppm. **^{13}C NMR** (125 MHz, $CDCl_3$): δ 190.70, 166.67, 166.44, 153.08, 150.05, 131.73–130.79, 129.11, 128.90, 126.16, 112.79, 109.74, 70.64, 66.97, 63.34, 55.79 ppm. **GPC**: M_n = 3.9 kDa, $Đ$ = 1.13. **DSC**: T_g = 62 °C.

PA-*alt*-VG Copolymer, ^{1}H NMR Spectrum (500 MHz, $CDCl_3$)

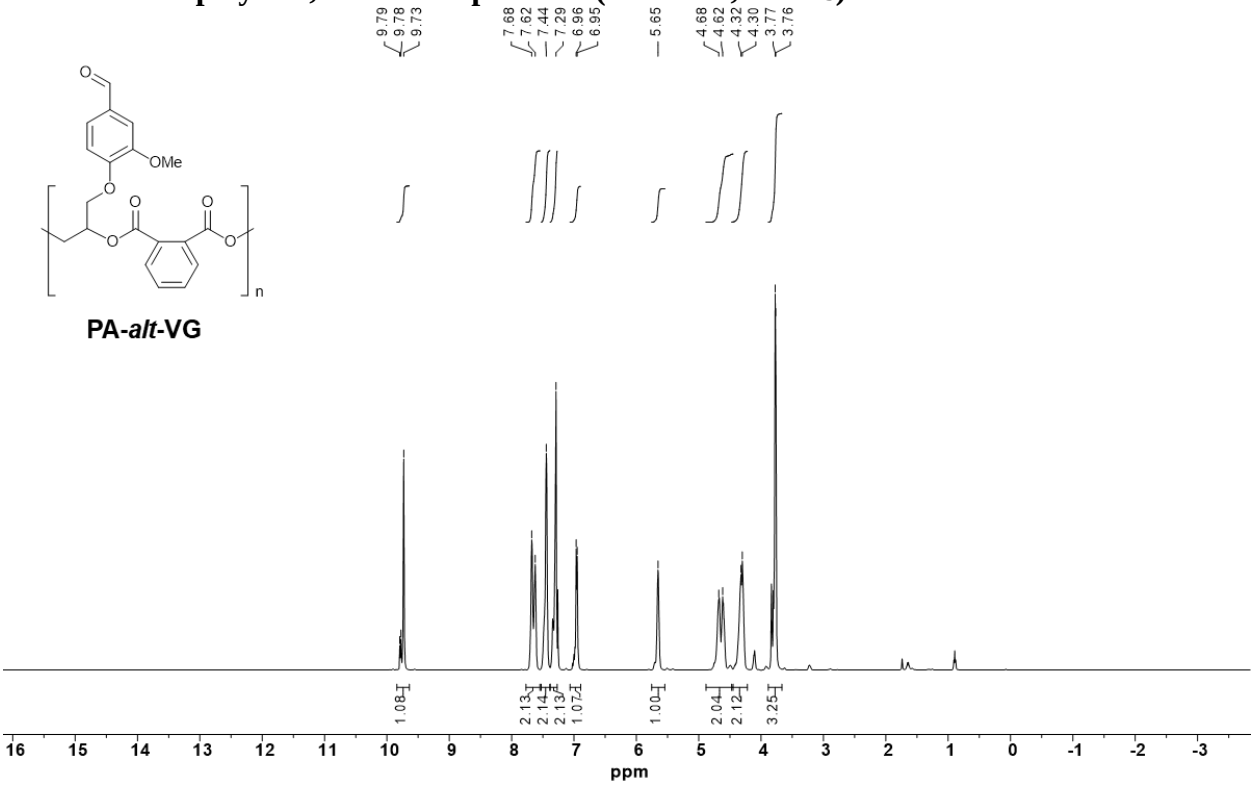

PA-*alt*-VG Copolymer, ^{13}C NMR Spectrum (125 MHz, $CDCl_3$)

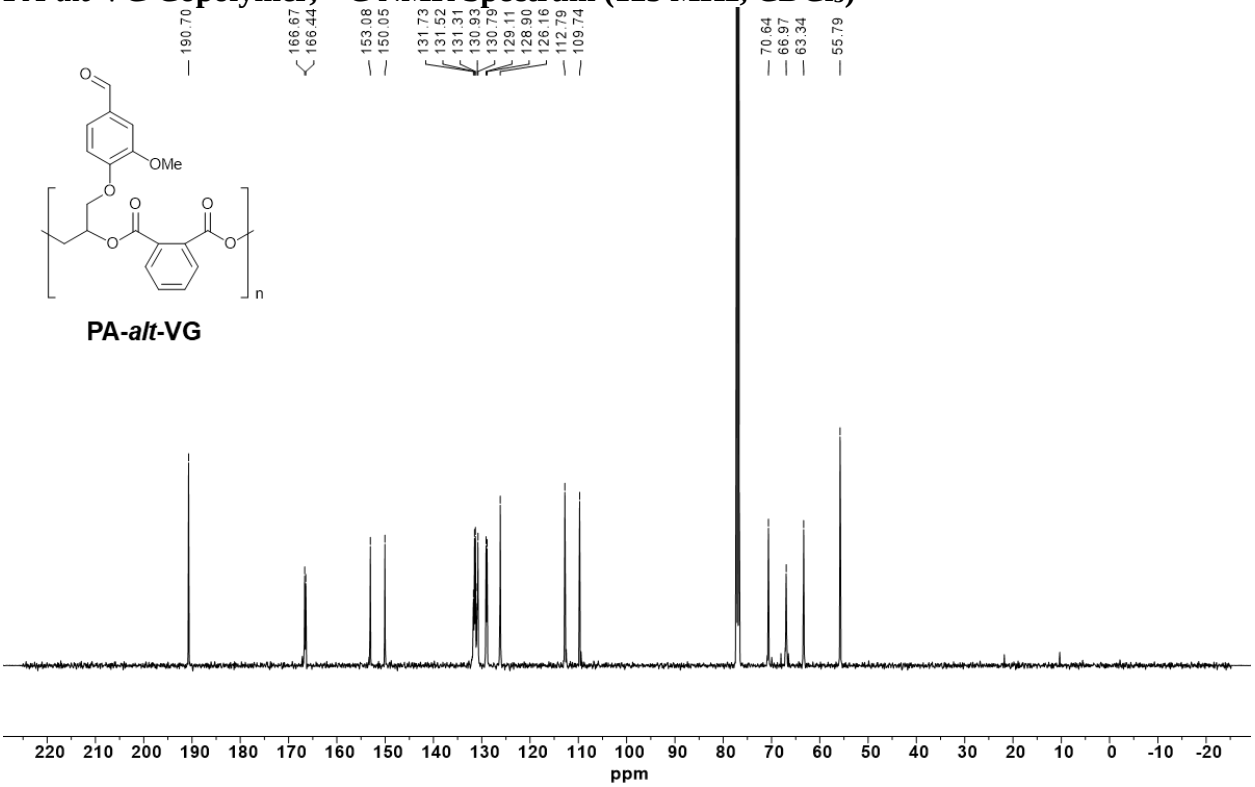

PA-*alt*-GG Copolymer

In a glovebox, catalyst (4.1 mg, 0.0038 mmol, 1 equiv) was weighed into an oven-dried 4 mL vial equipped with an oven-dried Teflon-coated stir bar. **PA** (0.225 g, 1.52 mmol, 400 equiv) was then weighed into the vial followed by **GG** (0.274 g, 1.52 mmol, 400 equiv). Dry, degassed THF (4 mL) was added to fully dissolve the phthalic anhydride. The vial was sealed with a Teflon-lined cap, removed from the glovebox, and placed in an oil bath preheated to 60 °C for 3 days. After cooling to room temperature, the polymer was precipitated into MeOH (15 mL) and dried in vacuo at 22 °C for 16 h to afford a glassy, pale yellow solid. **^{1}H NMR** (500 MHz, $CDCl_3$): δ 7.65 (d, 2H), 7.44 (m, 2H), 6.87 (m, 2H), 5.65 (s, 1H), 4.68 (m, 2H), 4.25 (m, 2H), 3.73 (m, 3H) ppm. **^{13}C NMR** (125 MHz, $CDCl_3$): δ 166.73, 166.51, 150.05, 147.96, 131.95, 131.30, 131.12, 129.09, 128.92, 122.29, 120.90, 115.42, 112.39, 71.12, 67.60, 63.69, 55.79 ppm. **GPC**: M_n = 8.3, $Đ$ = 1.16. **DSC**: T_g = 40 °C.

PA-*alt*-GG Copolymer, ^{1}H NMR Spectrum (500 MHz, $CDCl_3$)

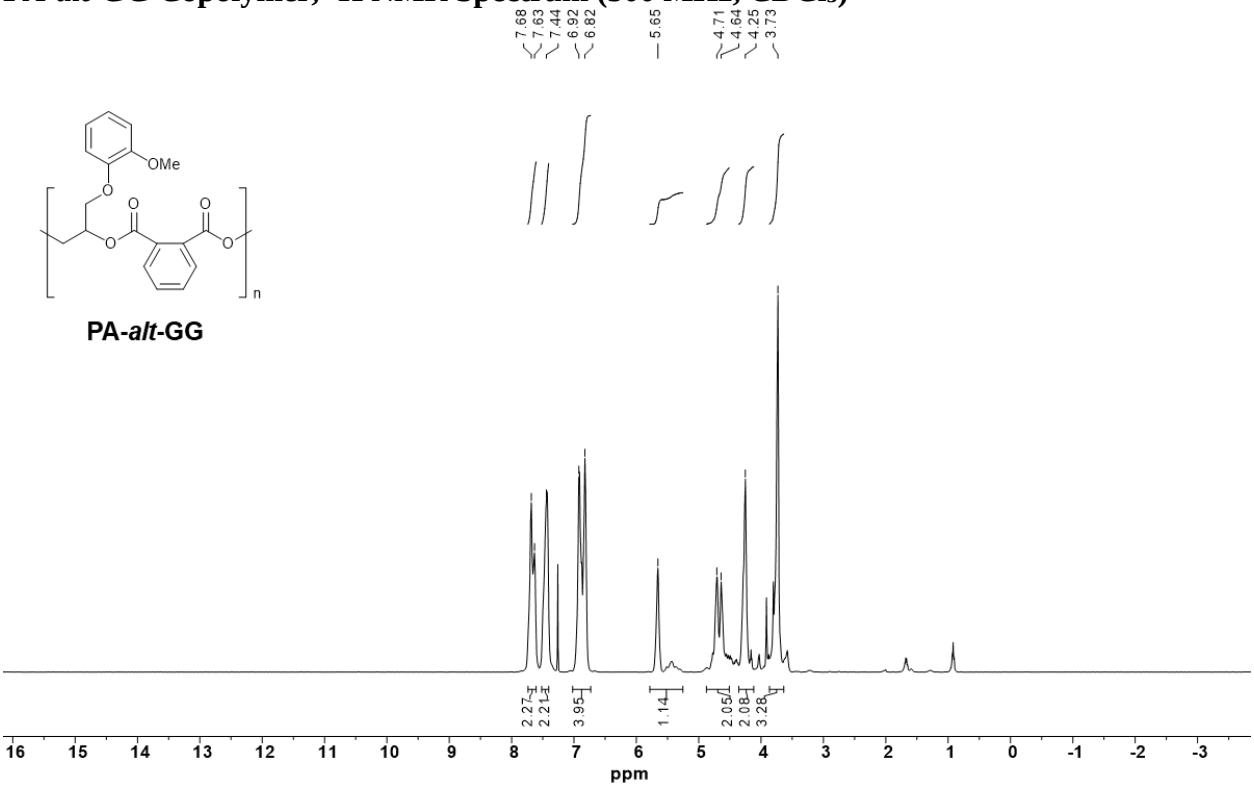

PA-*alt*-GG Copolymer, ^{13}C NMR Spectrum (125 MHz, $CDCl_3$)

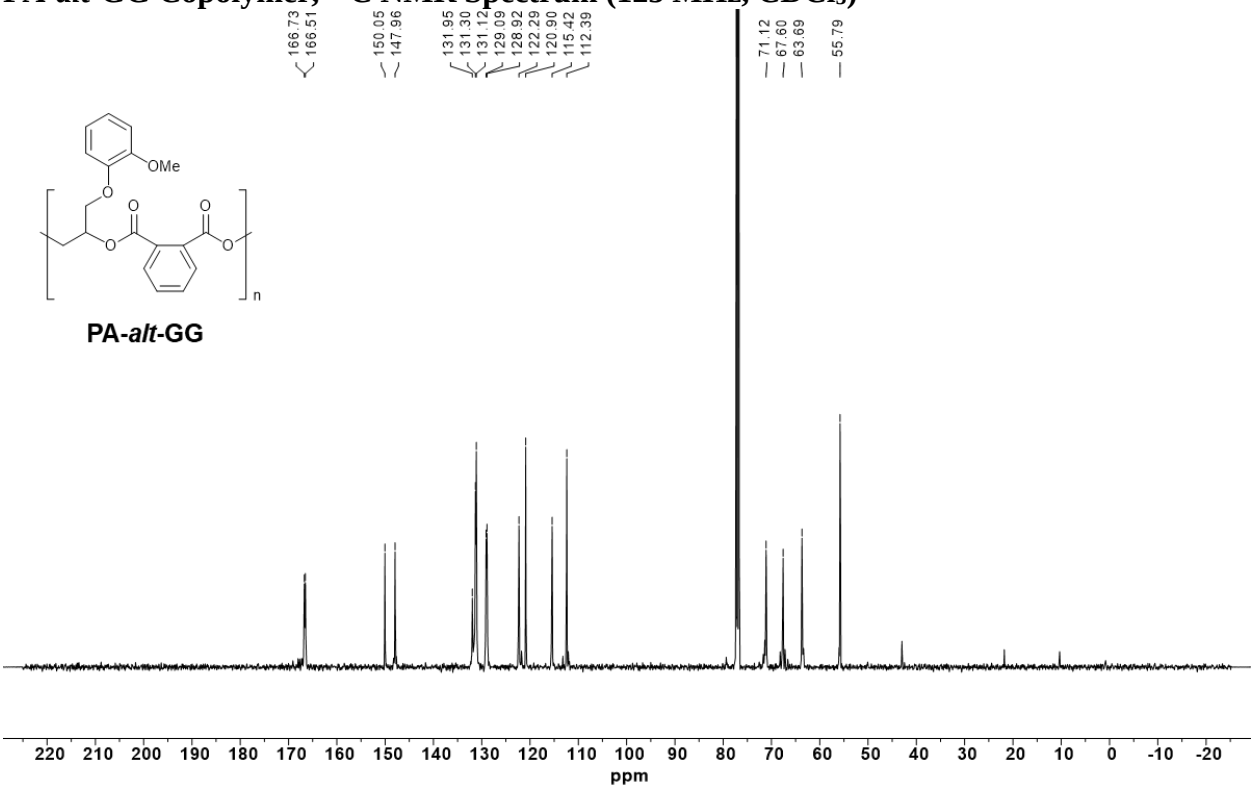

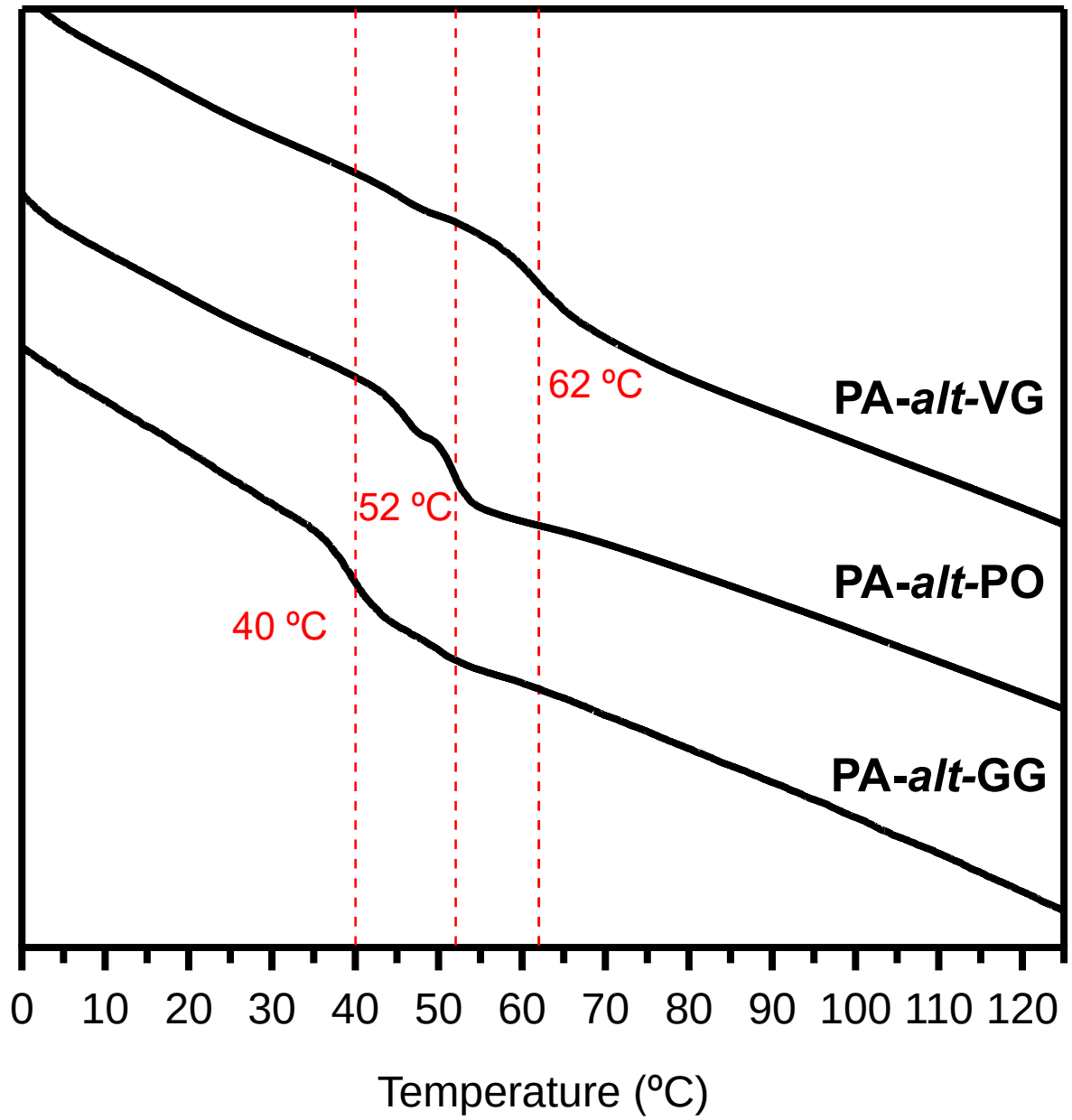

Figure S5. DSC traces from the second heating ramp for **PA-*alt*-VG**, **PA-*alt*-PO**, and **PA-*alt*-GG**.

Table S2. Properties of polyester copolymers.

Copolymer	$T_{g,\,DSC}$ (°C)	M_n (g/mol) [a]	$Đ$ [a]
PA-*alt*-PO	52	31.7	1.09
PA-*alt*-VG	62	3.9	1.13
PA-*alt*-GG	40	8.3	1.16

[a] Determined by GPC in THF, calibrated with polystyrene standards.

3.7. Imination vs. Amidation Control Reactions

To confirm that reaction of the diamine cross-linker occurred preferentially at the pendant aldehydes rather than the polyester backbone, **PA-*alt*-PO** and **pre-PO$_{62\%}$-*grad*** linear polyesters were reacted with *n*-hexylamine (0.38 equiv relative to **PA**) in THF (0.5 M relative to *n*-hexylamine) and subjected to the network curing conditions (*vide supra*). ^{1}H and ^{13}C NMR analysis of the **PA-*alt*-PO** and *n*-hexylamine reaction product showed no evidence of amide formation and was in good agreement with the spectra of the **PA-*alt*-PO** copolymer (Figure S6 and Figure S7). GPC analysis of the reaction products showed a small degree of low molecular weight tailing, consistent with a small amount of cleavage of the polyester backbone via amidation (Figure S8). In the presence of aldehyde, however, imination is strongly favored over amidation. The ^{1}H and ^{13}C NMR analysis of the **pre-PO$_{62\%}$-*grad*** and *n*-hexylamine reaction mixture revealed conversion of the pendant aldehydes to imines but exhibited no evidence of amide formation (Figure S9 and Figure S10). Moreover, the GPC trace of **pre-PO$_{62\%}$-*grad*** after treatment with *n*-hexylamine revealed that the molecular weight and dispersity were largely unchanged (Figure S11).

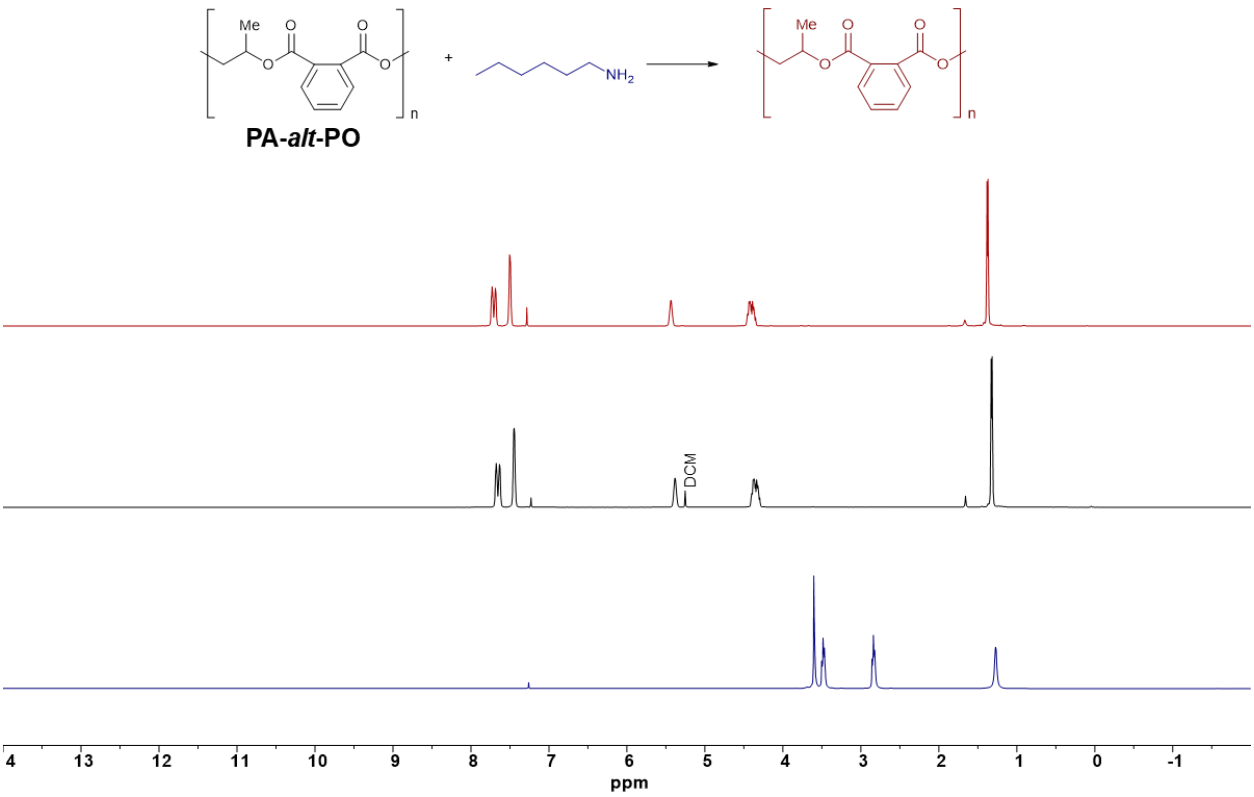

Figure S6. ^{1}H NMR spectra of *n*-hexylamine (bottom, blue), **PA-*alt*-PO** (middle, black), and their reaction product (top, red) showing no evidence of amidation.

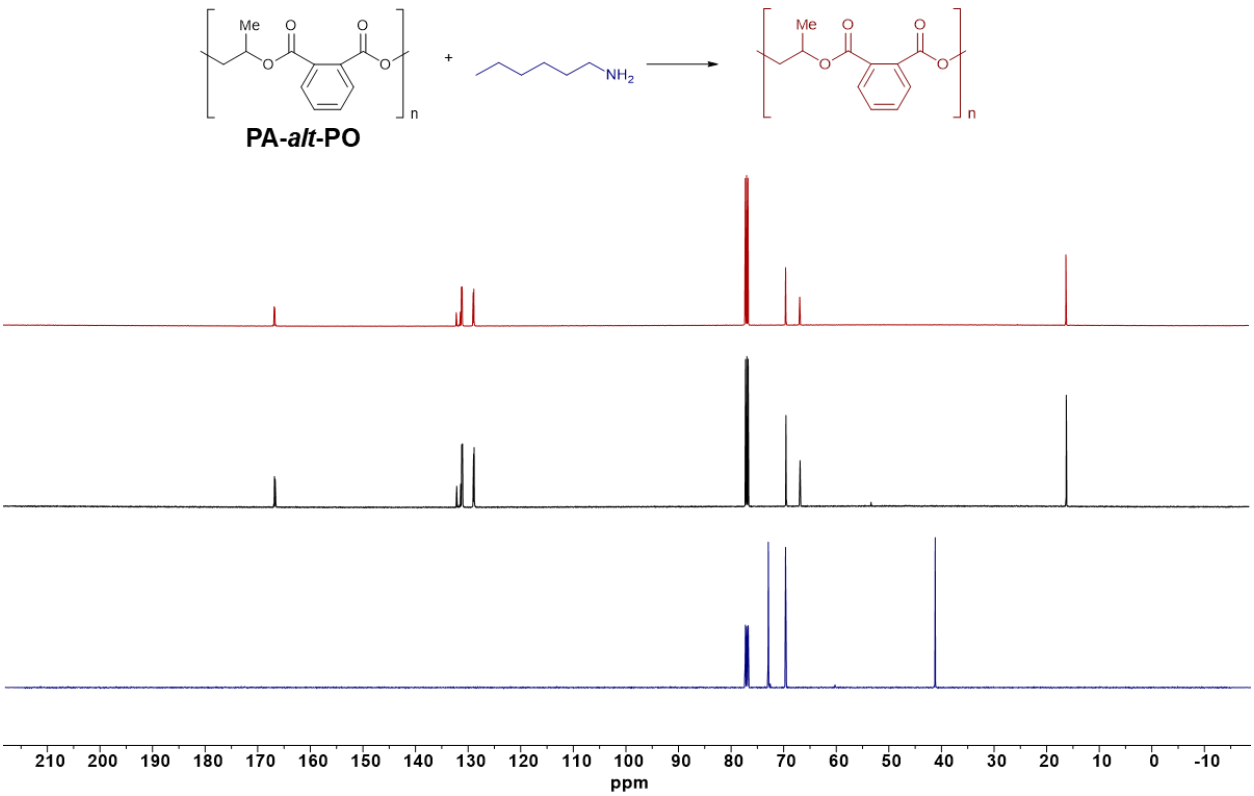

Figure S7. ^{13}C NMR spectra of *n*-hexylamine (bottom, blue), **PA-*alt*-PO** (middle, black), and their reaction product (top, red) showing no evidence of amidation.

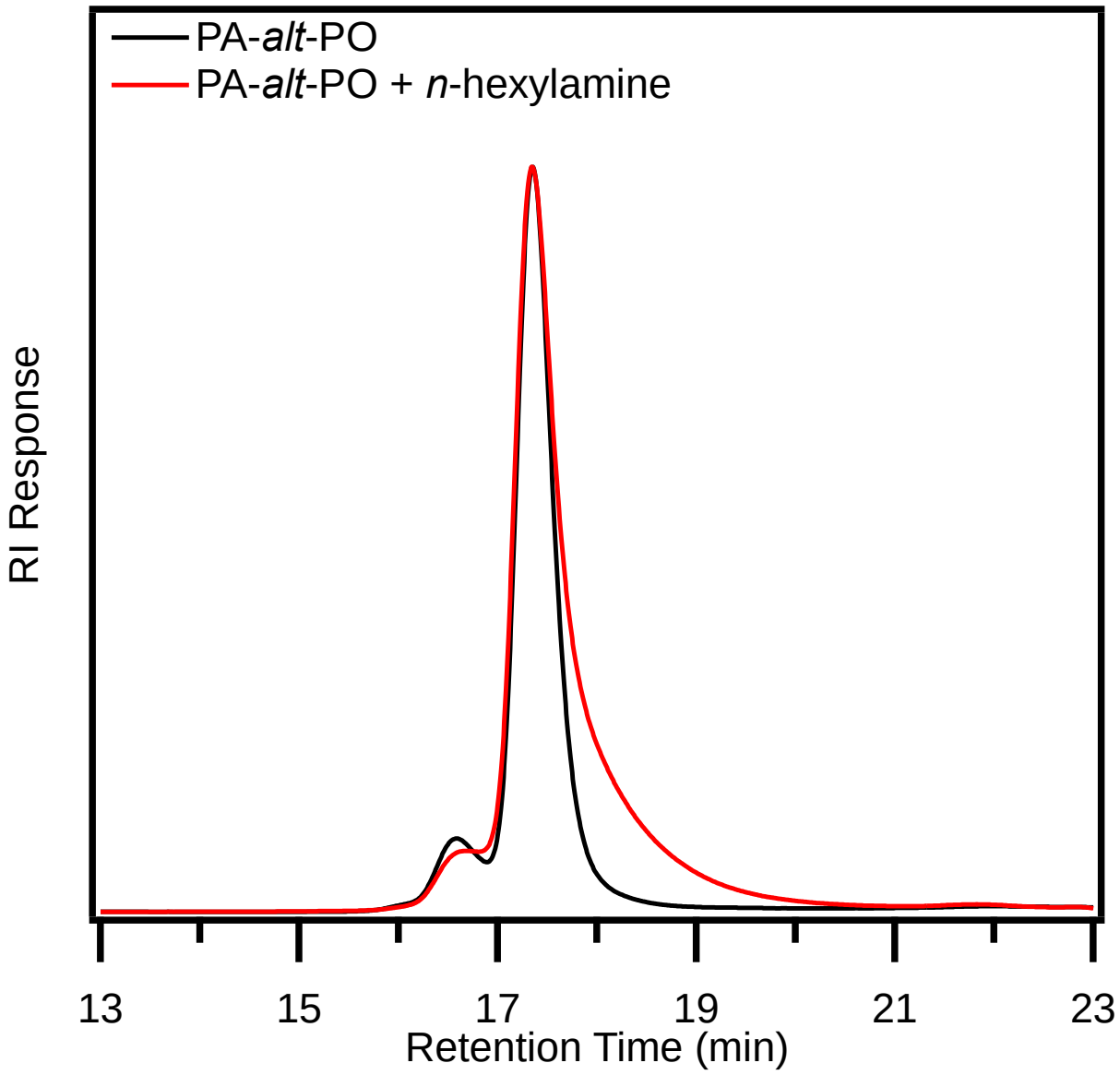

Figure S8. GPC traces of **PA-*alt*-PO** copolymer before (black) and after (red) reaction with *n*-hexylamine.

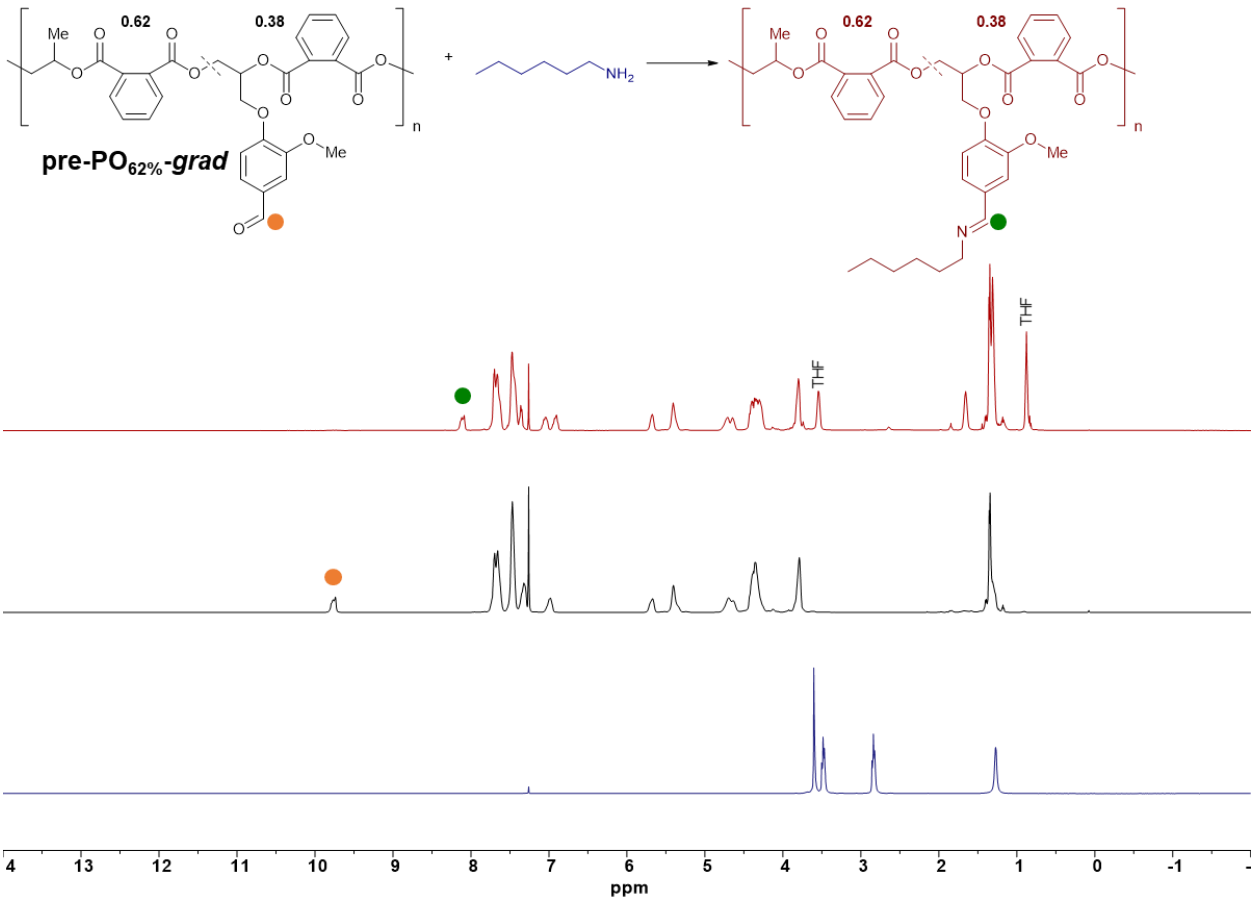

Figure S9. ^{1}H NMR spectra of *n*-hexylamine (bottom, blue), **pre-PO$_{62\%}$-*grad*** (middle, black), and their reaction product (top, red) showing full conversion of aldehyde to imine and no evidence of amidation.

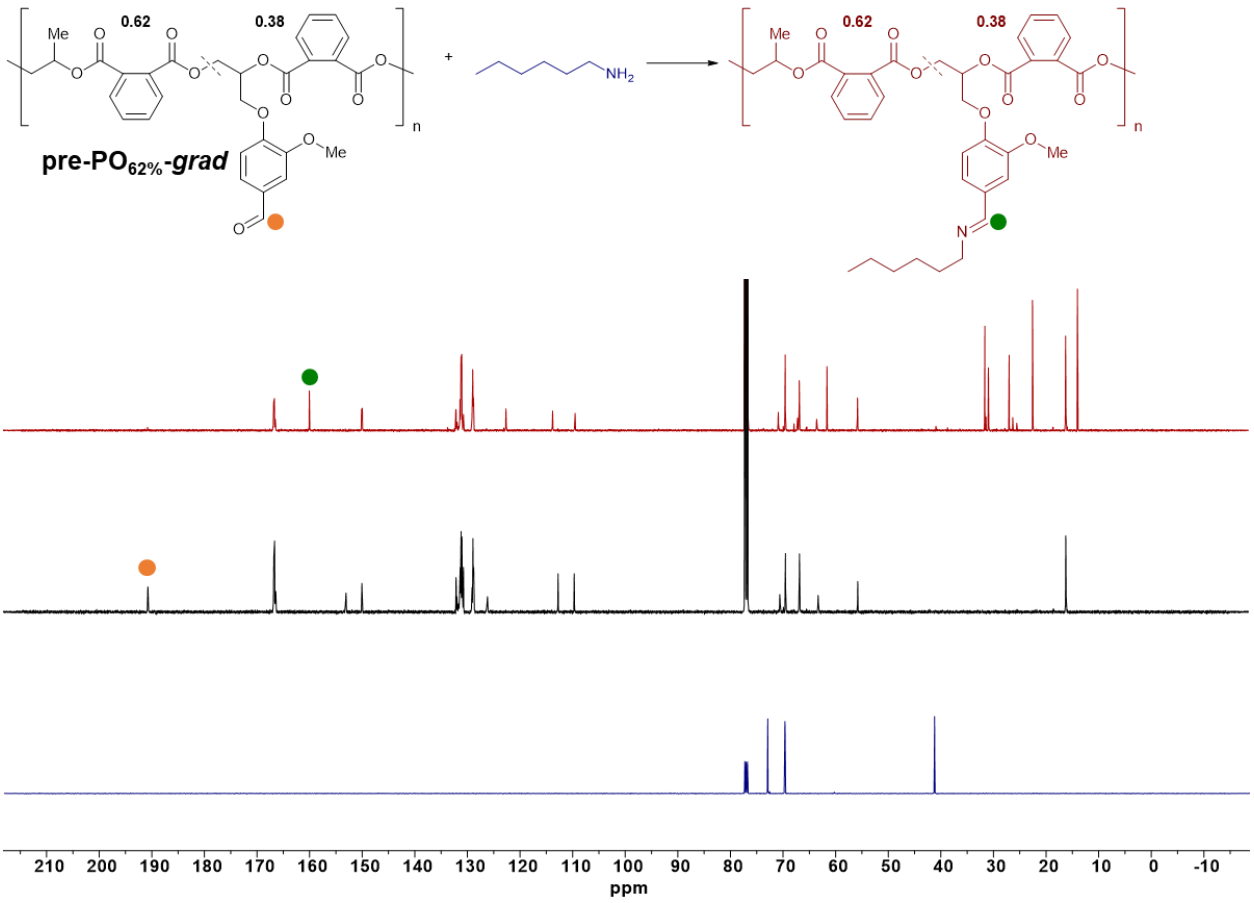

Figure S10. ^{13}C NMR spectra of *n*-hexylamine (bottom, blue), **pre-PO$_{62\%}$-*grad*** (middle, black), and their reaction product (top, red) showing full conversion of aldehyde to imine and no evidence of amidation.

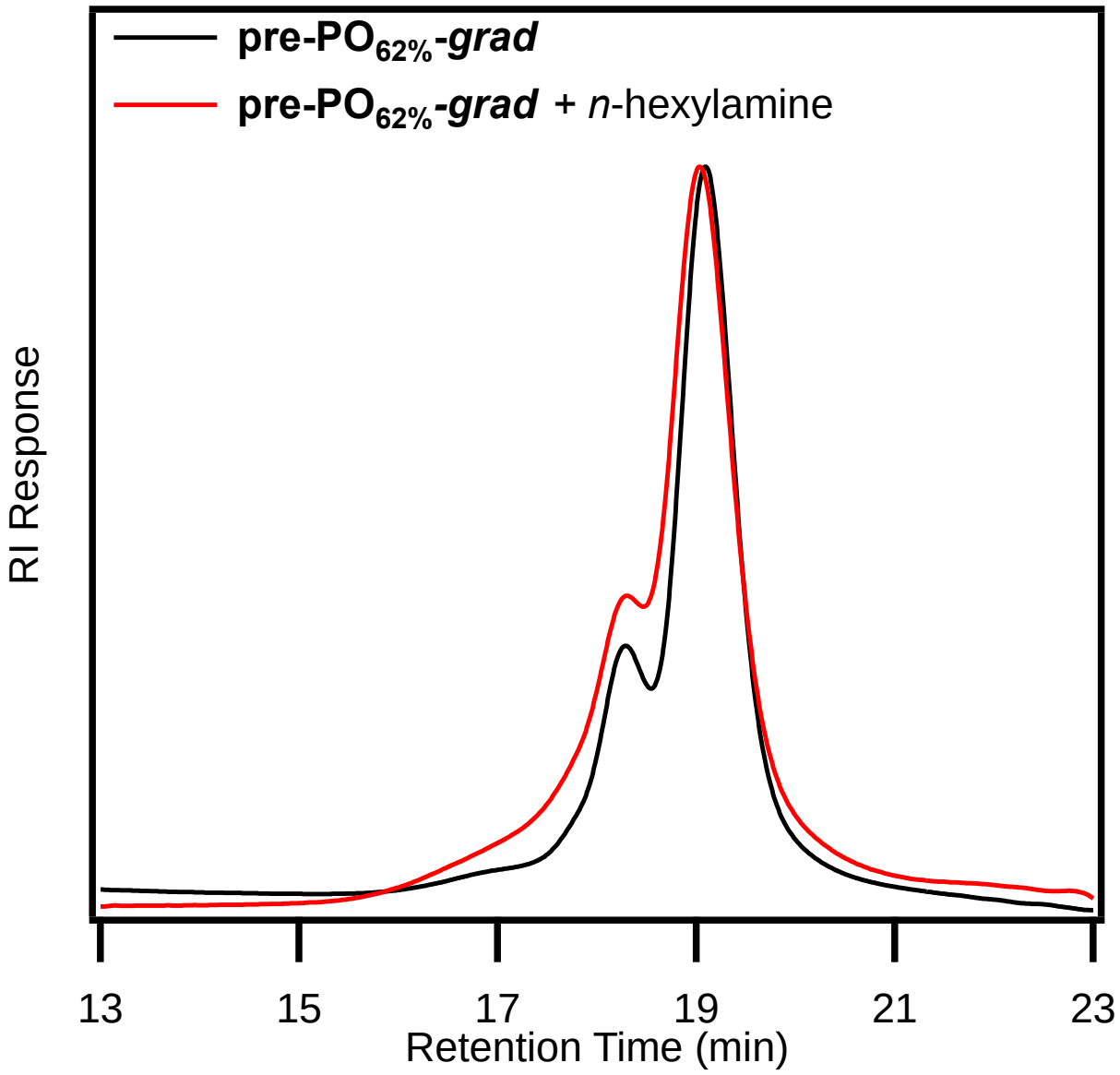

Figure S11. GPC traces of **pre-PO$_{62\%}$-*grad*** pre-polymer before (black) and after (red) reaction with *n*-hexylamine.

3.8. Reprocessing Procedure

Samples were ground to a ~1 mm particulate size using a Kitchenaid© BCG11ER Blade Coffee Grinder. Then, ~0.15 g of ground sample was loaded into a custom 0.5 mm thick dogbone-shaped aluminum mold (Figure S4). The mold was sandwiched between two aluminum plates (~2 mm thick) that were covered with Durafilm. The assembly was then placed in a Wabash-MPI

compression mold (Wabash, IN) or Carver hot press, preheated to the desired temperature (90 or 100 °C), and allowed to thermally equilibrate for 5 min. The pressure was rapidly increased to 1 metric ton and released repetitively ~10× to remove air bubbles. Then, a constant pressure of 1 or 3 metric tons was applied to the sample for a designated period of time, after which the pressure was released. The sample was rapidly cooled to 22 °C over five min by water cooling the hot press. The resulting tensile bars were then removed from the mold, trimmed, and sanded to smooth the edges before characterization.

4. Tabulated Polymer Properties

4.1. Pre-Polymers

Table S3. Pre-polymer properties.

Pre-Polymer	M_n (kg/mol) [a]	$Đ$ [a]	$T_{g,\,DSC}$ (°C)	Avg. Aldehydes per Chain [b]
pre-PO$_{62}$-*grad*	6.0	1.38	47	8–9
pre-PO$_{42}$-*grad*	3.8	1.12	52	7–8
pre-PO$_{23}$-*grad*	3.1	1.23	58	7–8
pre-PO$_{35}$-*stat*	5.1	1.13	71	10–11
pre-GG$_{43}$-*stat*	3.7	1.41	61	6–7

[a] Determined by GPC in THF, calibrated with polystyrene standards. [b] Calculated by dividing M_n by the molecular weight of an average repeat unit.

Table S4. Aliquots from pre-polymer syntheses illustrating relative incorporation of epoxide comonomers throughout reaction progress.

Pre-Polymer [a]	% conv. [b]	**VG:PO** [c]
pre-PO$_{62}$-*grad*	65	59:41
	100	38:62
pre-PO$_{42}$-*grad*	44	71:29
	77	66:34
	92	60:40
	100	58:42
pre-PO$_{23}$-*grad*	74	95:5
	79	91:9
	100	77:23
pre-PO$_{35}$-*stat*	30	72:28
	49	70:30
	63	68:32
	73	67:33
	80	66:34
	100	65:35

[a] The first aliquot taken during the synthesis of **pre-GG$_{43\%}$-*stat*** revealed full consumption of monomer. [b] Determined by ^{1}H NMR spectroscopy. [c] Determined by relative integrations of methine protons.

4.2. Pristine Networks

Table S5. Properties of pristine cross-linked networks.

Network	Gel %	ρ (g/mL)	$T_{d,\,5\%}$ (°C)	$T_{g,\,DSC}$ (°C)	$T_{g,\,DMTA}$ (°C)	G' (GPa)[a]	ν_e [b]	$M_{x,eff}$ [b] (g/mol)	T_v [c] (°C)
PO$_{62\%}$-*grad*	76	1.23	318	64	65	4.48	1.48	276	N.D.
PO$_{42\%}$-*grad*	99	1.25	306	67	76	6.21	1.06	202	N.D.
PO$_{23\%}$-*grad*	94	1.27	315	69	85	8.38	2.70	157	N.D.
PO$_{35\%}$-*stat*	99	1.31	319	57	61	9.52	3.07	140	N.D.
GG$_{43\%}$-*stat*	99	1.29	321	62	64	9.07	2.92	149	–22

[a] Determined at 90 °C (**PO$_{62\%}$-*grad*** and **PO$_{42\%}$-*grad***) or 100 °C (**PO$_{23\%}$-*grad***, **PO$_{35\%}$-*stat***, and **GG$_{43\%}$-*stat***). [b] Calculated using Equation S1. [c] Calculated using Equation S2. N.D. = not determined.

4.3. Reprocessed Networks

Table S6. Properties of cross-linked polymer network **PO$_{62\%}$-*grad***.

Cycle	$T_{g,\,DSC}$ (°C)	$T_{g,\,DMTA}$ (°C)	G' (GPa)[a]	$M_{x,eff}$ (g/mol)[b]	σ (MPa)	ε (%)	E (GPa)[c]
Pristine	64	65	4.48	276	60.3 ± 4.3	3.65 ± 0.48	2.09 ± 0.10
Reprocess 1	65	63	4.67	265	44.3 ± 6.9	2.12 ± 0.35	2.28 ± 0.11
Reprocess 2	65	61	4.62	268	57.4 ± 5.1	3.07 ± 0.38	2.15 ± 0.15
Reprocess 3	64	72	4.58	270	60.1 ± 3.6	3.04 ± 0.45	2.36 ± 0.14

[a] Determined at 90 °C. [b] Calculated using Equation S1. [c] Calculated using the slope of the stress-strain curve from 0 to 0.1% strain.

Table S7. Properties of cross-linked polymer network **PO$_{42\%}$-*grad***.

Cycle	$T_{g,\,DSC}$ (°C)	$T_{g,\,DMTA}$ (°C)	G' (GPa)[a]	$M_{x,eff}$ (g/mol)[b]	σ (MPa)	ε (%)	E (GPa)[c]
Pristine	67	76	6.21	202	77.1 ± 3.7	5.74 ± 0.94	2.08 ± 0.14
Reprocess 1	67	77	5.62	224	46.7 ± 4.8	2.32 ± 0.48	2.30 ± 0.05
Reprocess 2	64	76	6.96	181	53.4 ± 3.5	2.63 ± 0.25	2.28 ± 0.08
Reprocess 3	69	76	7.52	267	75.3 ± 3.8	4.20 ± 0.43	2.75 ± 0.12

[a] Determined at 90 °C. [b] Calculated using Equation S1. [c] Calculated using the slope of the stress-strain curve from 0 to 0.1% strain.

Table S8. Properties of cross-linked polymer network **PO$_{23\%}$-*grad***.

Cycle	$T_{g,\,DSC}$ (°C)	$T_{g,\,DMTA}$ (°C)	G' (GPa)[a]	$M_{x,eff}$ (g/mol)[b]	σ (MPa)	ε (%)	E (GPa)[c]
Pristine	69	85	8.38	157	68.3 ± 3.9	4.50 ± 0.29	2.16 ± 0.10
Reprocess 1	70	75	7.85	167	30.1 ± 6.3	2.06 ± 0.66	1.62 ± 0.33
Reprocess 2	68	70	7.77	169	57.8 ± 7.4	3.19 ± 0.62	2.17 ± 0.11
Reprocess 3	71	75	8.65	152	62.6 ± 6.2	3.65 ± 0.90	2.22 ± 0.09

[a] Determined at 100 °C. [b] Calculated using Equation S1. [c] Calculated using the slope of the stress-strain curve from 0 to 0.1% strain.

Table S9. Properties of cross-linked polymer network **PO$_{35\%}$-*stat***.

Cycle	$T_{g,\,DSC}$ (°C)	$T_{g,\,DMTA}$ (°C)	G' (GPa)[a]	$M_{x,eff}$ (g/mol)[b]	σ (MPa)	ε (%)	E (GPa)[c]
Pristine	57	61	9.52	140	60.6 ± 1.5	4.50 ± 0.36	2.20 ± 0.08
Reprocess 1	57	63	8.26	161	31.3 ± 12.3	1.94 ± 0.78	2.09 ± 0.11
Reprocess 2	61	63	9.05	147	39.4 ± 4.5	3.39 ± 1.01	2.09 ± 0.17
Reprocess 3	58	63	8.69	153	65.3 ± 5.1	4.55 ± 0.77	2.31 ± 0.06

[a] Determined at 100 °C. [b] Calculated using Equation S1. [c] Calculated using the slope of the stress-strain curve from 0 to 0.1% strain.

Table S10. Properties of cross-linked polymer network **GG$_{43\%}$-*stat***.

Cycle	$T_{g,\,DSC}$ (°C)	$T_{g,\,DMTA}$ (°C)	G' (GPa)[a]	$M_{x,eff}$ (g/mol)[b]	σ (MPa)	ε (%)	E (GPa)[c]
Pristine	62	64	9.07	149	65.2 ± 7.3	4.49 ± 0.56	1.99 ± 0.17
Reprocess 1	64	71	8.80	154	52.8 ± 6.7	3.22 ± 0.73	2.06 ± 0.07
Reprocess 2	64	66	6.94	195	57.0 ± 5.2	2.83 ± 0.37	2.33 ± 0.06
Reprocess 3	63	68	8.18	166	59.7± 6.2	3.40 ± 0.69	2.28 ± 0.03

[a] Determined at 100 °C. [b] Calculated using Equation S1. [c] Calculated using the slope of the stress-strain curve from 0 to 0.1% strain.

Table S11. Values of τ* measured in triplicate at each temperature by stress relaxation analysis for a single sample of **GG$_{43\%}$-*stat***.

T (°C)	85	90	95	100	105	110	115	120	125	130
Run 1	7.50	7.89	6.97	5.92	4.78	3.47	2.56	2.00	1.71	1.45
Run 2	7.10	8.28	6.84	6.05	4.64	3.66	2.68	2.14	1.81	1.68
Run 3	7.89	8.28	7.36	5.93	4.90	3.72	2.61	2.11	1.84	1.58
Average	7.50	8.15	7.06	5.97	4.77	3.62	2.62	2.08	1.84	1.57
St. Dev.	0.4	0.26	0.27	0.07	3.62	0.13	0.06	0.07	0.15	0.12

5. Images and Graphical Data

5.1. Images of Pristine and Reprocessed Networks

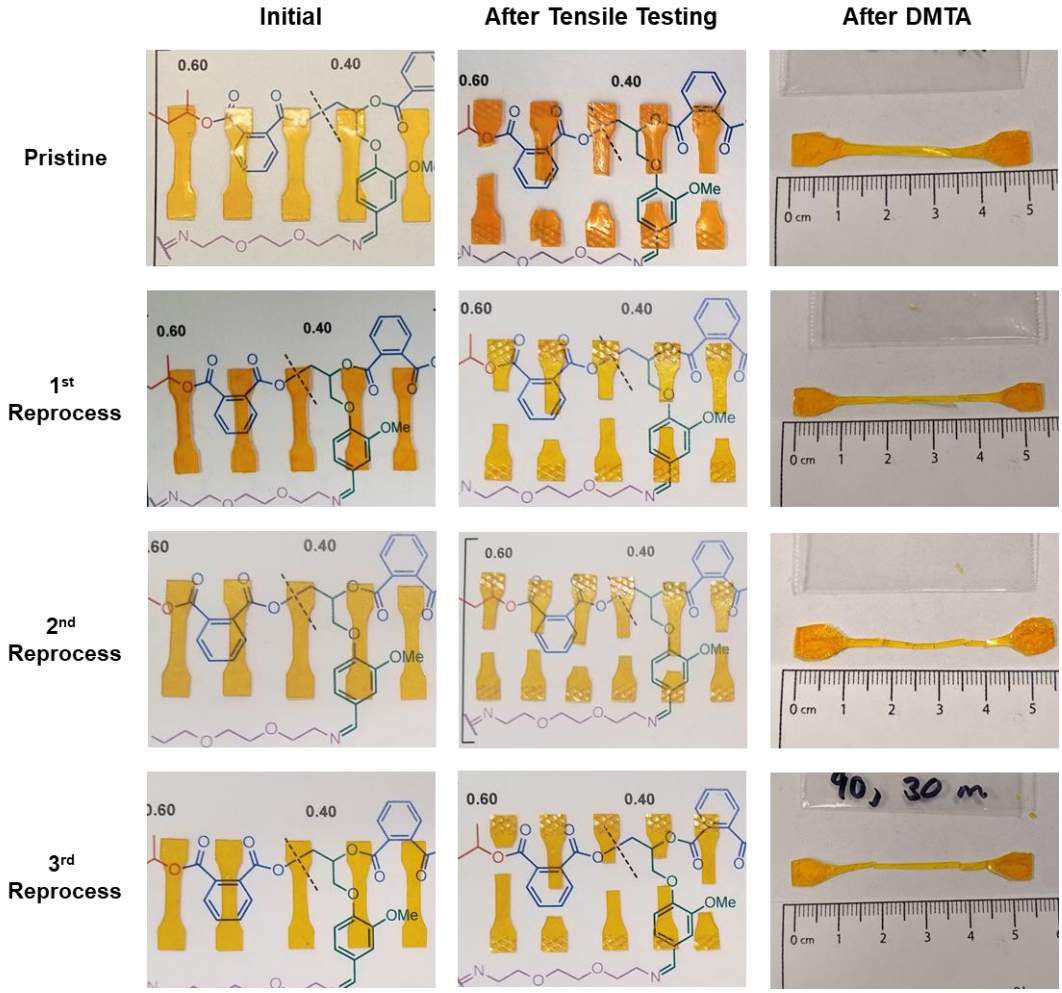

Figure S12. Images of **PO$_{62\%}$-*grad*** network before and after three reprocessing cycles (left), after tensile testing (middle), and after DMTA (right).

Figure S13. Images of ground and reprocessed **PO$_{62\%}$-*grad*** network in the dogbone mold.

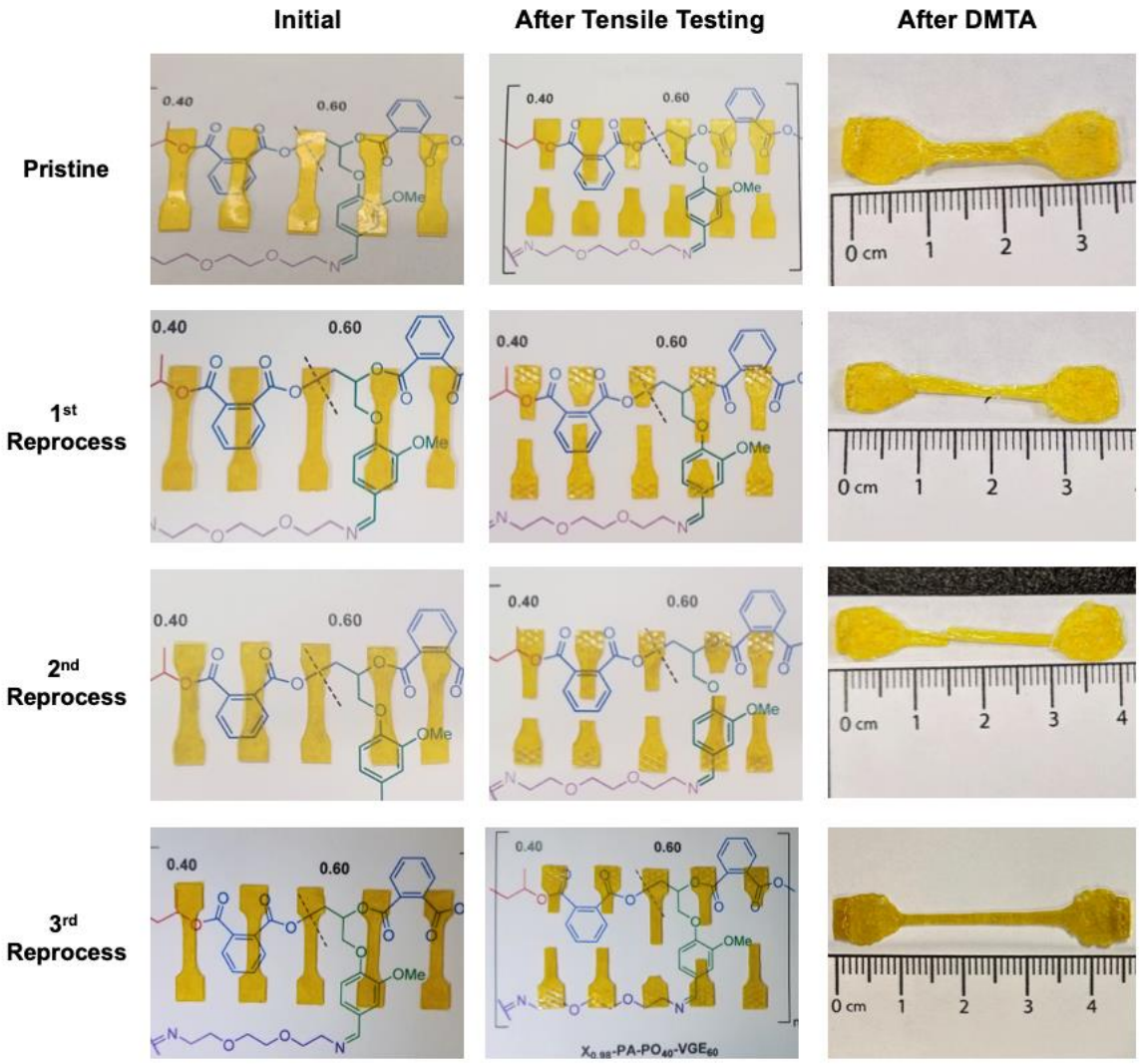

Figure S14. Images of **PO$_{42\%}$-*grad*** network before and after three reprocessing cycles (left), after tensile testing (middle), and after DMTA (right)

Figure S15. Images of ground and reprocessed **PO$_{42\%}$-*grad*** network in the dogbone mold.

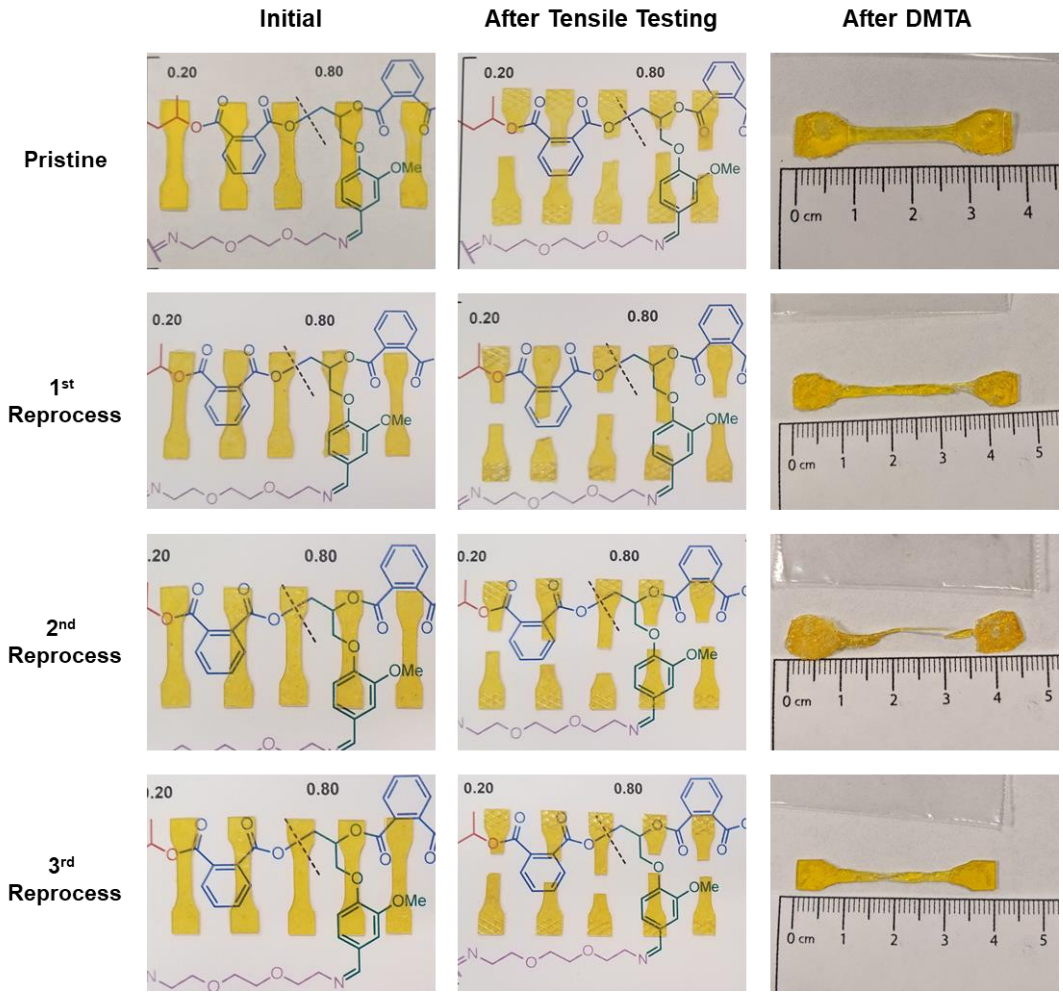

Figure S16. Images of **PO$_{23\%}$-*grad*** network before and after three reprocessing cycles (left), after tensile testing (middle), and after DMTA (right)

Figure S17. Image of ground **PO$_{23\%}$-*grad*** network in the dogbone mold. Unintentionally, no image was taken directly after reprocessing.

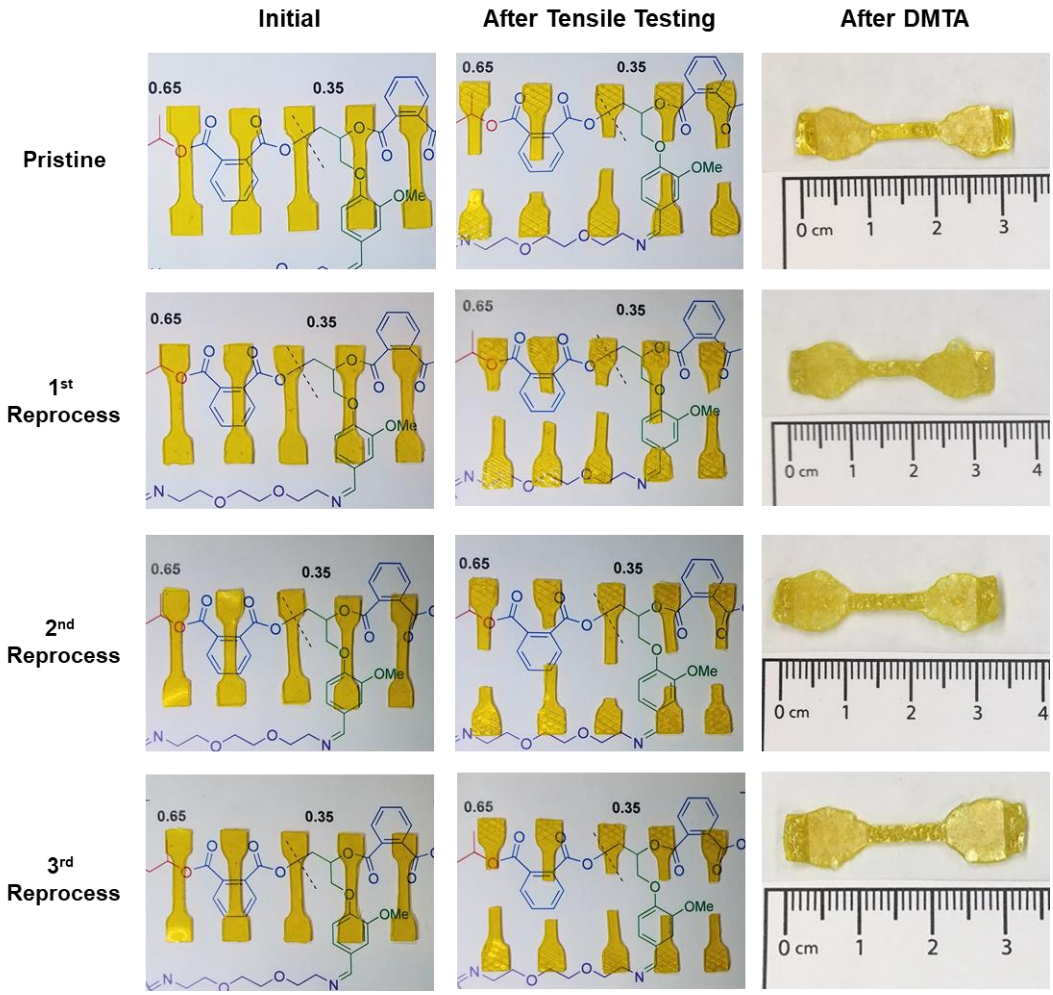

Figure S18. Images of **PO$_{35\%}$-*stat*** network before and after three reprocessing cycles (left), after tensile testing (middle), and after DMTA (right).

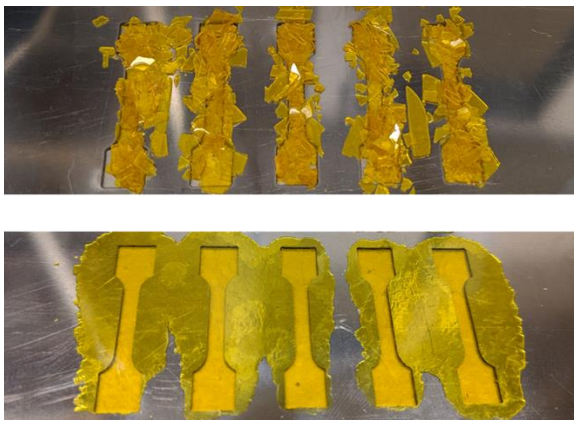

Figure S19. Images of ground and reprocessed **PO$_{35\%}$-*stat*** network in the dogbone mold.

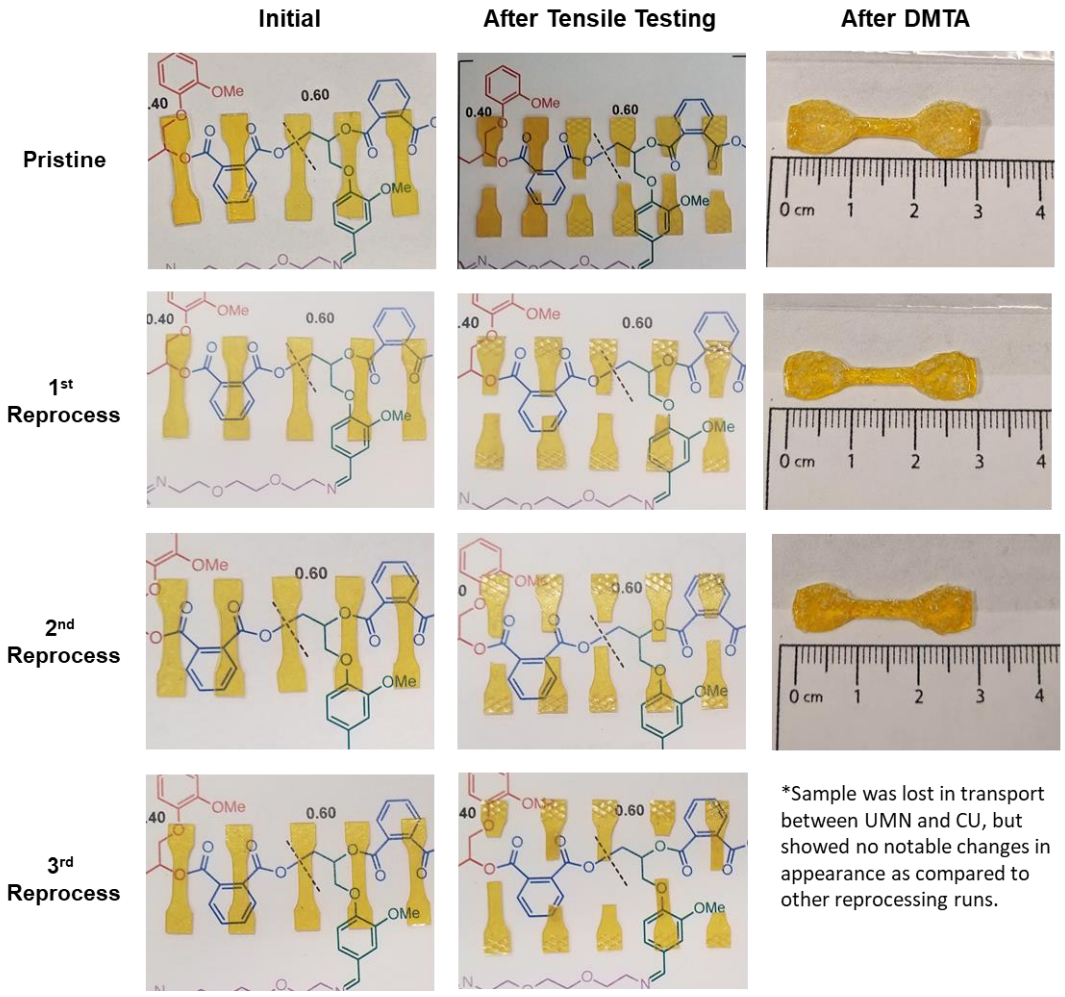

Figure S20. Images of **GG$_{43\%}$-*stat*** network before and after three reprocessing cycles (left), after tensile testing (middle), and after DMTA (right).

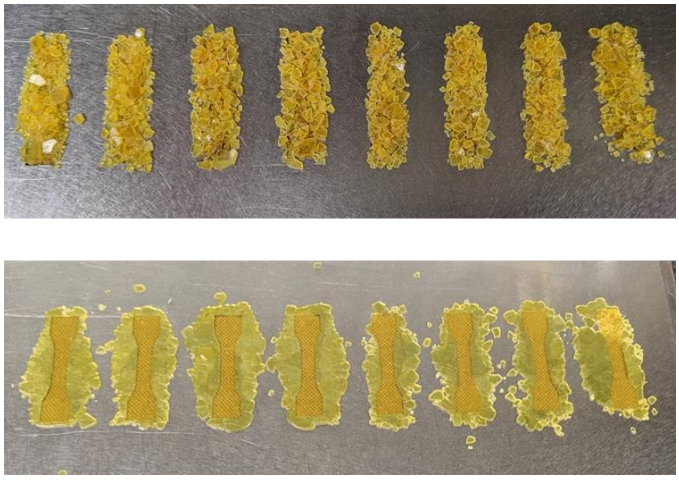

Figure S21. Images of ground and reprocessed **GG$_{43\%}$-*stat*** network in the dogbone mold.

5.2. Dynamic Mechanical Thermal Analysis

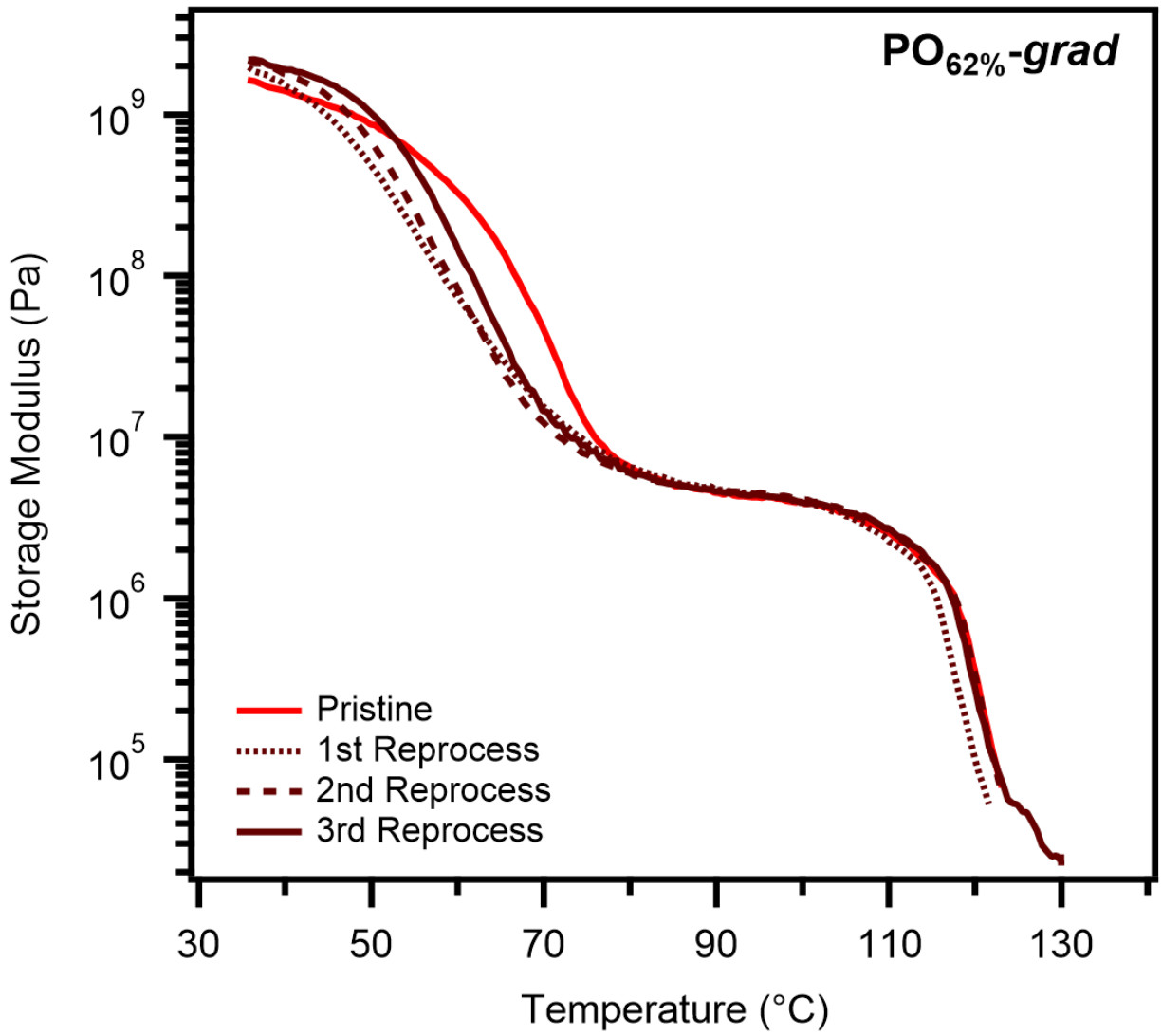

Figure S22. DMTA of **PO$_{62\%}$-*grad*** network before and after each of three reprocessing cycles.

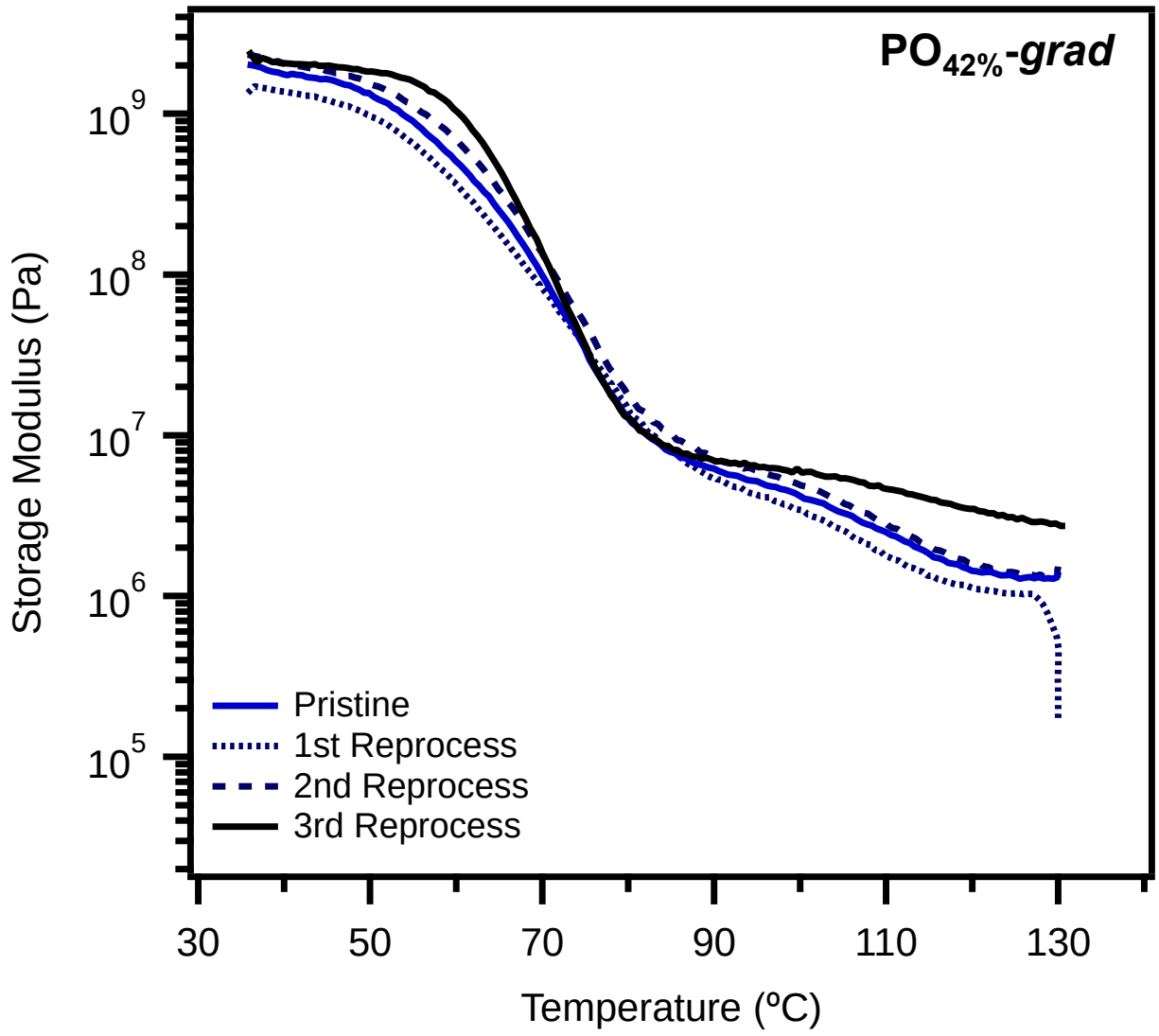

Figure S23. DMTA of **PO$_{42\%}$-*grad*** network before and after each of three reprocessing cycles.

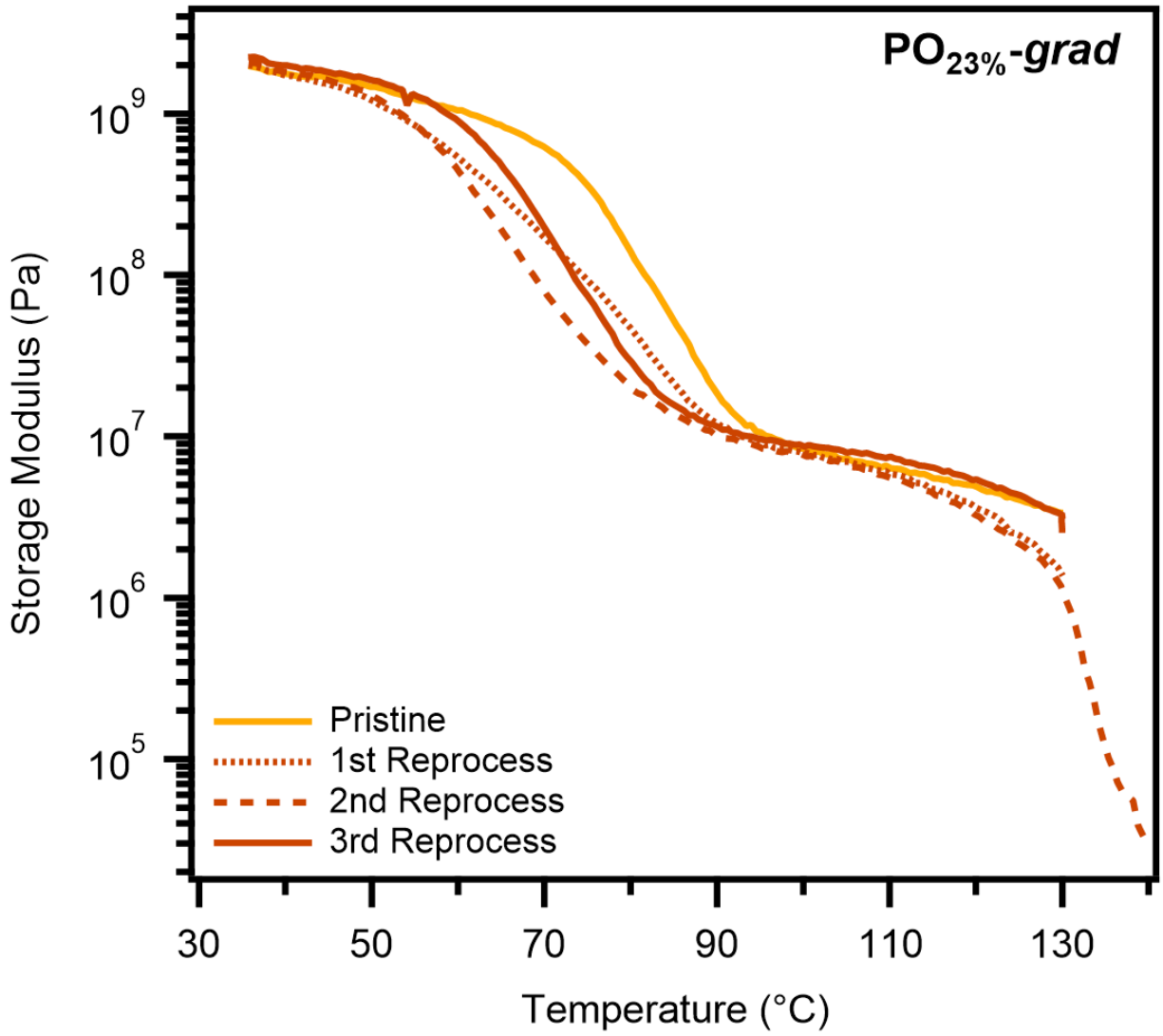

Figure S24. DMTA of **PO$_{23\%}$-*grad*** network before and after each of three reprocessing cycles.

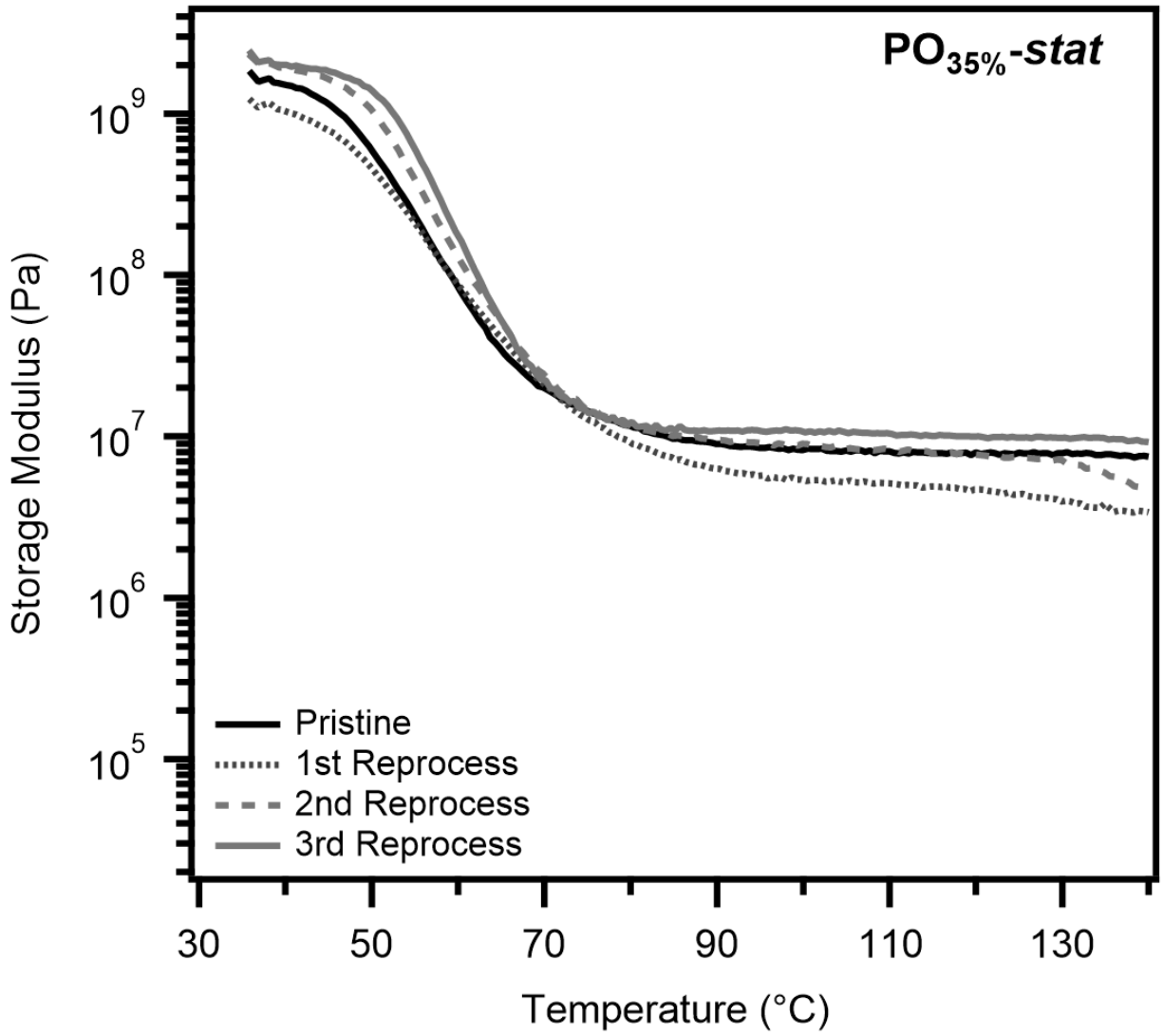

Figure S25. DMTA of **PO$_{35\%}$-*stat*** network before and after each of three reprocessing cycles.

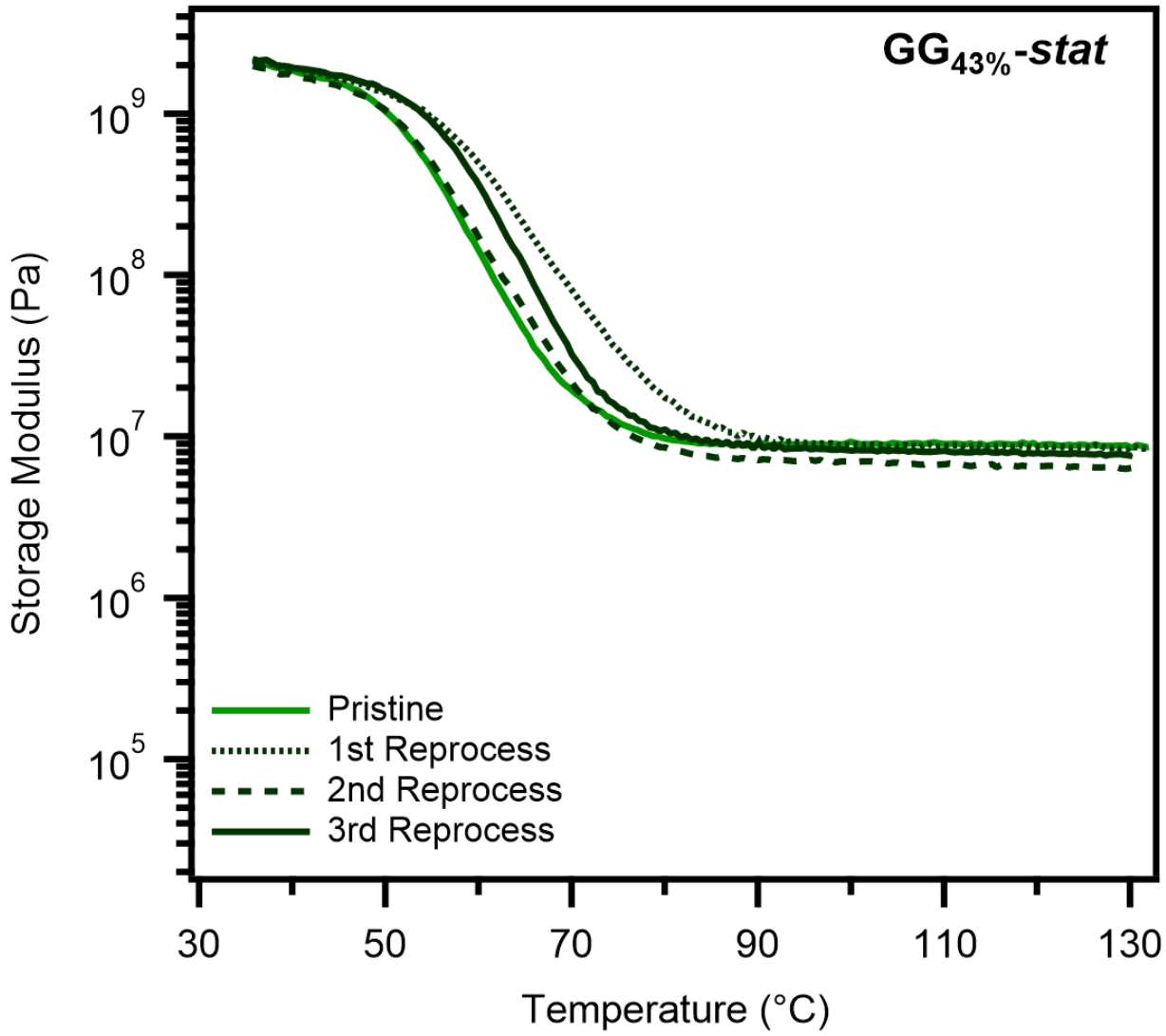

Figure S26. DMTA of **GG$_{43\%}$-*stat*** network before and after each of three reprocessing cycles.

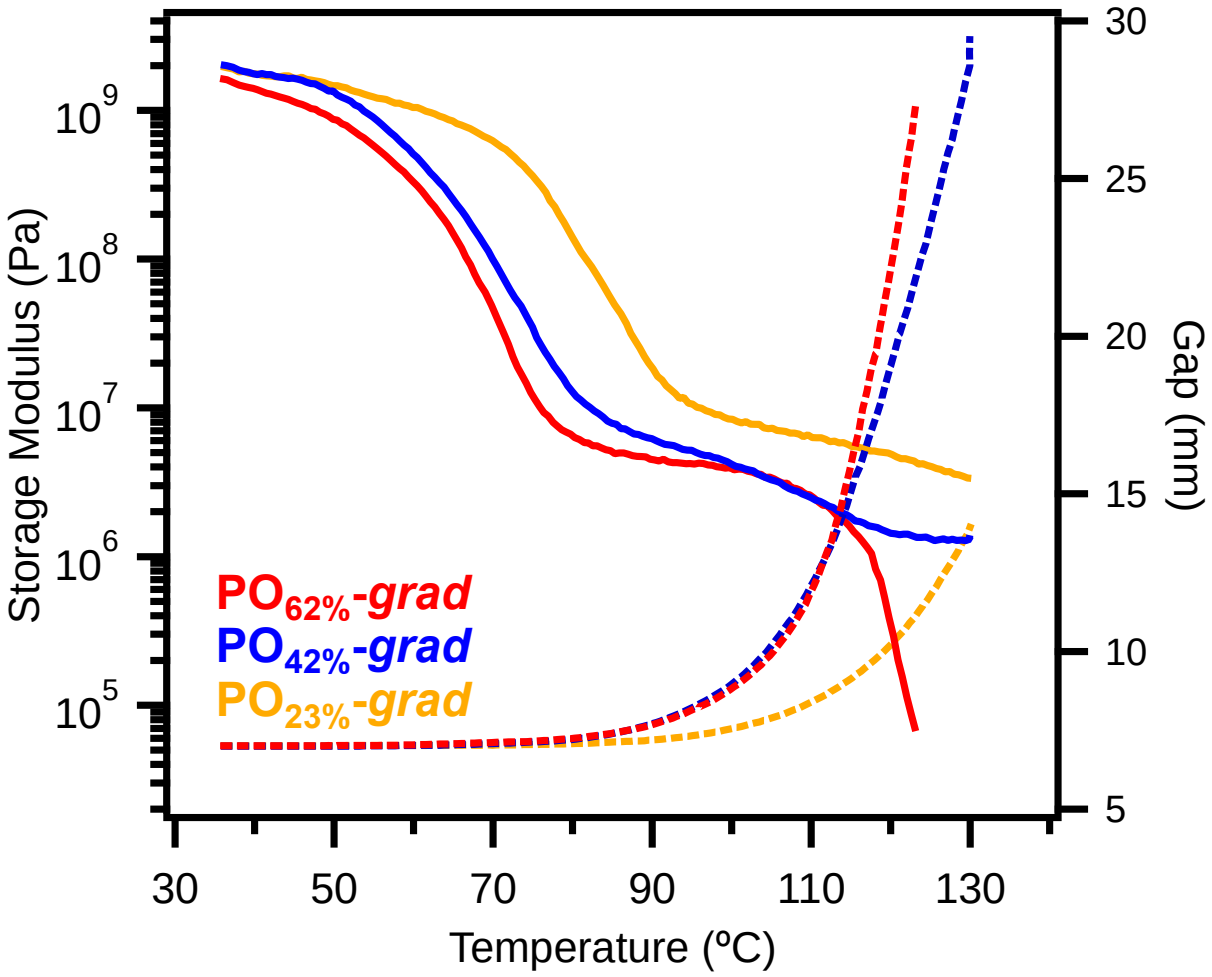

Figure S27. DMTA analysis of pristine gradient polyester imine networks showing storage moduli (solid) and gap length (dashed) as a function of temperature while oscillating at 1 Hz.

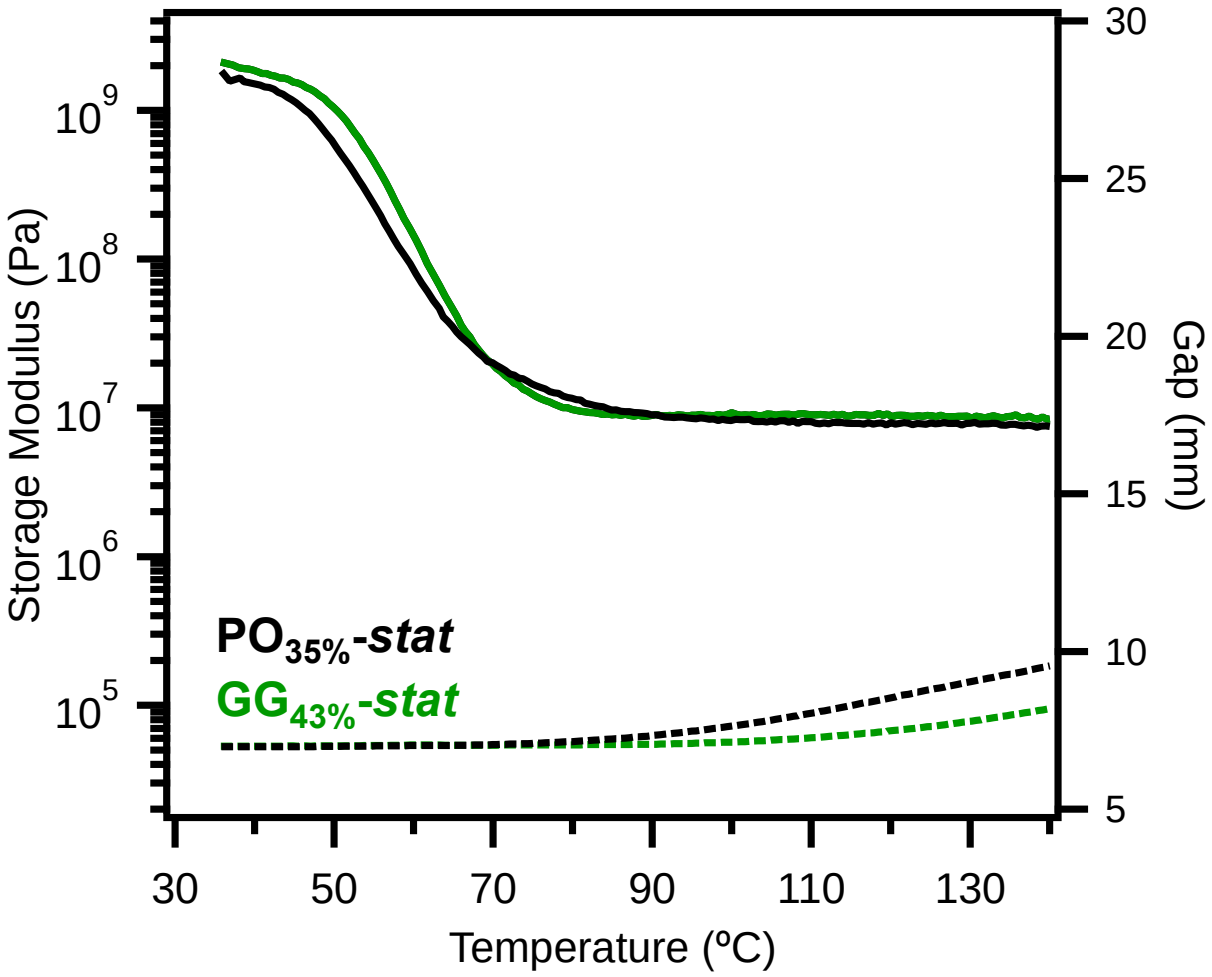

Figure S28. DMTA analysis of statistical polyester imine networks showing storage moduli (solid) and gap length (dashed) as a function of temperature while oscillating at 1 Hz.

5.3. Stress Relaxation Analysis

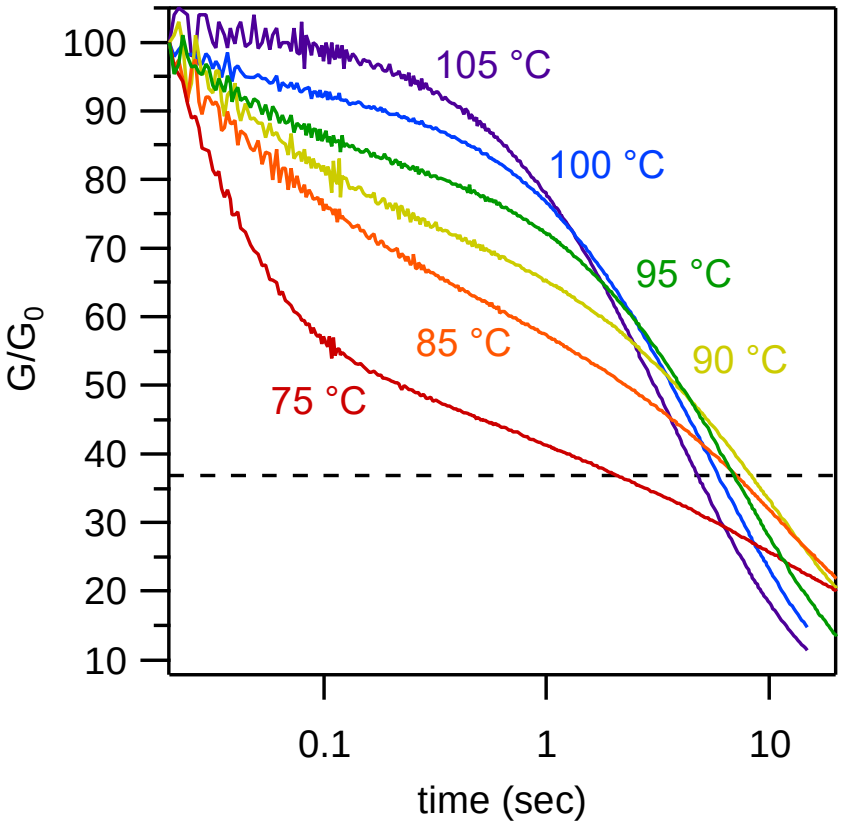

Figure S29. Representative stress relaxation curves for **GG$_{43\%}$-*stat*** at temperatures above the T_g. Close to the T_g, the SRA curves exhibit non-exponential shapes, and the Arrhenius activation energy was only determined using curves that demonstrated exponential decay.

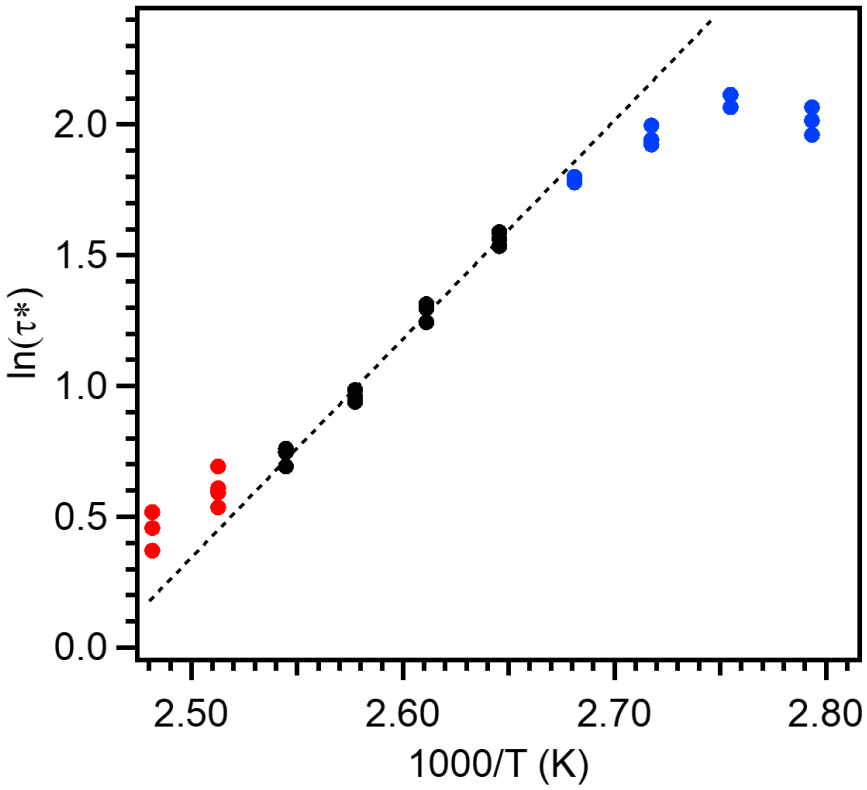

Figure S30. Arrhenius plot of ln(τ∗) versus inverse temperature for **GG$_{43\%}$-*stat***. The Arrhenius activation energy was determined at temperatures that demonstrated exponential decay (black). Close to the T_g, the SRA curves exhibit non-exponential shapes (blue). At temperatures above 120 °C, relaxation times of < 2 s resulted in significant instrument error across multiple runs (red).

5.4. Uniaxial Extension Tensile Testing

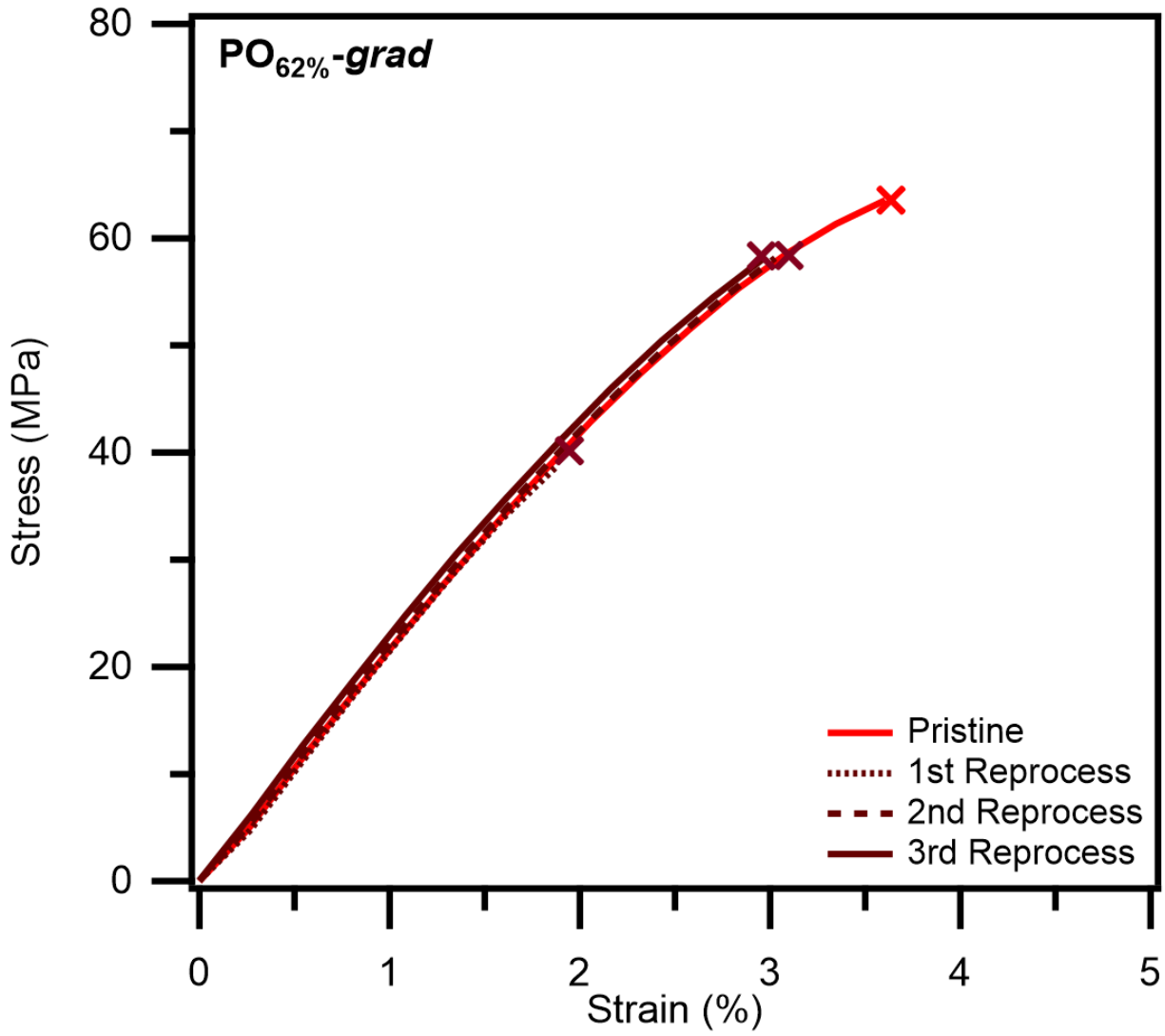

Figure S31. Overlay of representative uniaxial extension tensile testing data for pristine and reprocessed **PO62%-*grad***.

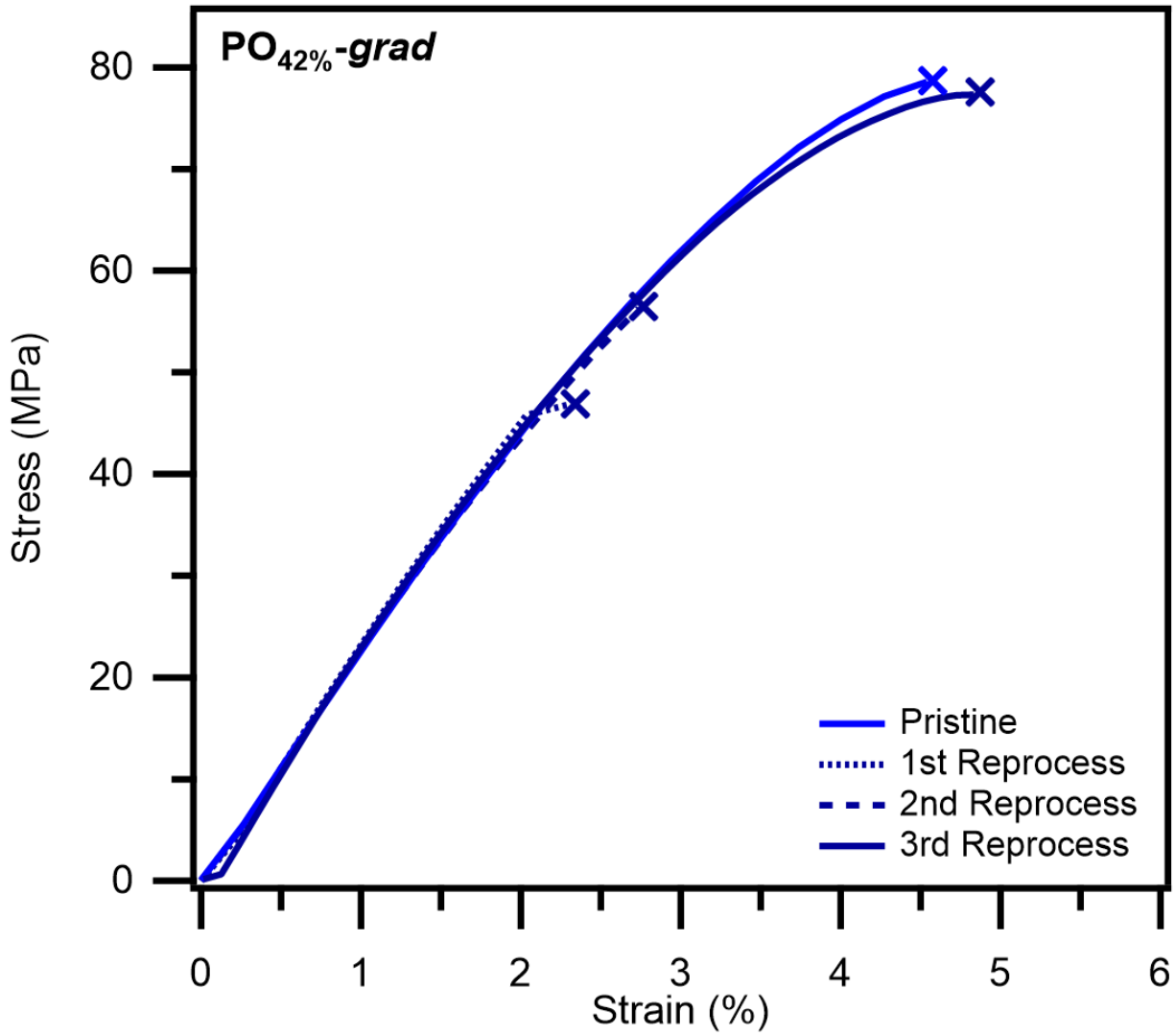

Figure S32. Overlay of representative uniaxial extension tensile testing data for pristine and reprocessed **PO$_{42\%}$-*grad***.

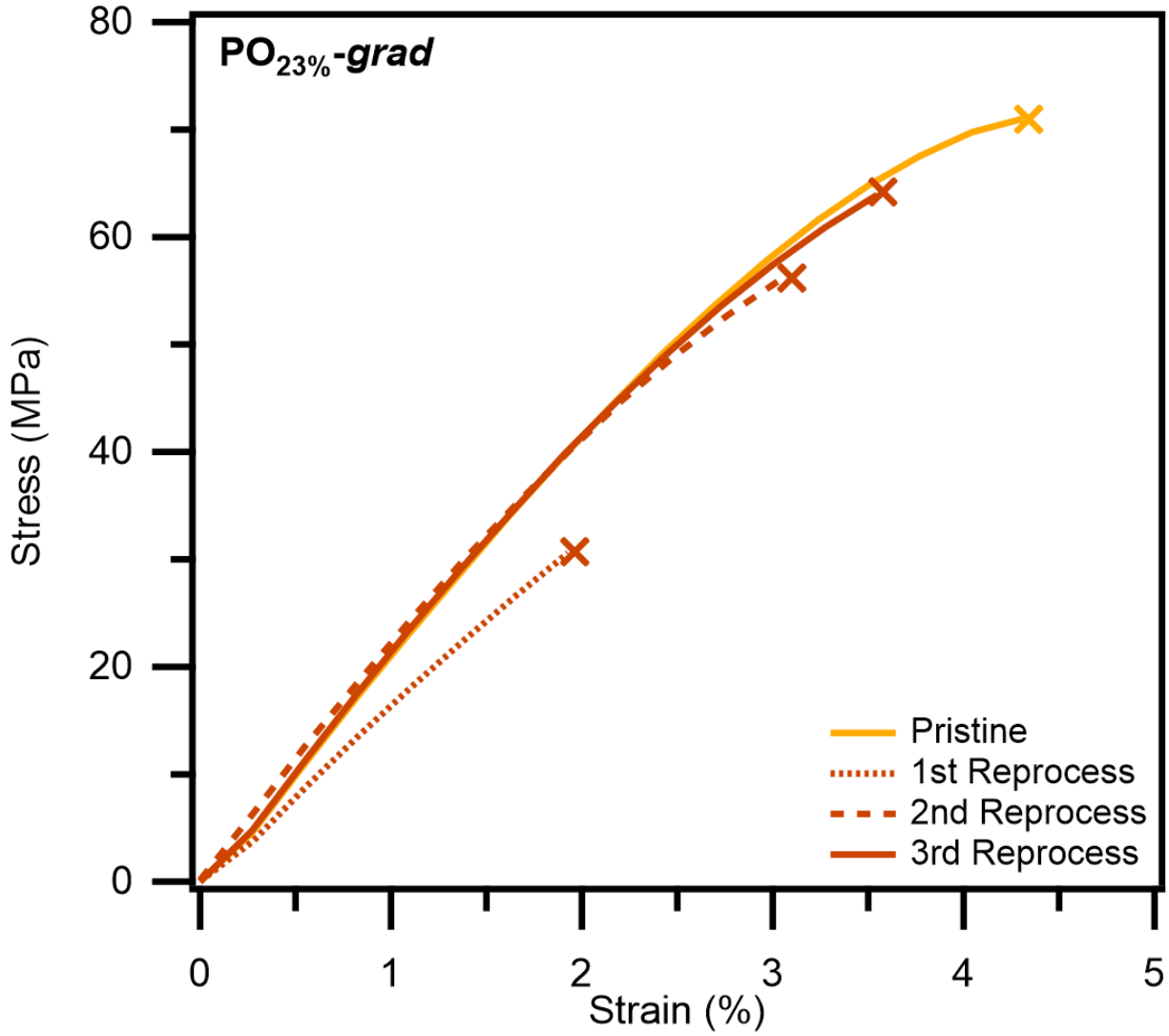

Figure S33. Overlay of representative uniaxial extension tensile testing data for pristine and reprocessed **PO$_{23\%}$-*grad***.

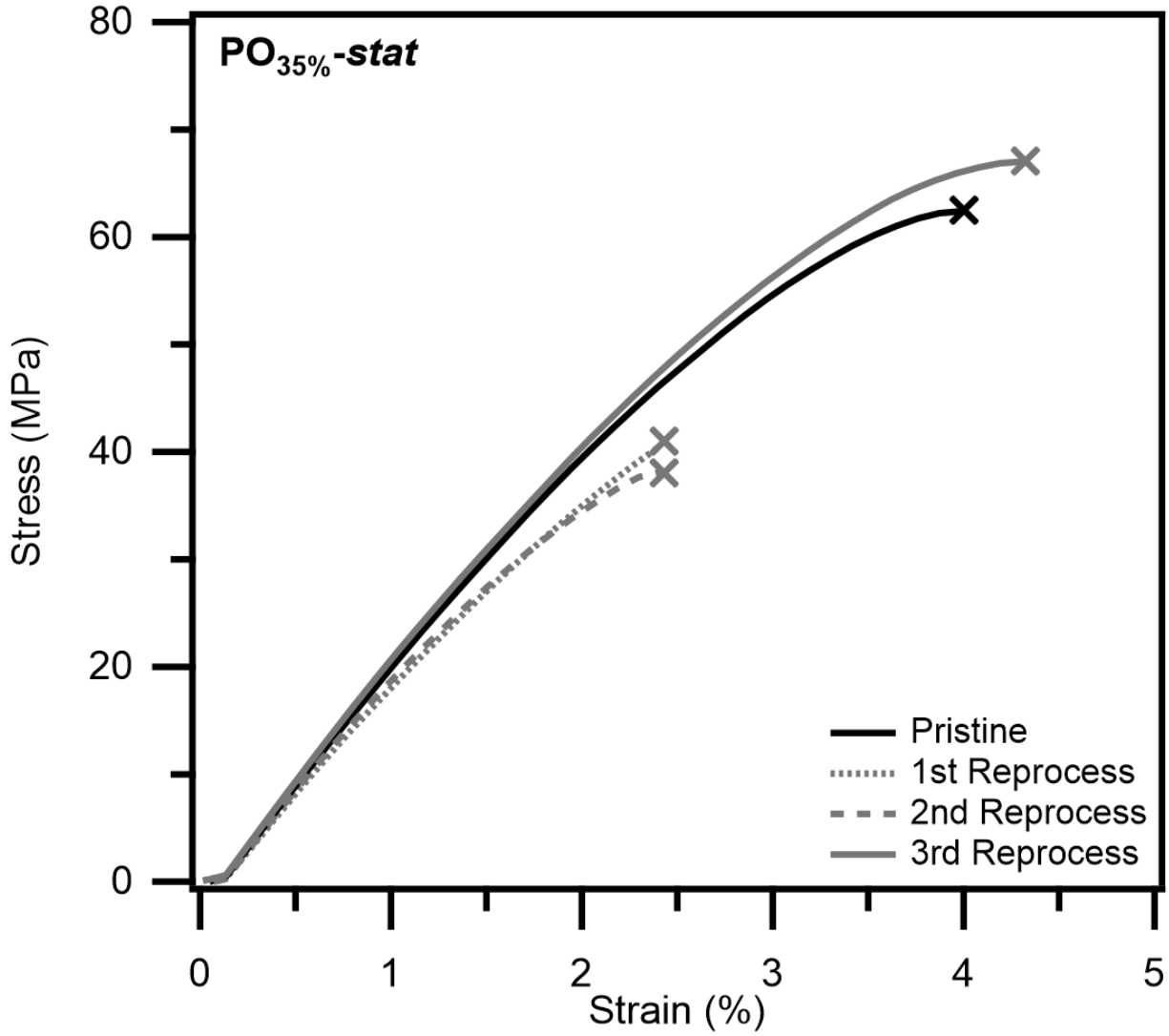

Figure S34. Overlay of representative uniaxial extension tensile testing data for pristine and reprocessed **PO$_{35\%}$-*stat***.

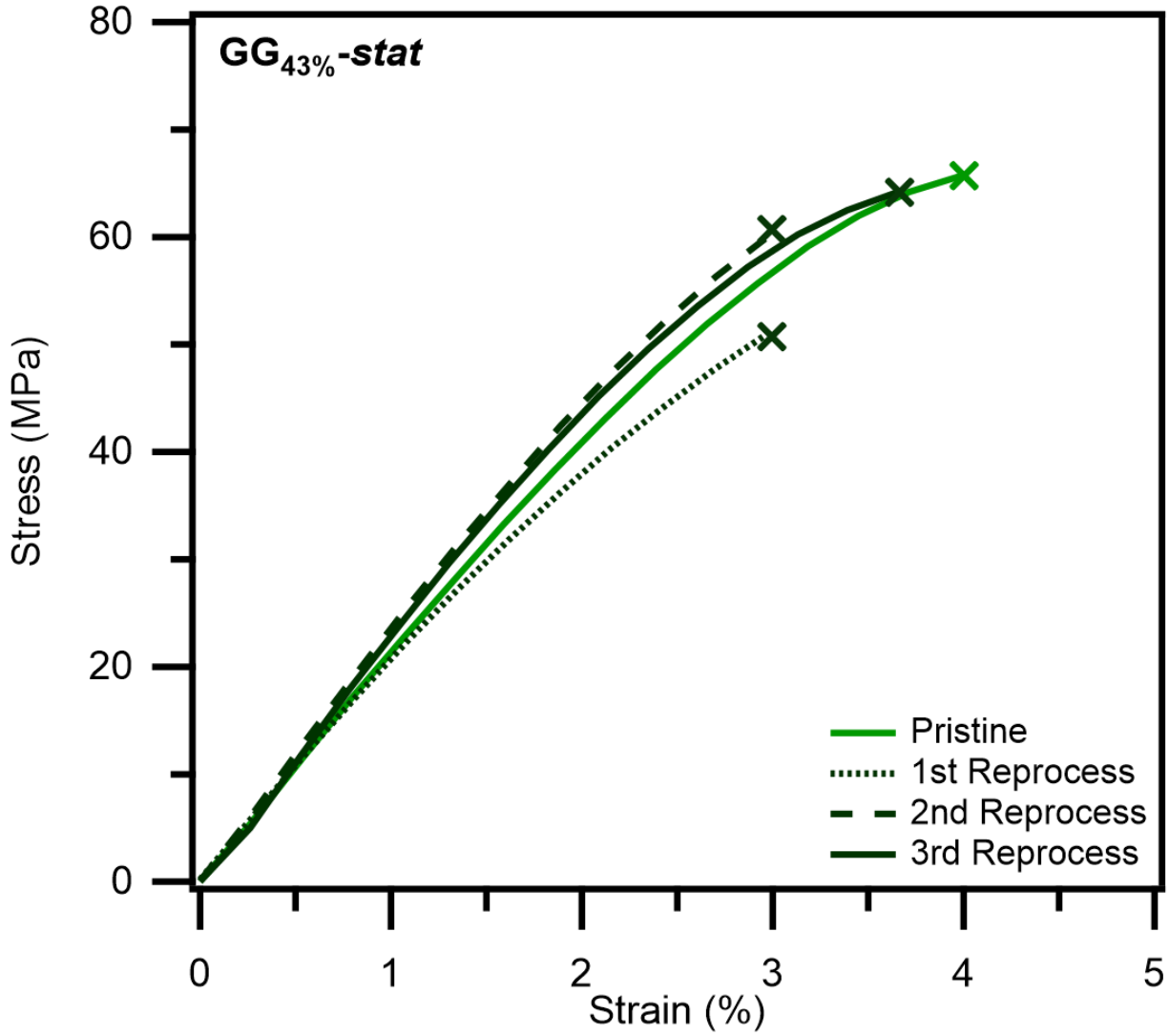

Figure S35. Overlay of representative uniaxial extension tensile testing data for pristine and reprocessed **GG$_{43\%}$-*stat***.

5.5. Fourier Transform Infrared Spectroscopy

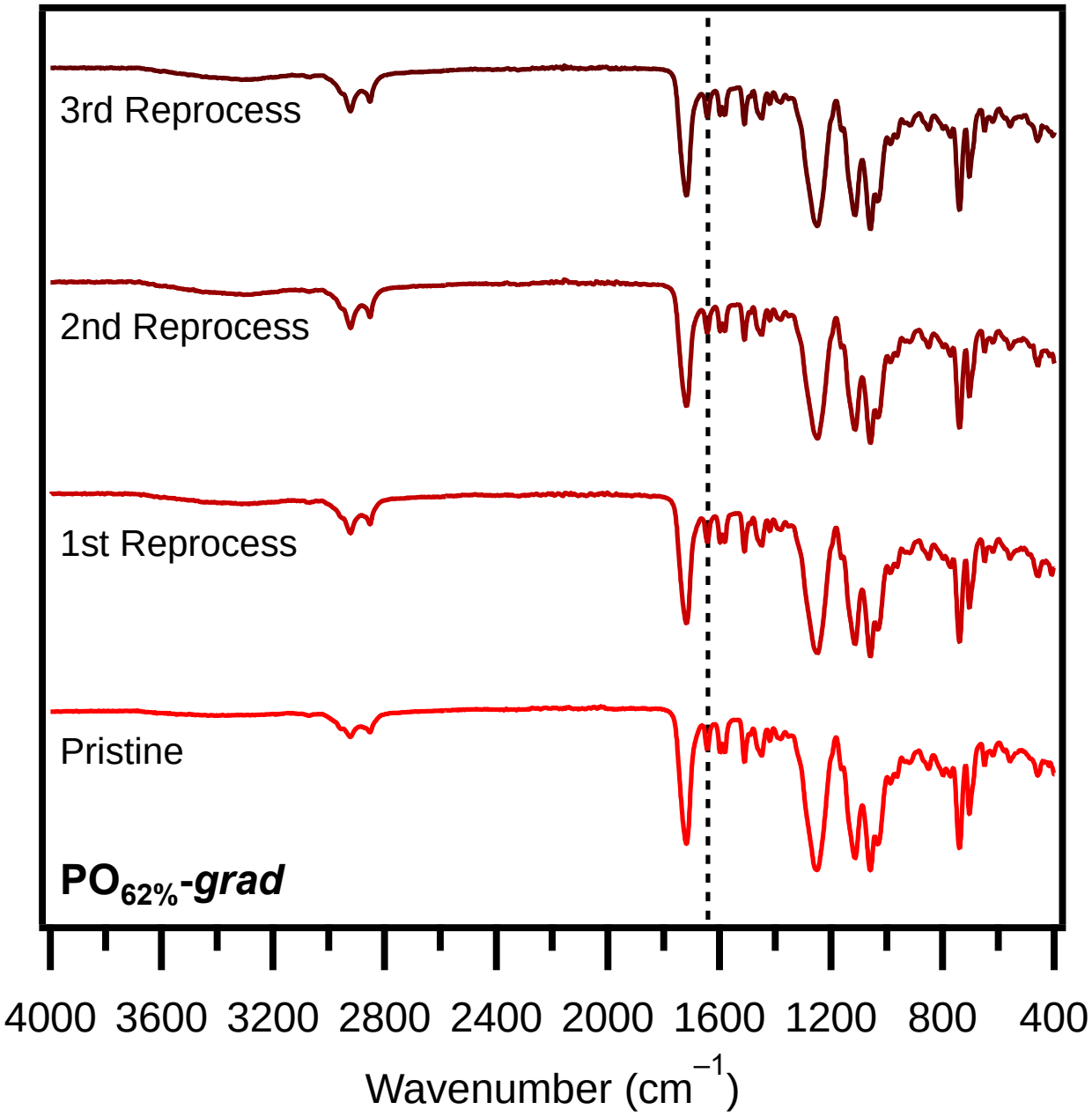

Figure S36. FT-IR spectra of **PO$_{62\%}$-*grad*** networks before and after each of three reprocessing cycles. The dashed line indicates the imine peak at 1642 cm^{-1}.

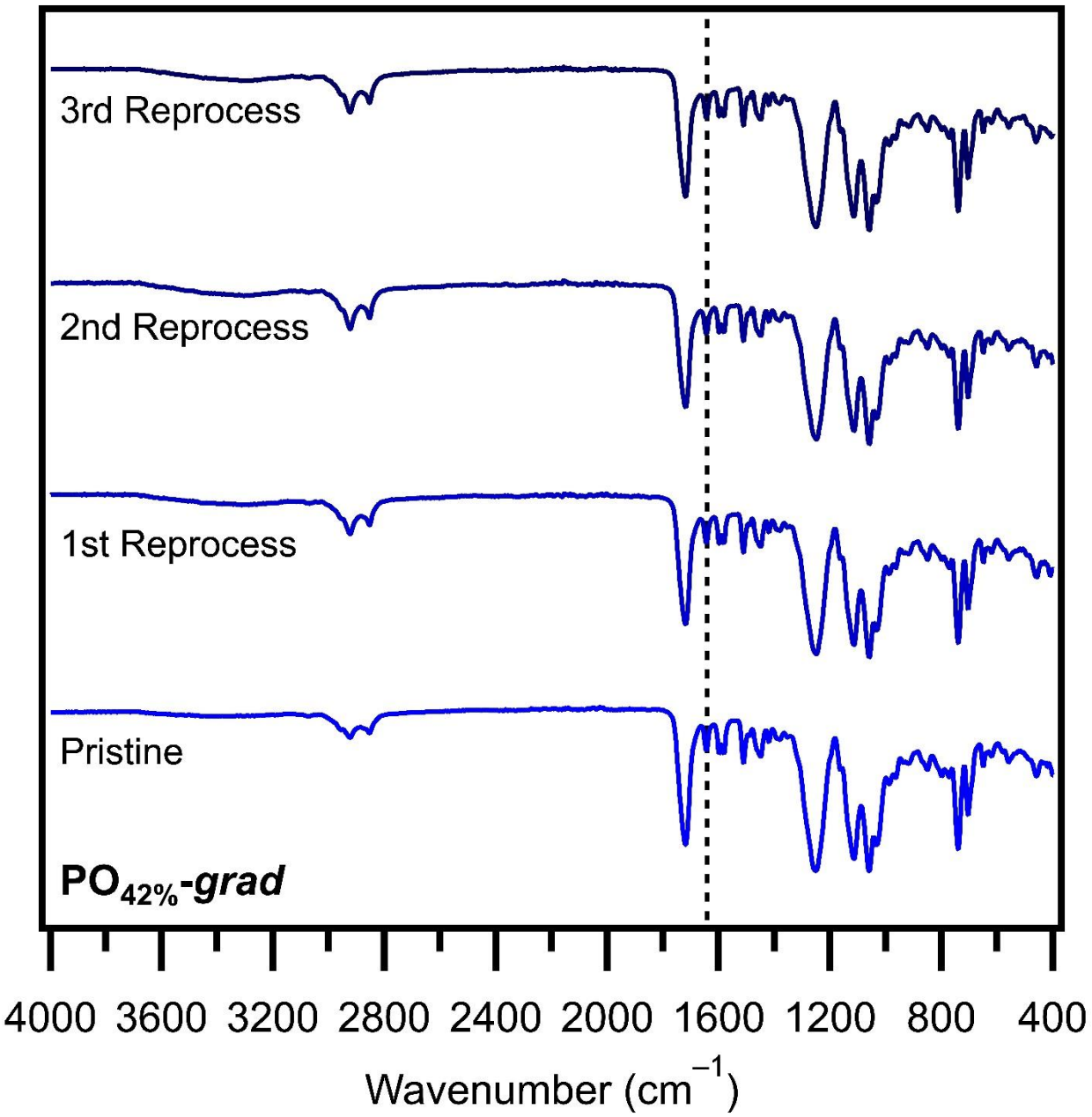

Figure S37. FT-IR spectra of **PO$_{42\%}$-*grad*** networks before and after each of three reprocessing cycles. The dashed line indicates the imine peak at 1642 cm^{-1}.

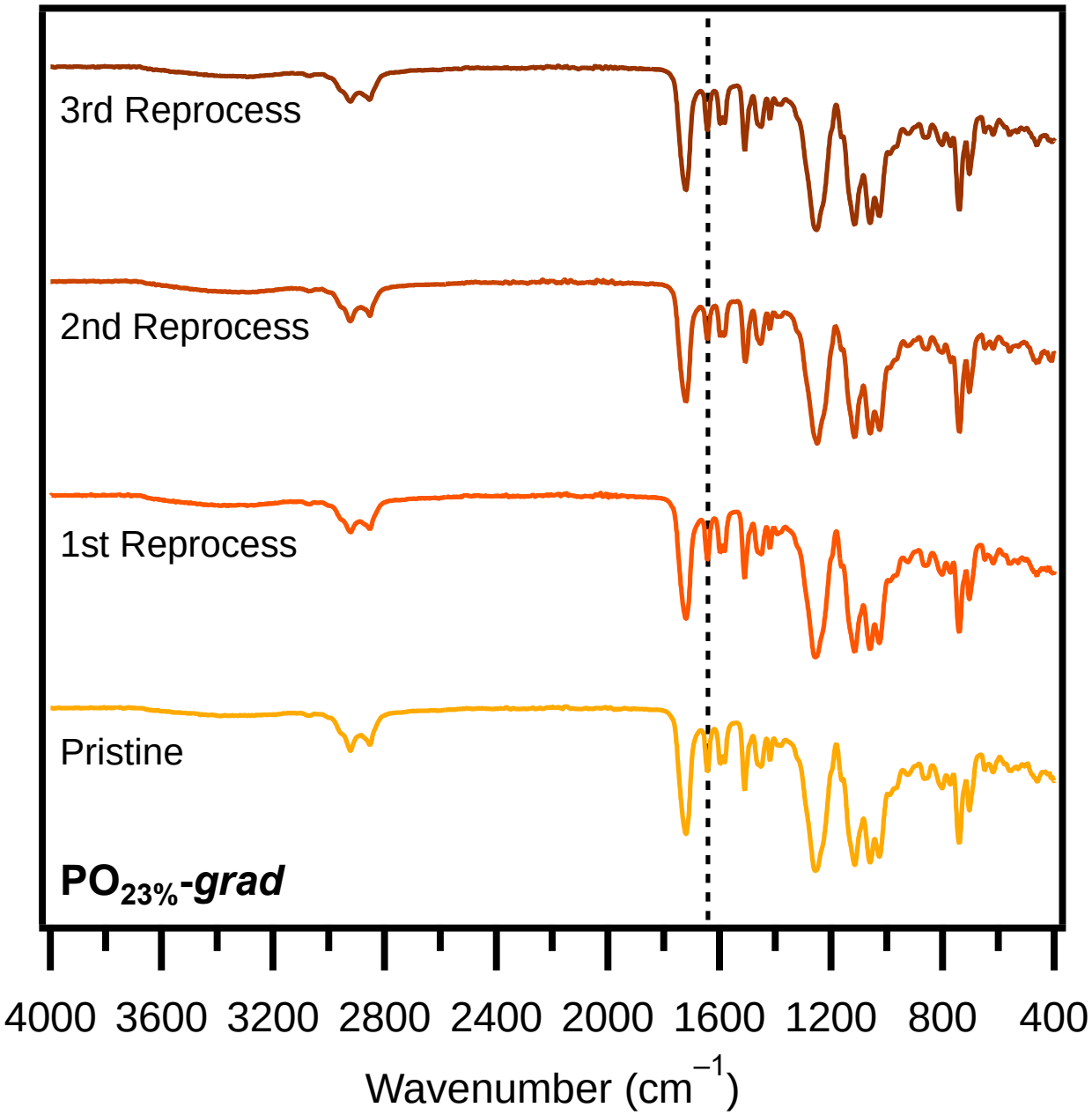

Figure S38. FT-IR spectra of **PO$_{23\%}$-*grad*** networks before and after each of three reprocessing cycles. The dashed line indicates the imine peak at 1642 cm^{-1}.

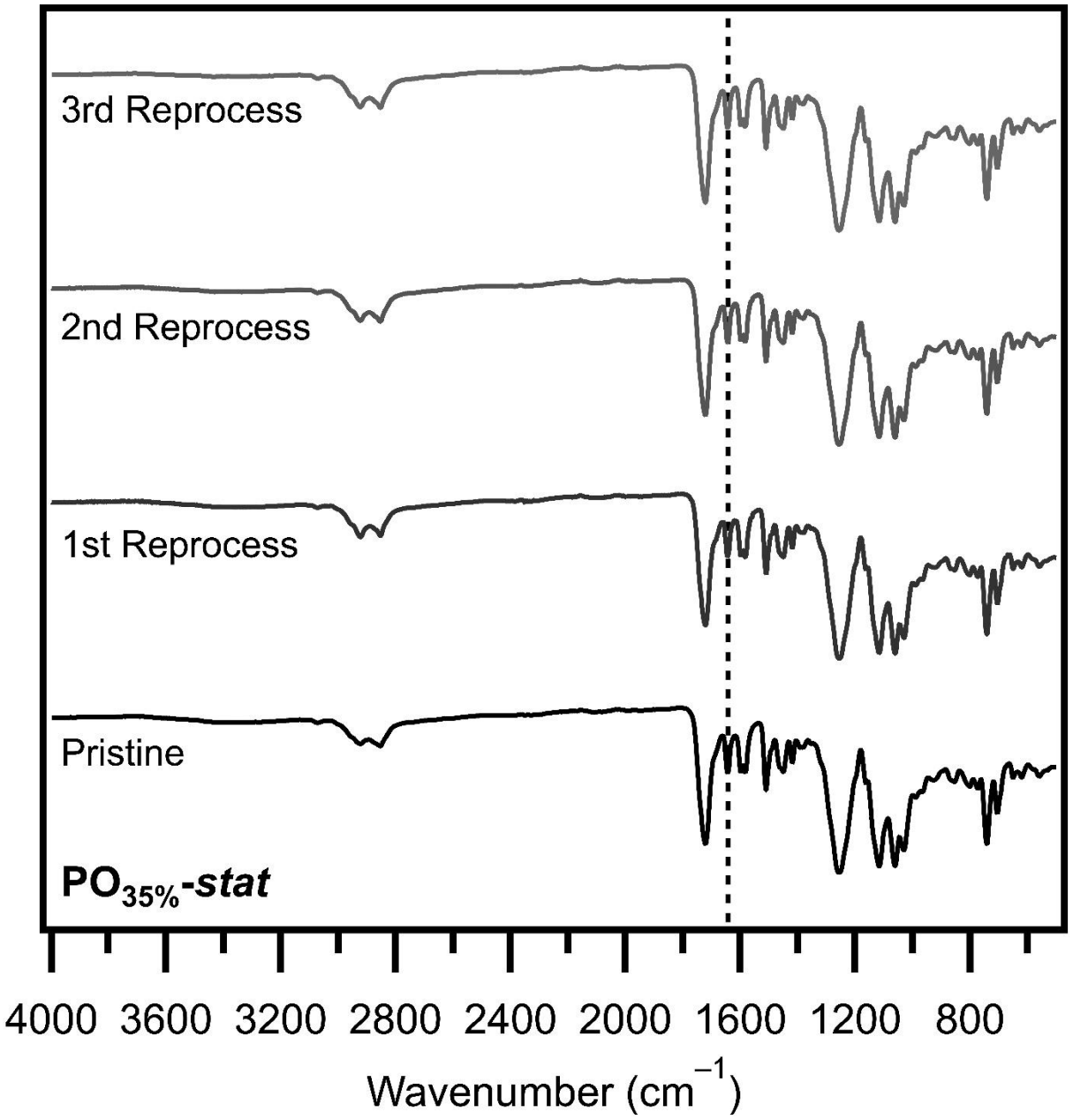

Figure S39. FT-IR spectra of **PO$_{35\%}$-*stat*** networks before and after each of three reprocessing cycles. The dashed line indicates the imine peak at 1642 cm^{-1}.

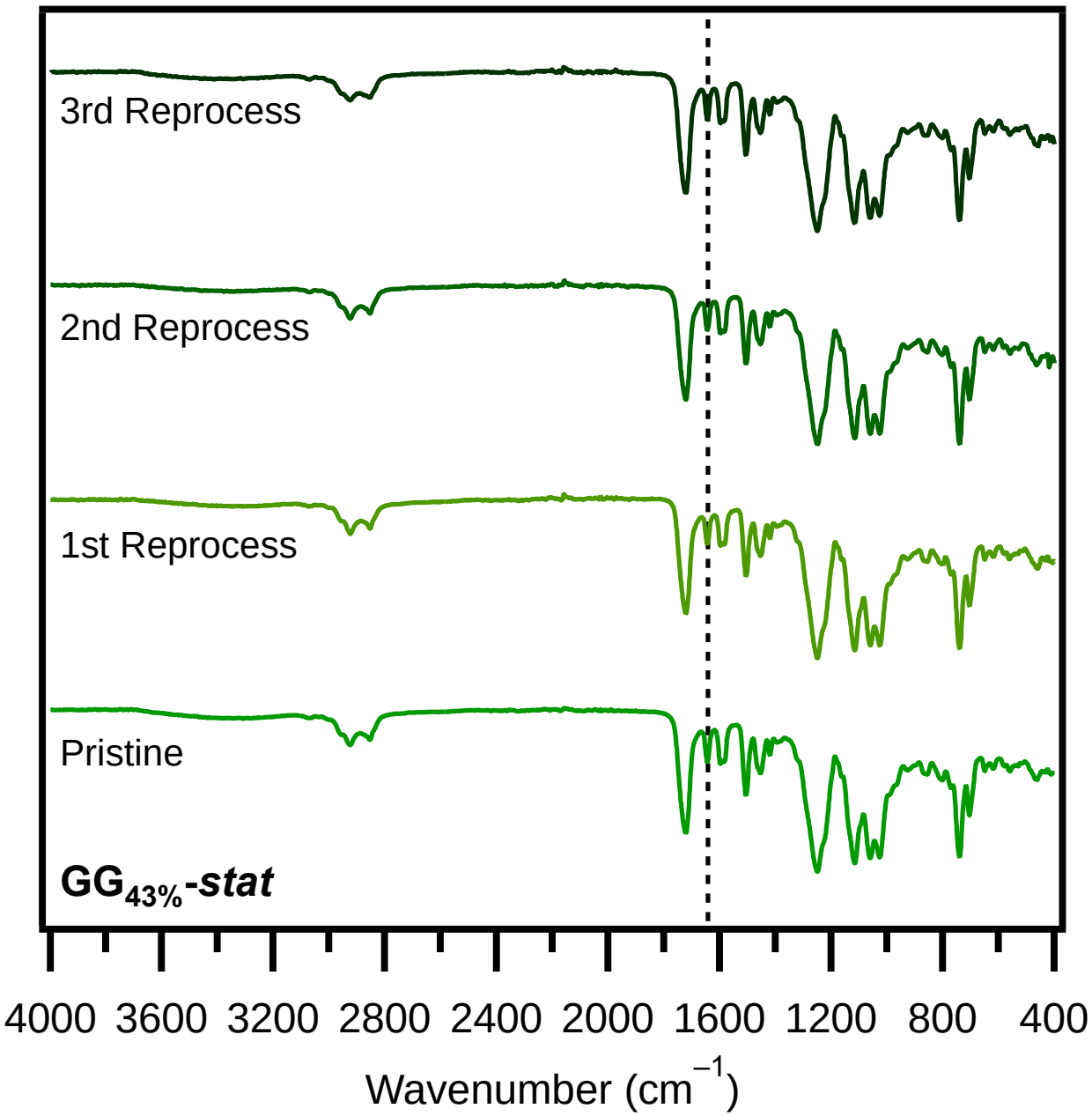

Figure S40. FT-IR spectra of **GG$_{43\%}$-*stat*** networks before and after each of three reprocessing cycles. The dashed line indicates the imine peak at 1642 cm^{-1}.

5.6. Differential Scanning Calorimetry

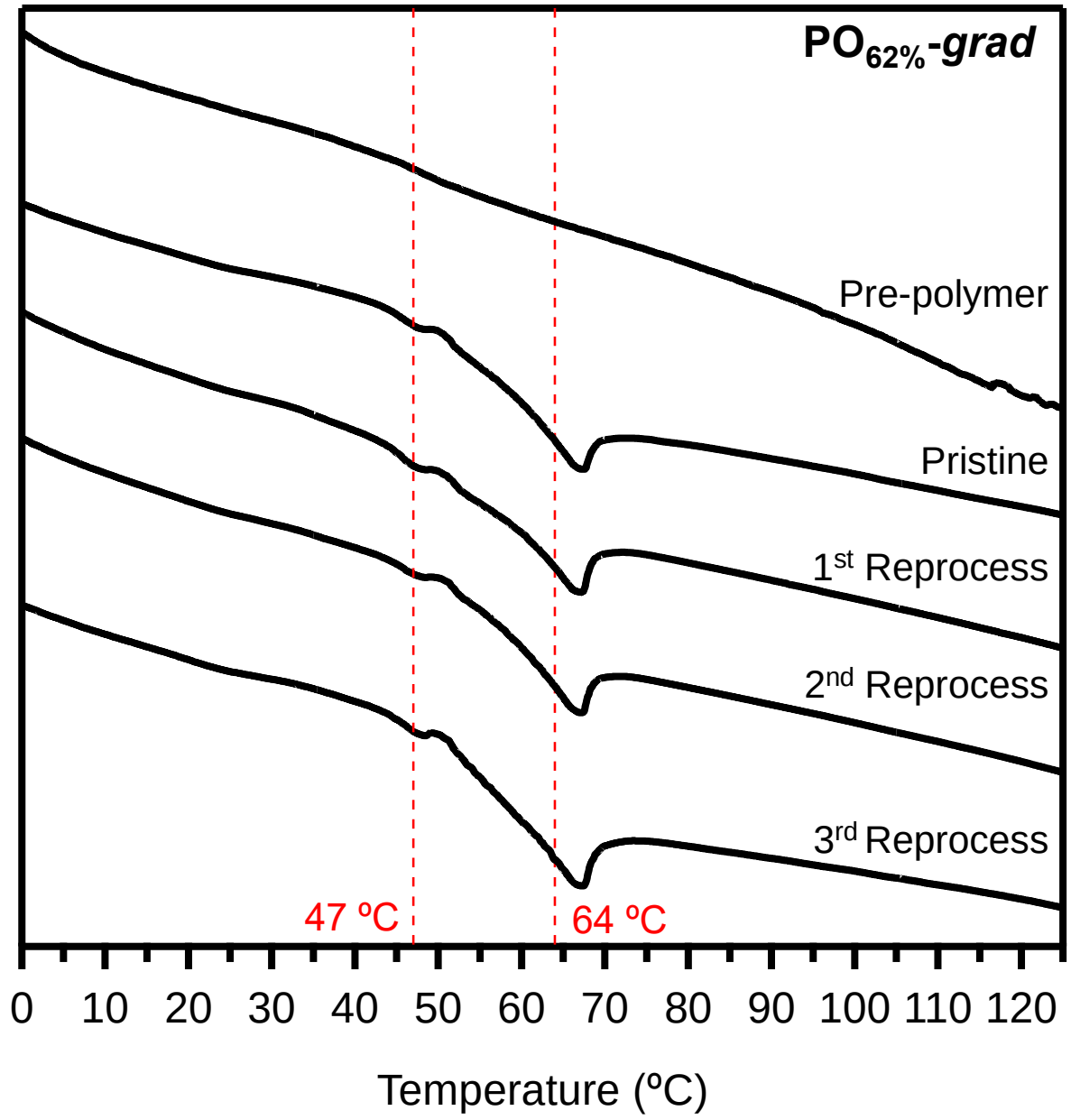

Figure S41. DSC traces from the second heating ramp for **pre-PO$_{62\%}$-*grad*** and **PO$_{62\%}$-*grad*** before and after each of three reprocessing cycles. The low intensity feature at 47 °C is a known artifact from the instrument.

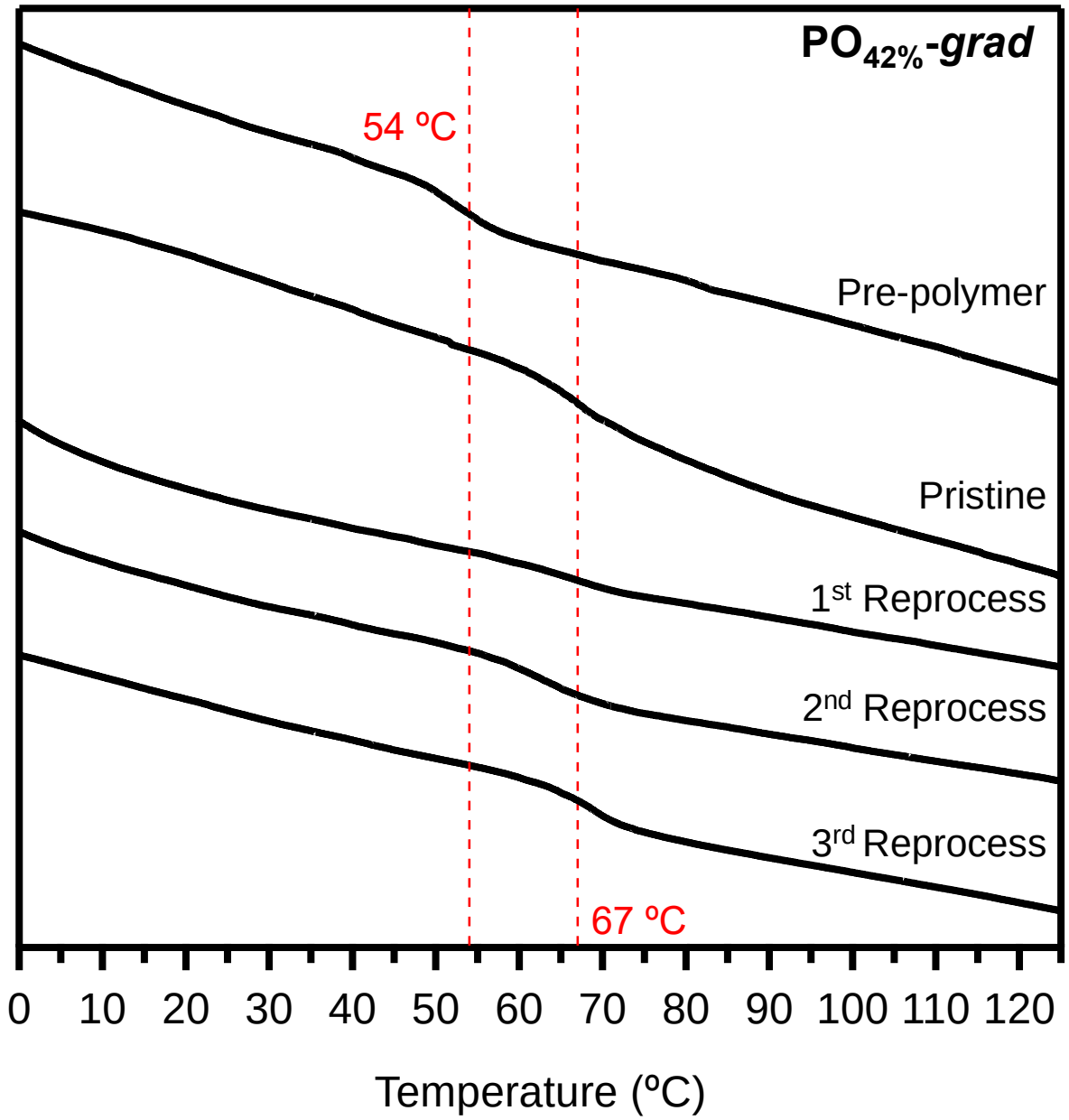

Figure S42. DSC traces from the second heating ramp for **pre-PO$_{42\%}$-*grad*** and **PO$_{42\%}$-*grad*** before and after each of three reprocessing cycles. The low intensity feature at 47 °C is a known artifact from the instrument.

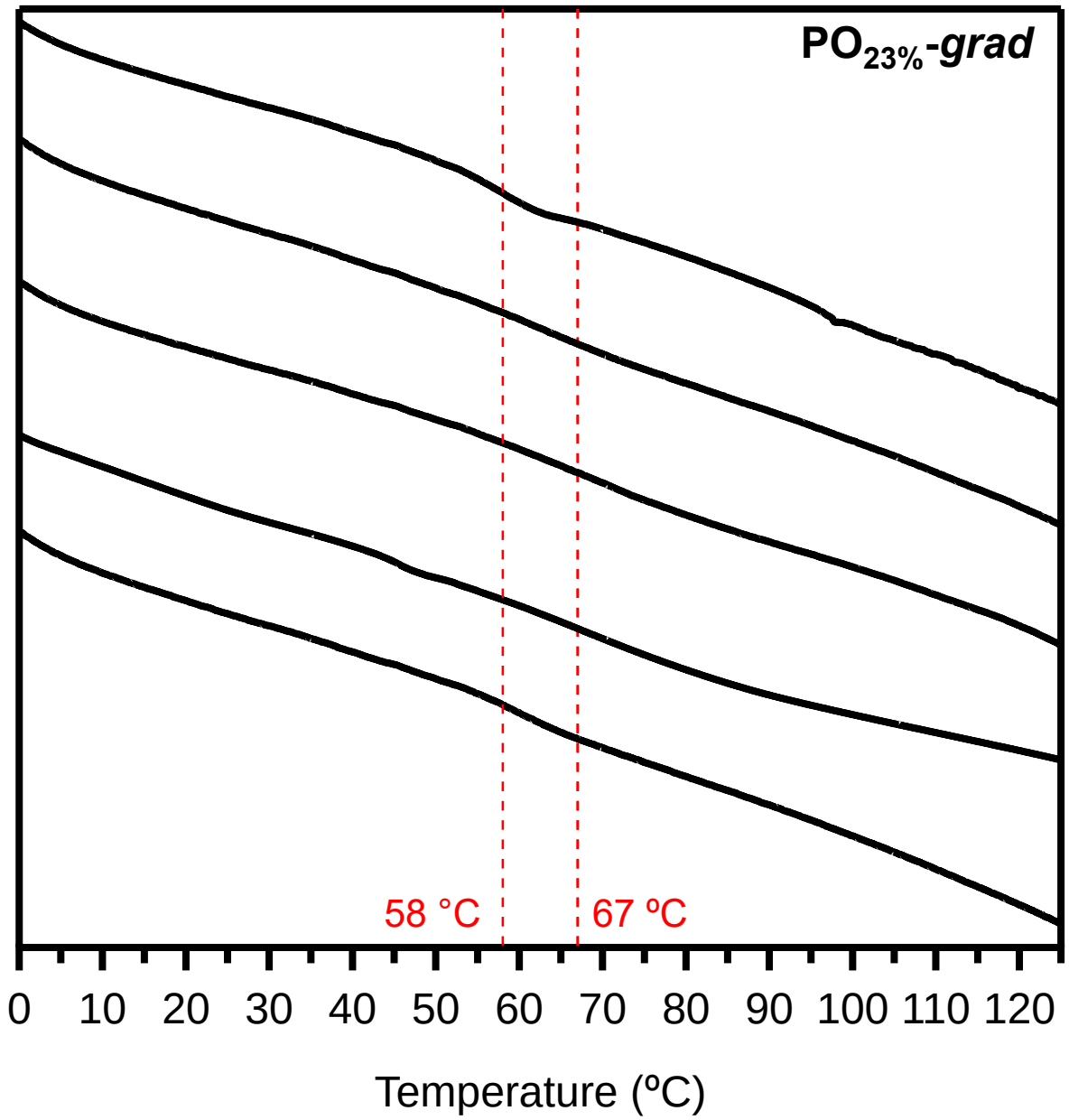

Figure S43. DSC traces from the second heating ramp for **pre-PO$_{23\%}$-*grad*** and **PO$_{23\%}$-*grad*** before and after each of three reprocessing cycles. The low intensity feature at 47 °C is a known artifact from the instrument.

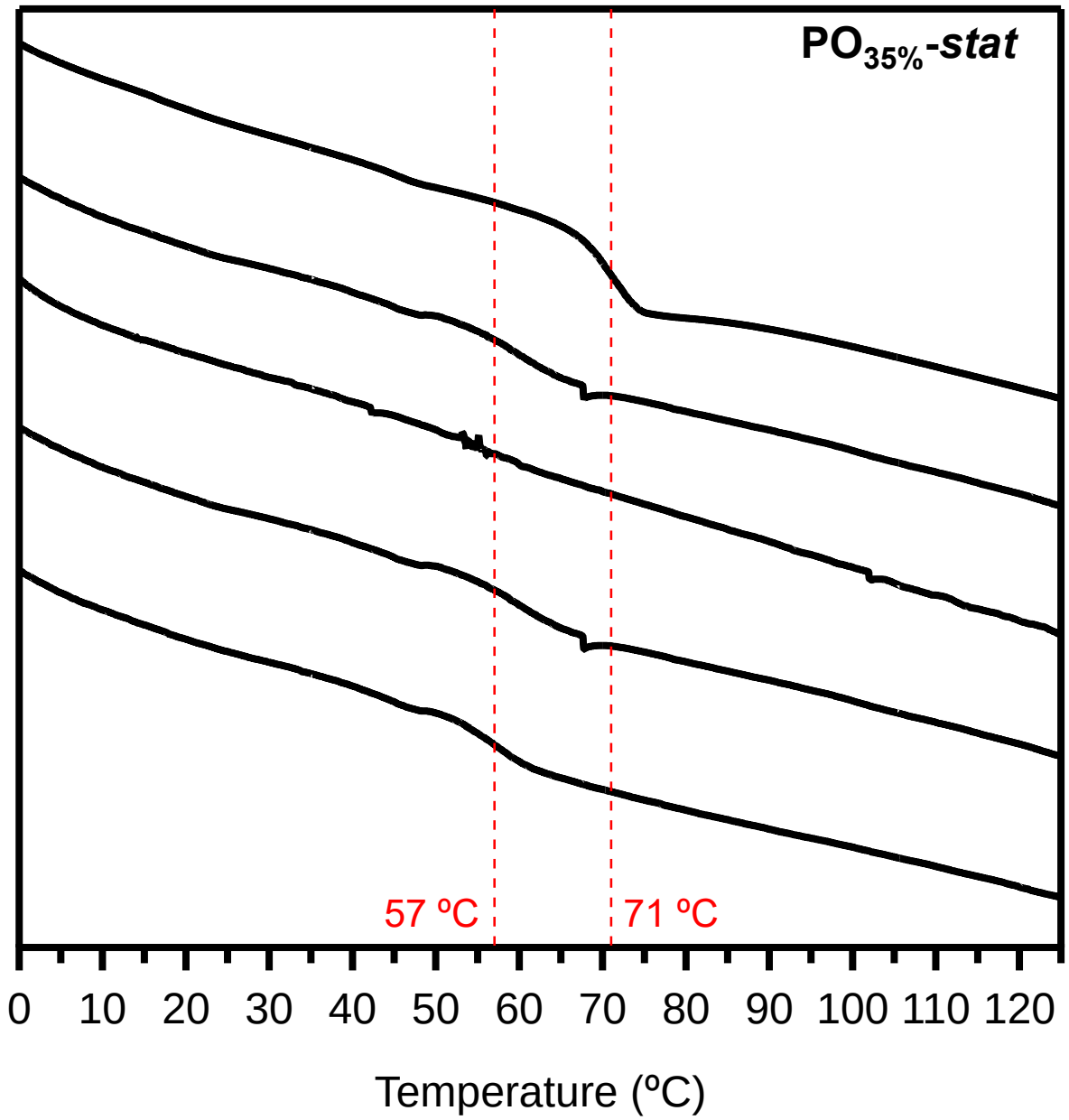

Figure S44. DSC traces from the second heating ramp for **pre-PO$_{35\%}$-*stat*** and **PO$_{35\%}$-*stat*** before and after each of three reprocessing cycles. The low intensity feature at 47 °C is a known artifact from the instrument.

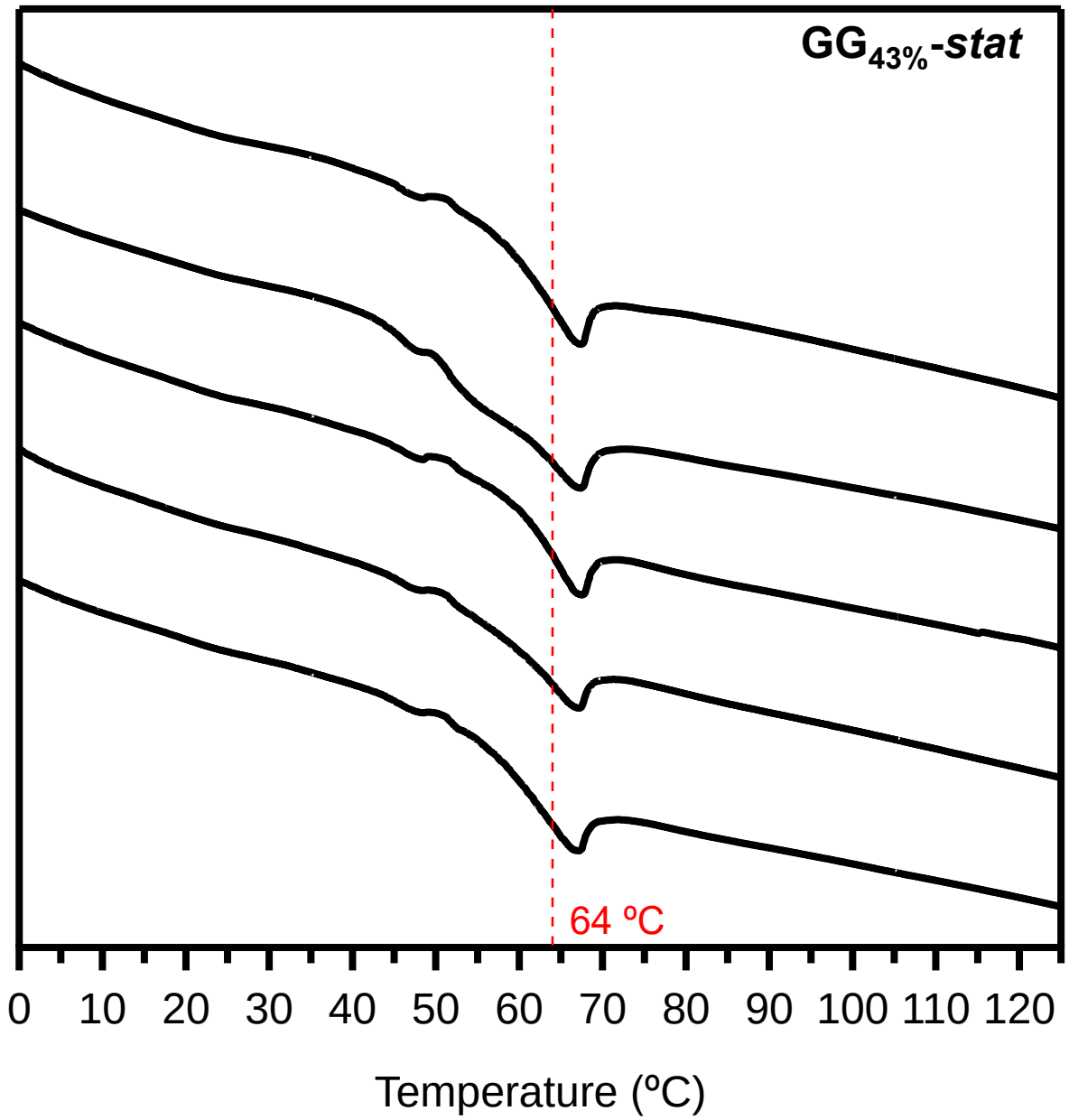

Figure S45. DSC traces from the second heating ramp for **pre-** **GG$_{43\%}$-*stat*** and **GG$_{43\%}$-*stat*** before and after each of three reprocessing cycles. The low intensity feature at 47 °C is a known artifact from the instrument.

5.7. Thermogravimetric Analysis

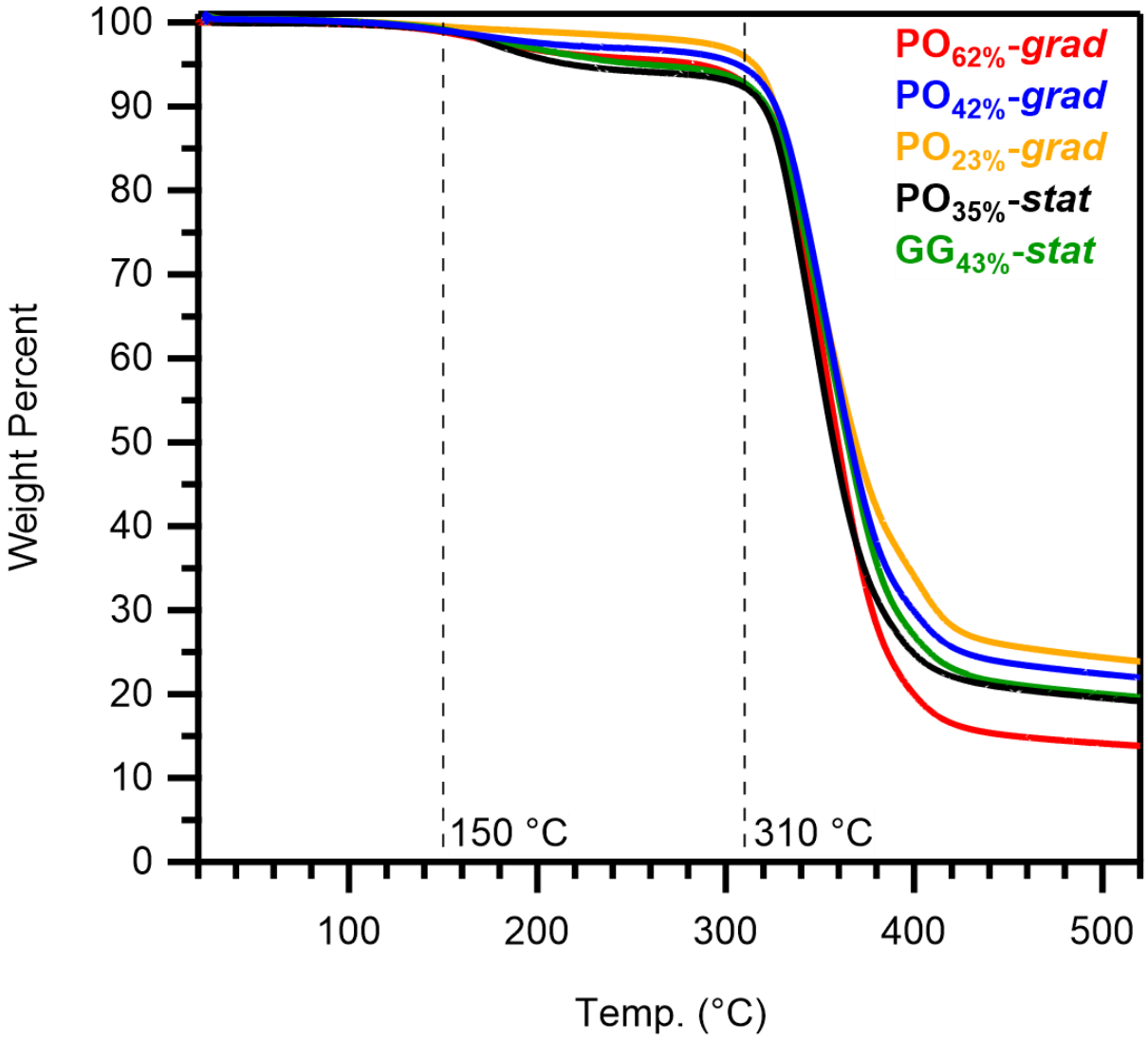

Figure S46. Dynamic thermogravimetric analysis of polyester imine networks. The networks lose ~6 wt% at 150 °C, which we attribute to loss of residual solvent, but most weight loss occurs above 300 °C.

6. Small Molecule Models

6.1. Synthesis of Small Molecule Imine Compounds

1-(4-Fluorophenyl)-*N*-propylmethanimine (Imine-1)

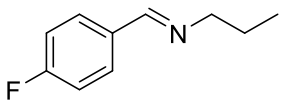

4-Fluorobenzaldehyde (1.1 mL, 10 mmol, 1.0 equiv) and *n*-propylamine (0.82 mL, 10 mmol, 1.0 equiv) were combined in a 20 mL vial with a Teflon-coated magnetic stir bar, DCM (15 mL), and anhydrous sodium sulfate (1 g). The reaction mixture was stirred at 22 °C for 3.5 h before decanting the solution and concentrating in vacuo. The imine was dried over activated 3 Å molecular sieves and degassed by three freeze-pump-thaw cycles. The imine was then taken into the glovebox and filtered through a 5 μm PTFE syringe filter to afford a pale yellow oil, which was stored at –20 °C under nitrogen (780 mg, 47% yield). **^{1}H NMR** (500 MHz, $CDCl_3$): δ 8.22 (s, 1H), 7.71 (m, 2H), 7.07 (t, *J* = 7.85 Hz, 2H), 3.56 (t, *J* = 7.08 Hz, 2H), 1.72 (m, 2H), 0.95 (t, *J* = 7.04, 3H) ppm. **^{13}C NMR** (125 MHz, $CDCl_3$): δ 165.26, 163.26, 159.45, 132.73, 130.00, 129.94, 115.80, 115.62, 63.47, 24.14, 11.93 ppm. **^{19}F NMR** (376 MHz, $CDCl_3$): δ –110.03 ppm. **DART-HRMS** calculated m/z for $C_{10}H_{13}NF$ [M+H] = 166.10265, found 166.10252.

1-(4-Fluorophenyl)-*N*-propylmethanimine, ^{1}H NMR Spectrum (500 MHz, $CDCl_3$)

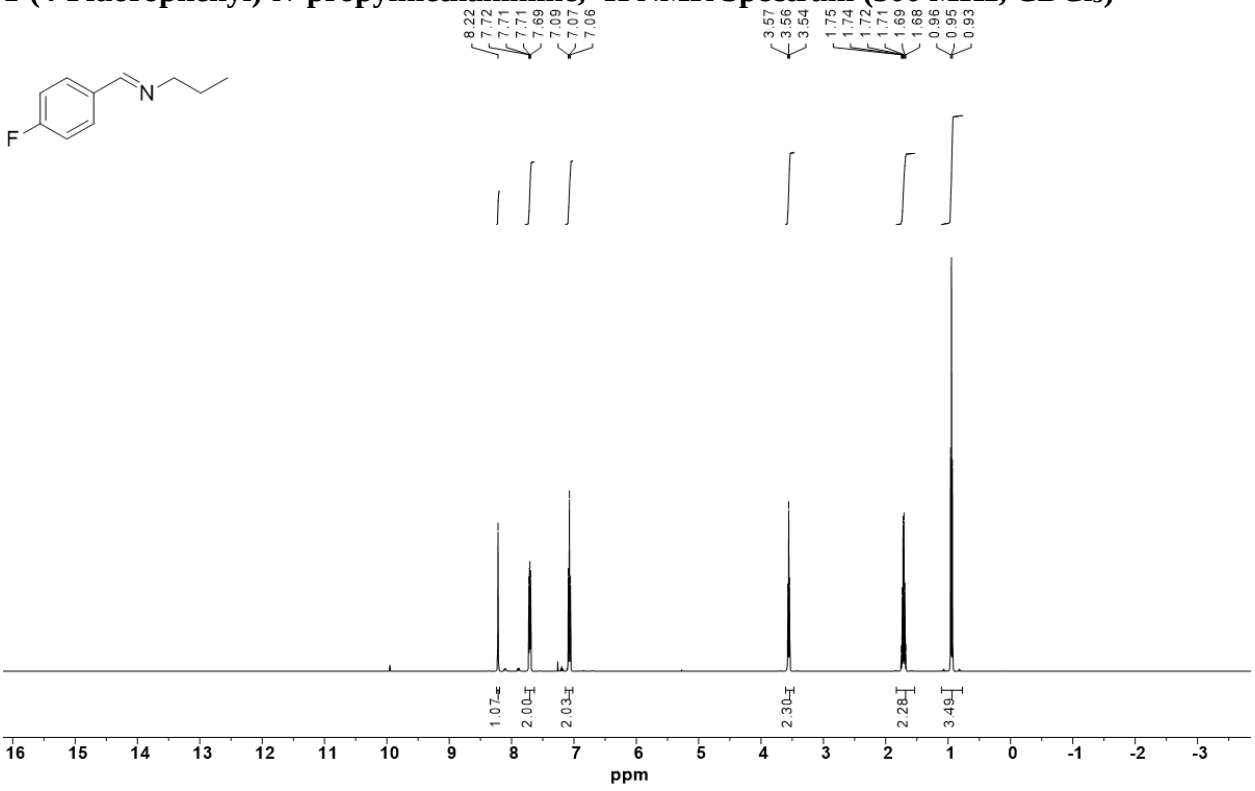

1-(4-Fluorophenyl)-*N*-propylmethanimine, ^{13}C NMR Spectrum (125 MHz, $CDCl_3$)

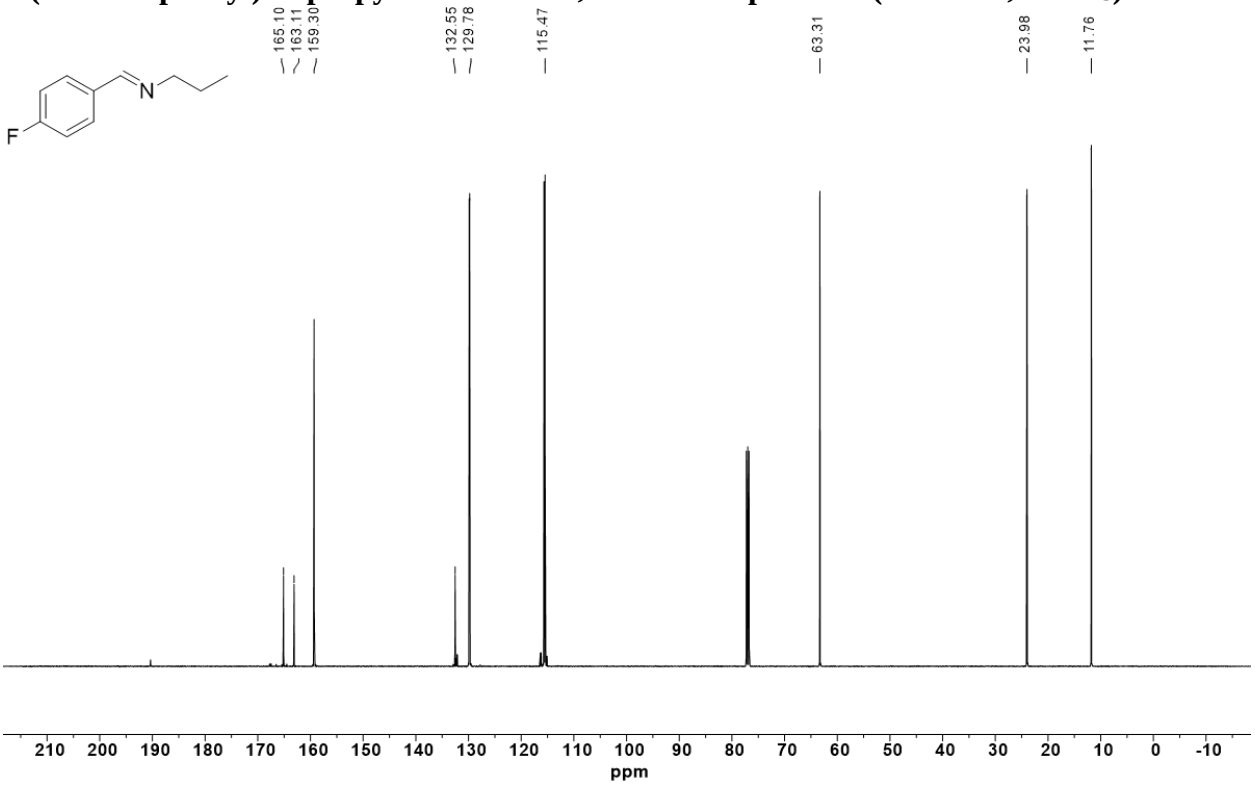

***N*-Neopentyl-1-phenylmethanimine (Imine-2)**

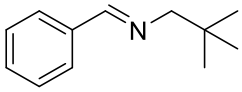

Benzaldehyde (1.02 mL, 10.0 mmol, 1.00 equiv) and neopentylamine (1.17 mL, 10.0 mmol, 1.00 equiv) were combined in a 20 mL vial with a stir bar, DCM (15 mL) and anhydrous sodium sulfate (1 g), and the reaction mixture stirred at 22 °C for 4 h. The solution was then decanted, and solvent was removed in vacuo. **Imine-2** was then dried over activated 3 Å molecular sieves, degassed by three freeze-pump-thaw cycles, taken into the glovebox, and filtered through a 5 μm PTFE syringe filter. The resulting clear colorless oil was stored at –20 °C under nitrogen (480 mg, 27% yield). **^{1}H NMR** (500 MHz, $CDCl_3$): δ 8.25 (s, 1H), 7.78 (m, 2H), 7.43 (m, 3H), 3.40 (s, 2H), 1.02 (s, 9H) ppm. **^{13}C NMR** (125 MHz, $CDCl_3$): δ 160.78, 136.65, 130.45, 128.63, 128.19, 74.08, 32.72, 28.13 ppm. **DART-HRMS** calculated m/z for $C_{12}H_{18}N$ [M+H] = 176.14338, found 176.14328.

***N*-Neopentyl-1-phenylmethanimine, ^{1}H NMR Spectrum (500 MHz, $CDCl_3$)**

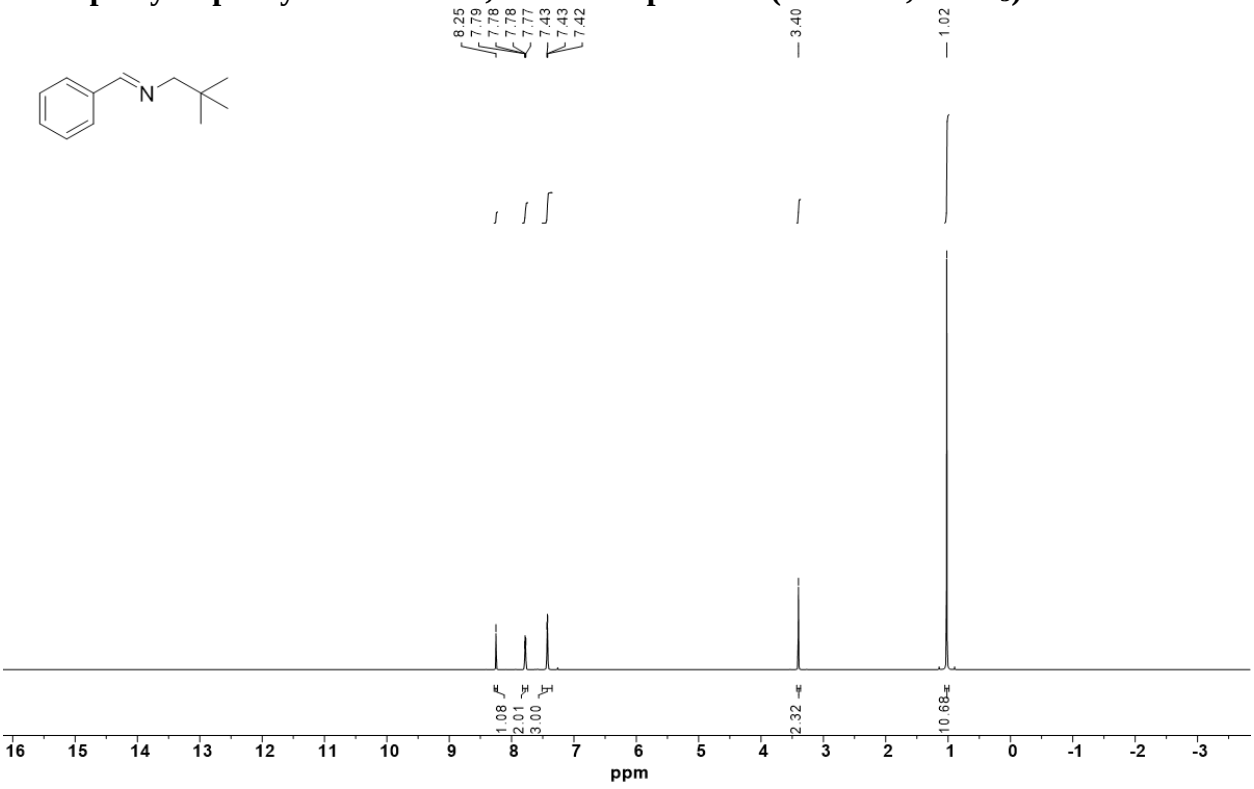

***N*-Neopentyl-1-phenylmethanimine, ^{13}C NMR Spectrum (125 MHz, $CDCl_3$)**

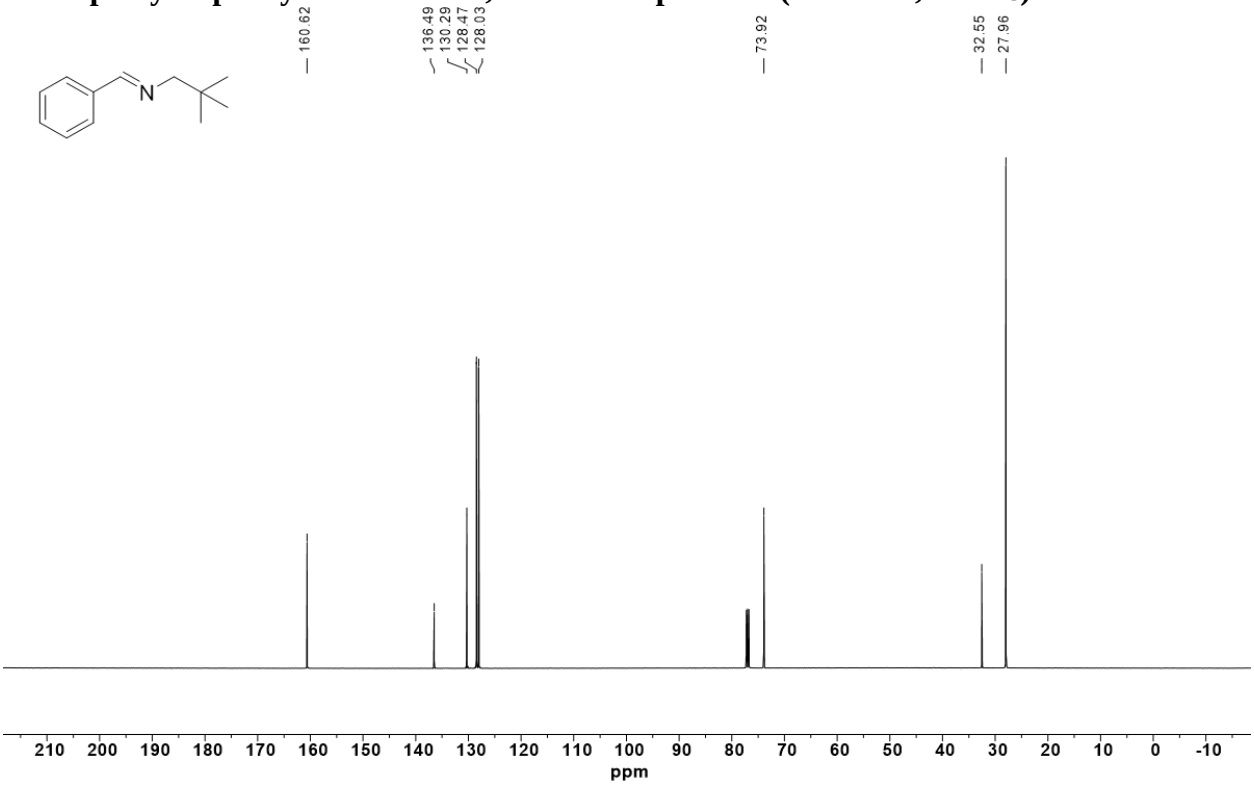

1-Phenyl-*N*-propylmethanimine (Imine-3)

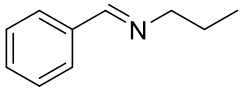

Benzaldehyde (1.0 mL, 10 mmol, 1.0 equiv) and *n*-propylamine (0.90 mL, 11 mmol, 1.1 equiv) were combined in a 20 mL vial with a stir bar, DCM (15 mL) and anhydrous sodium sulfate (250 mg). After stirring at 22 °C for 4 h, the solution was decanted, and solvent was removed in vacuo. **Imine-3** was then dried over activated 3 Å molecular sieves, degassed by three freeze-pump-thaw cycles, taken into the glovebox, and filtered through a 5 μm PTFE syringe filter. The resulting clear colorless oil was stored in the glovebox freezer at –20 °C under nitrogen. **^{1}H NMR** (500 MHz, $CDCl_3$): δ 8.28 (s, 1H), 7.73 (m, 2H), 7.42 (m, 3H), 3.59 (t, *J* = 7.32 Hz, 2H), 1.74 (m, 2H) 0.95 (t, *J* = 7.29 Hz, 3H) ppm. **^{13}C NMR** (125 MHz, $CDCl_3$): δ 160.93, 136.49, 130.56, 128.69, 128.14, 63.69, 24.20, 11.99 ppm. Characterization data were consistent with previous reports.[7]

1-(4-Fluorophenyl)-*N*-neopentylmethanimine (Imine-4)

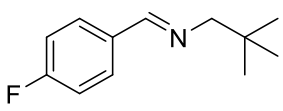

4-Fluorobenzaldehyde (1.07 mL, 10.0 mmol, 1.00 equiv) and neopentylamine (1.29 mL, 11.0 mmol, 1.10 equiv) were combined in a 20 mL vial with a magnetic stir bar, DCM (15 mL), and anhydrous sodium sulfate (250 mg). The reaction mixture was stirred at 22 °C for 4 h. The solution was then decanted, and solvent was removed in vacuo. **Imine-4** was dried over activated 3 Å molecular sieves, degassed by three freeze-pump-thaw cycles, and taken into the glovebox. **Imine-4** was filtered through a 5 μm PTFE syringe filter to afford a clear pale yellow oil that was stored in the glovebox freezer at –20 °C under nitrogen. **^{1}H NMR** (500 MHz, $CDCl_3$): δ 8.19 (s, 1H), 7.74 (t, *J* = 7.29 Hz, 2H), 7.09 (t, *J* = 8.28 Hz, 2H), 3.35 (s, 2H), 0.98 (s, 9H) ppm. **^{13}C NMR** (125 MHz, $CDCl_3$): δ 165.27, 163.28, 159.40, 132.94, 130.06, 115.80, 115.63, 73.97, 32.73, 27.95 ppm. **^{19}F NMR** (376 MHz, $CDCl_3$): δ 110.23 ppm. **DART-HRMS** calculated m/z for $C_{12}H_{17}NF$ [M+H] = 194.13395, found 194.13349.

1-(4-Fluorophenyl)-*N*-neopentylmethanimine, ^{1}H NMR Spectrum (500 MHz, $CDCl_3$)

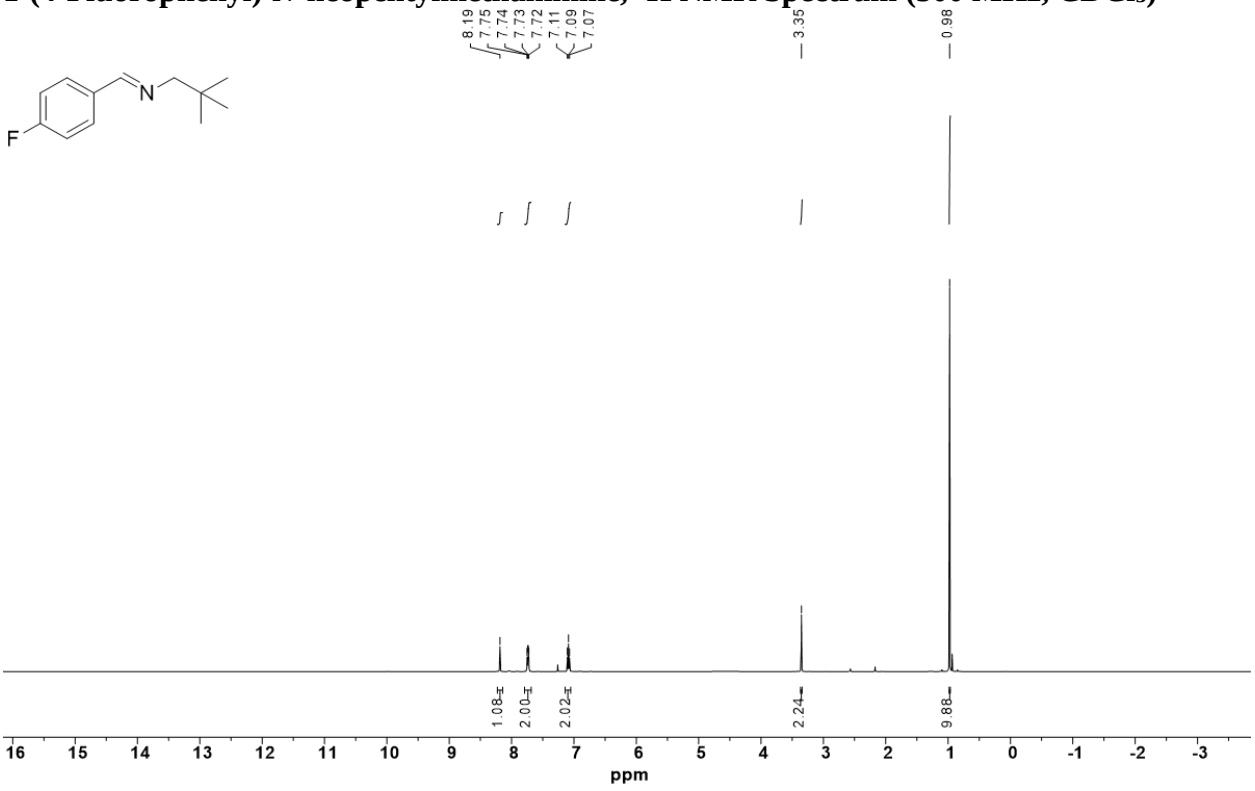

1-(4-Fluorophenyl)-*N*-neopentylmethanimine, ^{13}C NMR Spectrum (125 MHz, $CDCl_3$)

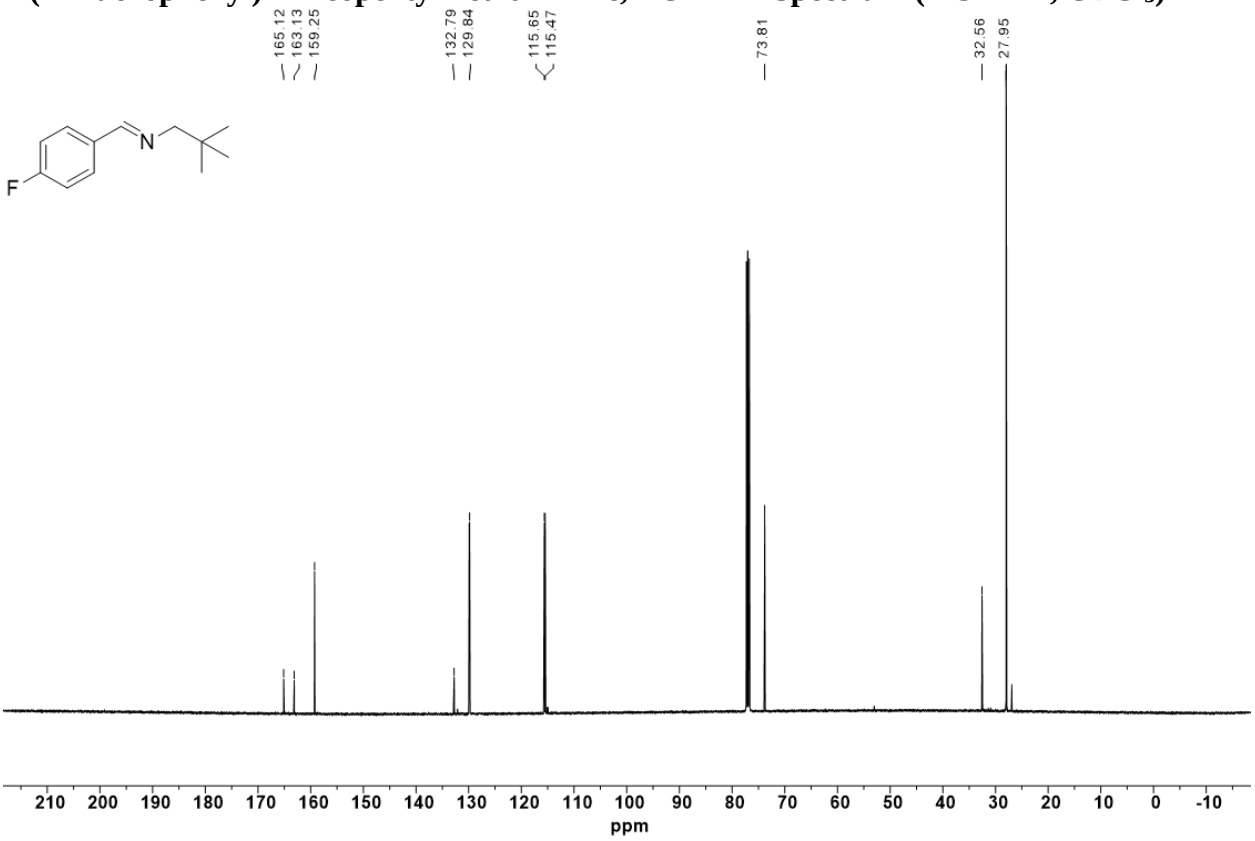

6.2. Small Molecule Imine Exchange ^{1}H NMR Kinetics

Small molecule models were studied in an attempt to elucidate the mechanism of dynamic imine exchange in the cross-linked materials. Exchange of **Imine-1** and **Imine-2** in CD_3CN was monitored using ^{1}H NMR spectroscopy in the presence and absence of a primary amine catalyst, and the distribution of exchange products (Imines-1–4) was observed (Scheme S1). Because the small molecule exchange reaction occurred rapidly in solution at ambient temperature, experiments were conducted at from –5 to –35 °C.

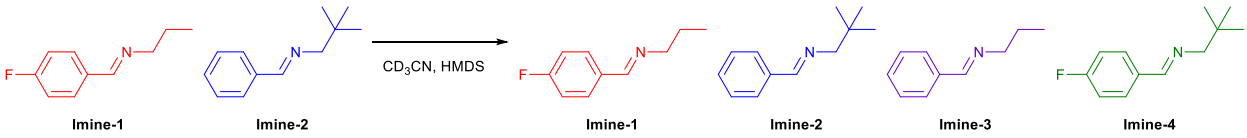

Scheme S1. Small molecule model used to determine the Arrhenius activation energy of imine exchange. **Imine-1** and **Imine-2** can exchange to give a statistical distribution of **Imines 1–4**.

In a glovebox, separate stock solutions of **Imine-1** (0.10 M) and an internal standard (hexamethyldisiloxane, HMDS, 0.051 M), **Imine-2** (0.10), and neopentylamine (0.010 M) were prepared in dried, degassed CD_3CN. CD_3CN and the stock solution comprising **Imine-1** and HMDS were added by volume to an oven-dried NMR tube, which was then sealed with a rubber septum (2.5 × 4.3 mm, inner diameter × outer diameter of bottom, Figure S47a). Outside the glovebox, the end of the septum was cut off with a razor blade (Figure S47b) to allow for a second rubber septum (10 mm outer diameter) to be turned down over the tube to create a double septa seal (Figure S47c). The NMR tube was then cooled to –78 °C in a dry ice/acetone bath to freeze the solution. Using a gas-tight syringe, the stock solutions of **Imine-2** and neopentyl amine (if required) were injected into the chilled NMR tube and immediately frozen. The resulting needle hole in the septa was sealed with a small amount of Krytox and wrapped in parafilm to prevent air and water from entering.

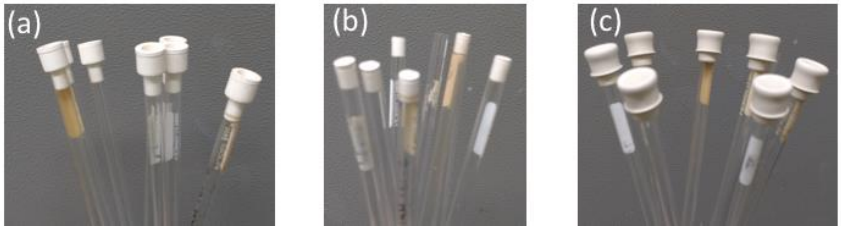

Figure S47. Double septa NMR tube set-up with (a) inner septa, (b) trimmed inner septa, and (c) double septa seal.

The NMR tube was placed into a 500 MHz Varian Spectrometer with Varian 500 MHz 5 mm inverse detection and a single-axis pulsed field-gradient probe, which had been pre-equilibrated to the appropriate temperature. The time required to tune, shim, and lock the instrument (2–5 min) was recorded so that a correction could be applied to the acquisition time. Generally, this setup period allowed the sample to melt and mix at temperatures above –25 °C. At –25 and –30 °C, mixing within the NMR tube was slow, causing fluctuations in the integration of the HMDS internal standard over the first few min of the acquisition (Figure S48). The inaccurate initial data points were therefore discarded.

The acquisition parameters were 8 scans with an acquisition time of 3 s and a relaxation delay of 4.5 s. The spectra were arrayed every 60 s. The arrayed spectra were analyzed in MestReNova using a full auto Bernstein polynomial baseline correction (Figure S49). The relative integrations of HMDS and the imine proton of cross-product **Imine-3** were used to determine the concentration of **Imine-3** throughout the reaction period (Figure S50). All rates were calculated based on the production of **Imine-3**.

First, the contribution of imine metathesis to the exchange reaction was measured by mixing equimolar amounts of **Imines-1** and **-2** in CD_3CN at –20 °C and monitoring the reaction by ^1H NMR spectroscopy. Minimal conversion to **Imine-3** was observed at –20 °C over a 1.5 h period (Figure S51). Upon warming the reaction mixture to 22 °C for 30 min, no further conversion

was observed. This result suggests that uncatalyzed exchange is negligible in the small molecule case.

In the presence of ≥ 5 mol% neopentyl amine catalyst, the reaction proceeded rapidly to form a statistical distribution of **Imines 1–4**. **Imine-3** concentration was plotted versus time and fit in IgorPro to Equation S4, where *a* is the initial concentration of **Imine-3**, *b* is the observed rate constant k_{obs}, and *c* is the y-intercept (Figure S52). At least three replicates of the kinetics experiments were performed at five temperatures from –35 to –5 °C to determine the average rate constant of imine exchange with 5 mol% neopentyl amine catalyst (Table S12). The Arrhenius activation energy was calculated by plotting the natural log of the average rate constant versus inverse temperature. Primary amine-catalyzed imine exchange has an Arrhenius activation energy of 36.5 ± 2.1 kJ/mol (Figure S53).

$$f(x) = a(1 - e^{-bx}) + c \qquad \text{Equation S4}$$

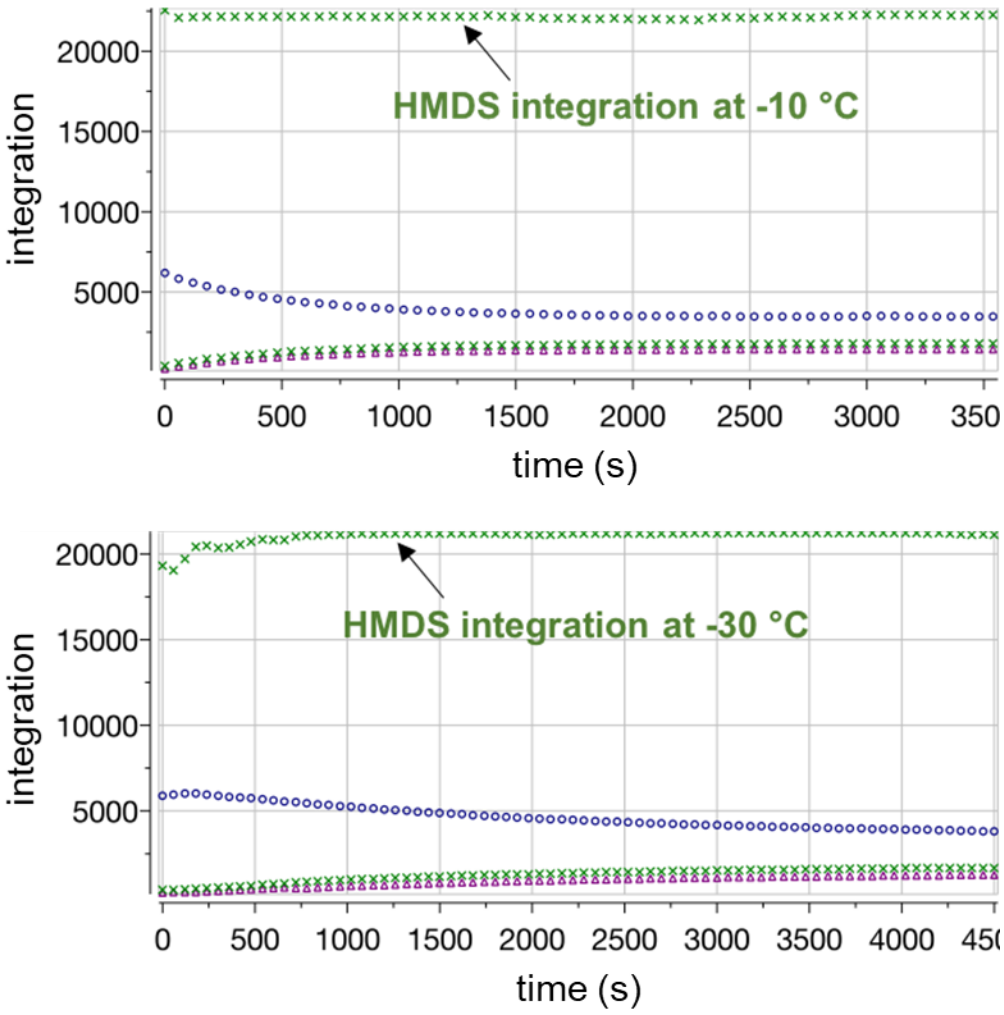

Figure S48. Comparison of the raw integral output plots from Mestrenova at –10 °C (top) versus –30 °C (bottom) showing fluctuation in the HMDS signal at lower temperatures.

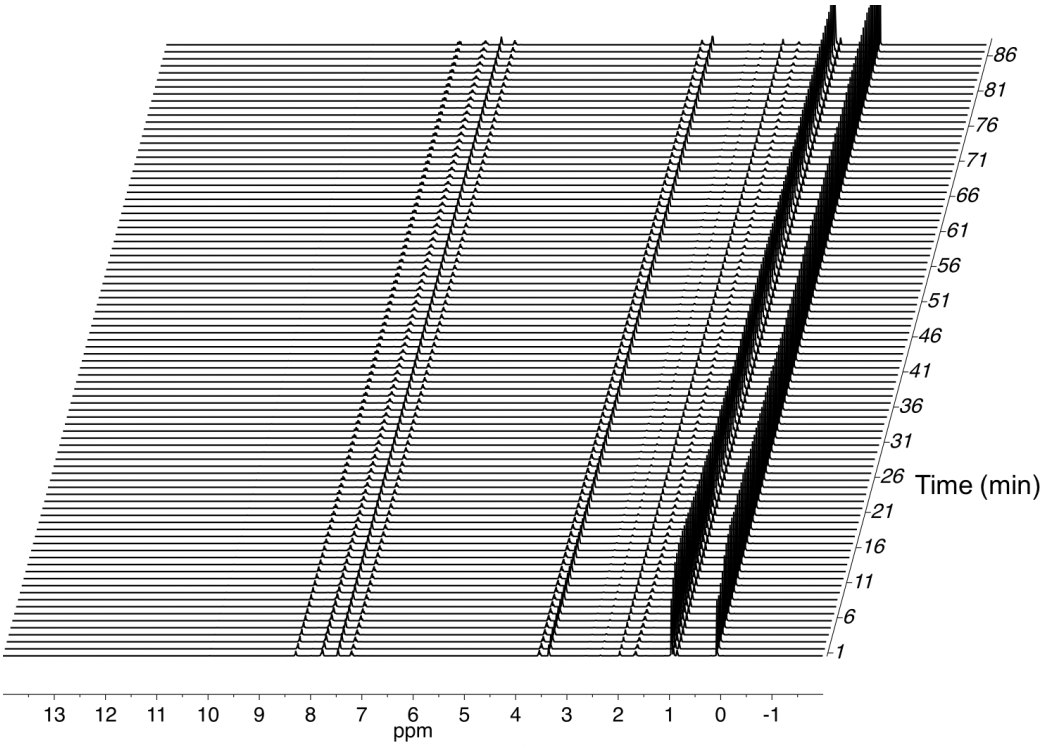

Figure S49. Representative arrayed spectra for ^{1}H NMR imine exchange kinetics experiments.

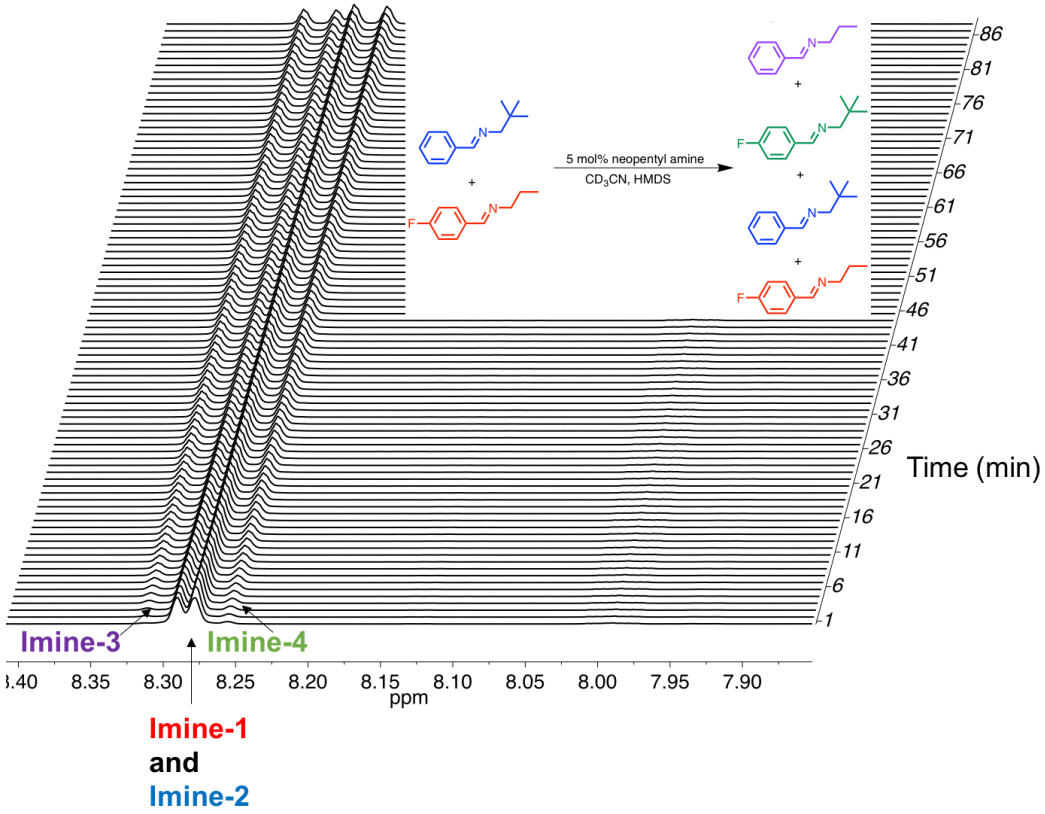

Figure S50. Representative arrayed spectra of the imine region used for quantification in ^{1}H NMR imine exchange kinetics experiments.

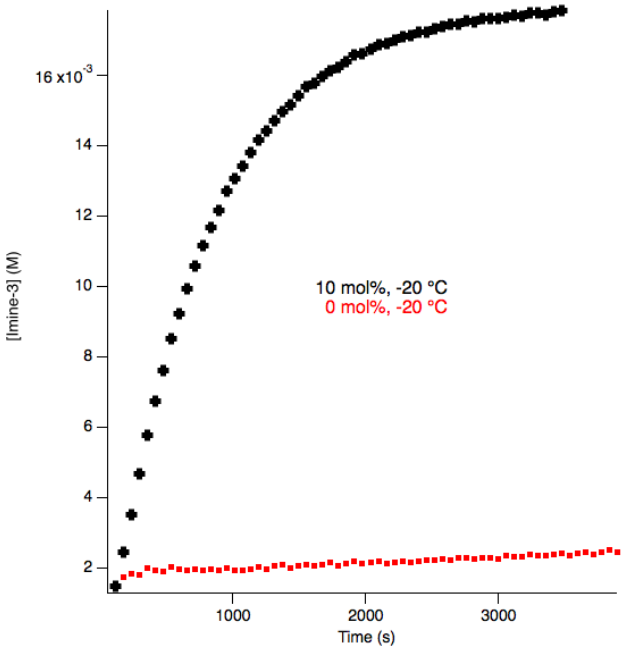

Figure S51. Comparison of imine exchange without catalyst (red) or in the presence of 10 mol% neopentylamine catalyst (black) at –20 °C.

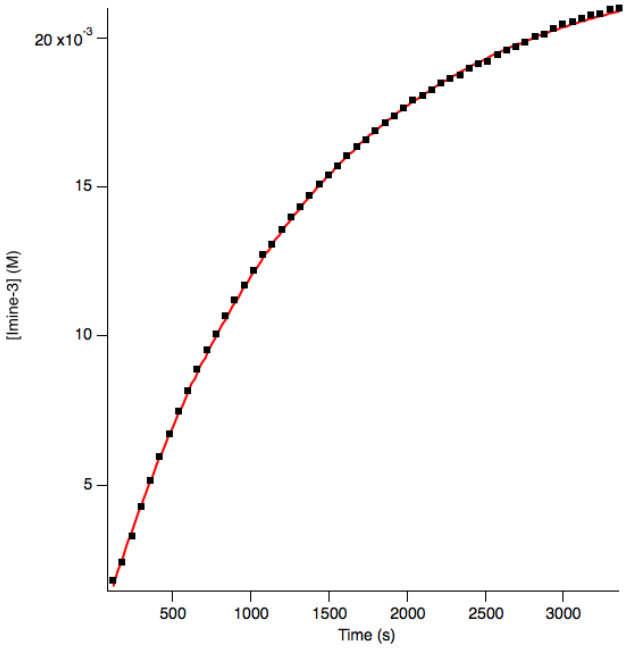

Figure S52. Representative fitted curve (red) for changing concentration of **Imine-3** over time (black) to find k_{obs}.

Table S12. Rate constants (k_{obs}) calculated for the amine-catalyzed exchange of **Imine-1** and **Imine-2**.

Entry	Temp (°C)	k (s^{-1})
1	–30	4.61×10^{-4}
2	–30	4.82×10^{-4}
3	–30	3.18×10^{-4}
4	–30	4.21×10^{-4}
5	–25	5.86×10^{-4}
6	–25	7.75×10^{-4}
7	–25	7.31×10^{-4}
8	–25	7.55×10^{-4}
9	–20	1.04×10^{-3}
10	–20	9.62×10^{-4}
11	–20	9.64×10^{-4}
12	–10	1.87×10^{-3}
13	–10	1.74×10^{-3}
14	–10	1.85×10^{-3}
15	–5	2.33×10^{-3}
16	–5	2.44×10^{-3}
17	–5	2.23×10^{-3}

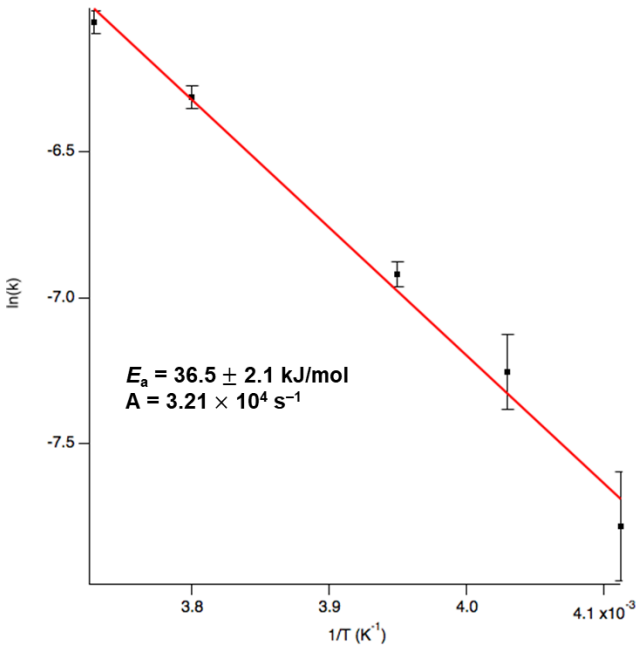

Figure S53. Arrhenius plot of amine-catalyzed imine exchange.

7. Network Solvation and Dissociation

Network dissolution of **GG$_{43\%}$-*stat*** and **PO$_{35\%}$-*stat*** was studied in various solvents to identify conditions under which the materials are susceptible to degenerative dissociative exchange (Figure S54 and Figure S55). Samples of **GG$_{43\%}$-*stat*** and **PO$_{35\%}$-*stat*** (ca. 2 mm × 3 mm × 1 mm) were stirred in solvent (10 mg/mL) at 22 °C. **GG$_{43\%}$-*stat*** and **PO$_{35\%}$-*stat*** neither visibly swelled nor dissolved in acetone, EtOAC, PhMe, or hexane over the course of a week. The networks swelled in THF and water but did not dissolve, even over a one-week period. **GG$_{43\%}$-*stat*** and **PO$_{35\%}$-*stat*** swelled and slowly disintegrated into DCM over one week and fully dissolved in $CHCl_3$ in 2–6 h. We hypothesized that acid-catalyzed hydrolysis in $CHCl_3$ promotes imine dissociation. A mixture of water in $CHCl_3$ (100 μL in 5 mL) did not accelerate dissolution, but rather produced swelling and disintegration into small particulates that slowly dissolved over days. Submerging the networks in a mixture of 5% triethylamine in $CHCl_3$ caused the networks to swell

but not dissolve; this insolubility in neutral or slightly basic $CHCl_3$ further corroborates that network dissolution in untreated $CHCl_3$ results from acid-catalyzed dissociation (Figure S56).

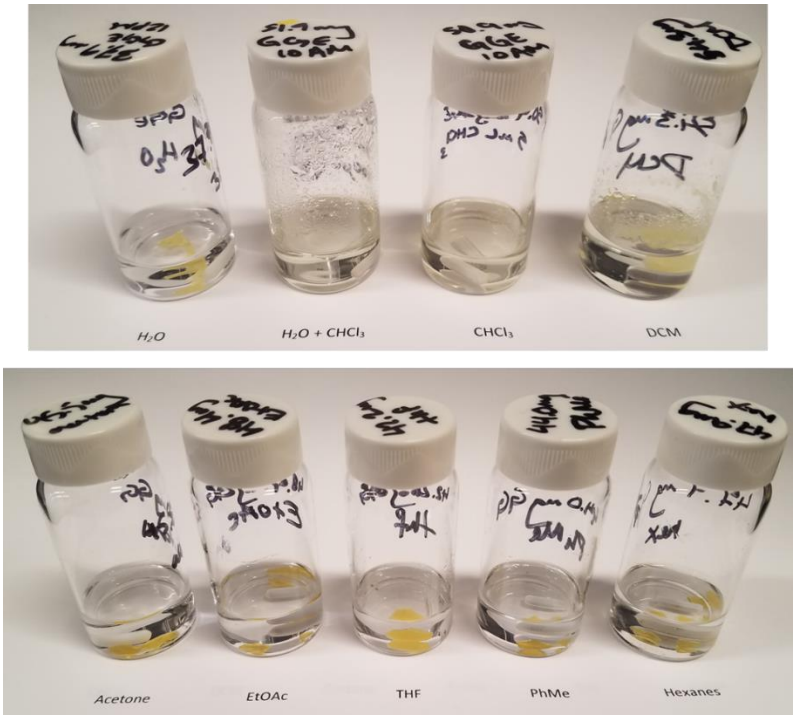

Figure S54. Solubility studies of **GG$_{43\%}$-*stat***. Top: water, water/$CHCl_3$, $CHCl_3$, and DCM. Bottom: acetone, EtOAc, THF, PhMe, hexanes.

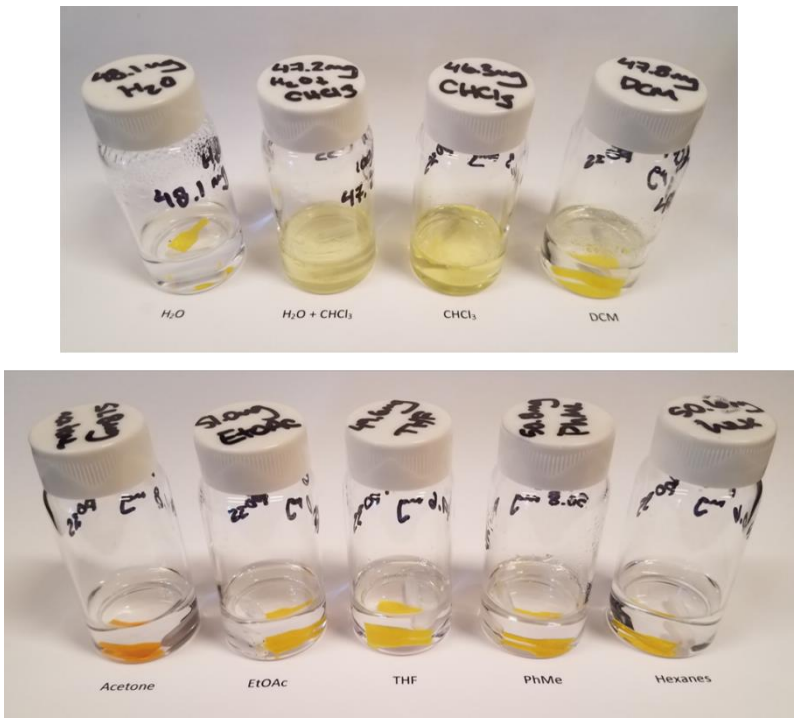

Figure S55. Solubility studies of **PO$_{35\%}$-*stat***. Top: water, water/$CHCl_3$, $CHCl_3$, and DCM. Bottom: acetone, EtOAc, THF, PhMe, hexanes.

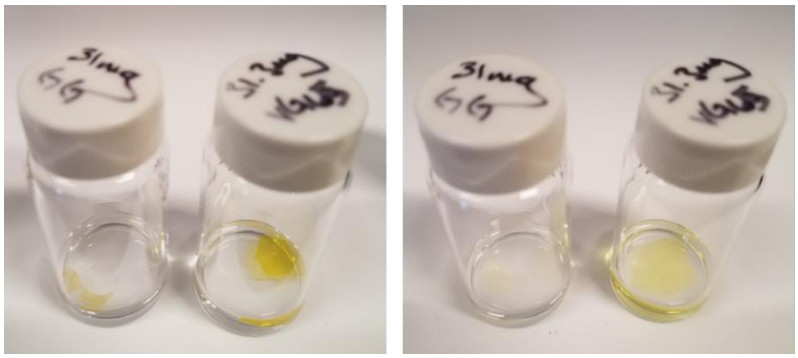

Figure S56. GG$_{43\%}$-*stat* (left vial in each image) and **PO$_{35\%}$-*stat*** (right vial in each image) networks submerged in 5% triethylamine in $CHCl_3$ initially (left image) and after 24 h (right image).

To corroborate that a dissociative imine exchange mechanism is not operative, **PO$_{35\%}$-*stat*** (61.6 mg) and **GG$_{43\%}$-*stat*** (56.8 mg) were submerged in 1,4-dioxane (a good pre-polymer solvent) and heated to 120 °C overnight. The networks swelled and darkened but did not dissolve (Figure S57). Drying overnight at 100 °C in vacuo revealed >97% mass was recovered (**PO$_{35\%}$-*stat*** final mass of 59.8 mg and **GG$_{43\%}$-*stat*** 55.8 mg).

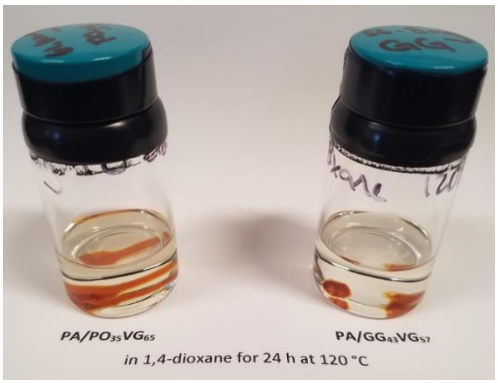

Figure S57. Networks **PO$_{35\%}$-*stat*** and **GG$_{43\%}$-*stat*** after being submerged in 1,4-dioxane at 120 °C for 24 h.

PO$_{35\%}$-*stat* (25 mg) was submerged in $CDCl_3$ (1 mL) at 22 °C for 16 h. Of the resulting solution, 0.5 mL was transferred to an oven-dried NMR tube, and 25 μL tetramethylsilane was added as an internal standard. ^{1}H NMR analysis revealed a 93:7 ratio of imine:aldehyde. Concentrated HCl (12 M, 1.5 μL, 1 equiv relative to **VG** based on TMS integration) was added via gas-tight syringe. Analysis by 1H NMR revealed increased imine dissociation to aldehyde 53:47. Addition of a second equivalent of HCl promoted full imine dissociation (Figure S58).

PO$_{35\%}$-*stat* (255 mg) was treated with HCl (91 μL, ~2 equiv relative to **VG**) in CH_3Cl (5 mL) and stirred at 22 °C for 48 h until fully dissolved (Figure S59). Solvent was removed by rotary evaporation, and the residue was then re-dissolved in minimal $CHCl_3$ (~ 0.5 mL) and precipitated into MeOH (5 mL). The pale yellow precipitate was dried in vacuo at 22 °C and analyzed by ^{1}H and ^{13}C NMR (Figure S60 and Figure S61) and GPC (Figure S62). NMR characterization was consistent with that of **pre-PO$_{35\%}$-*stat*** (Figure S60 and Figure S61), while the GPC trace showed a slight increase in molecular weight (Figure S62).

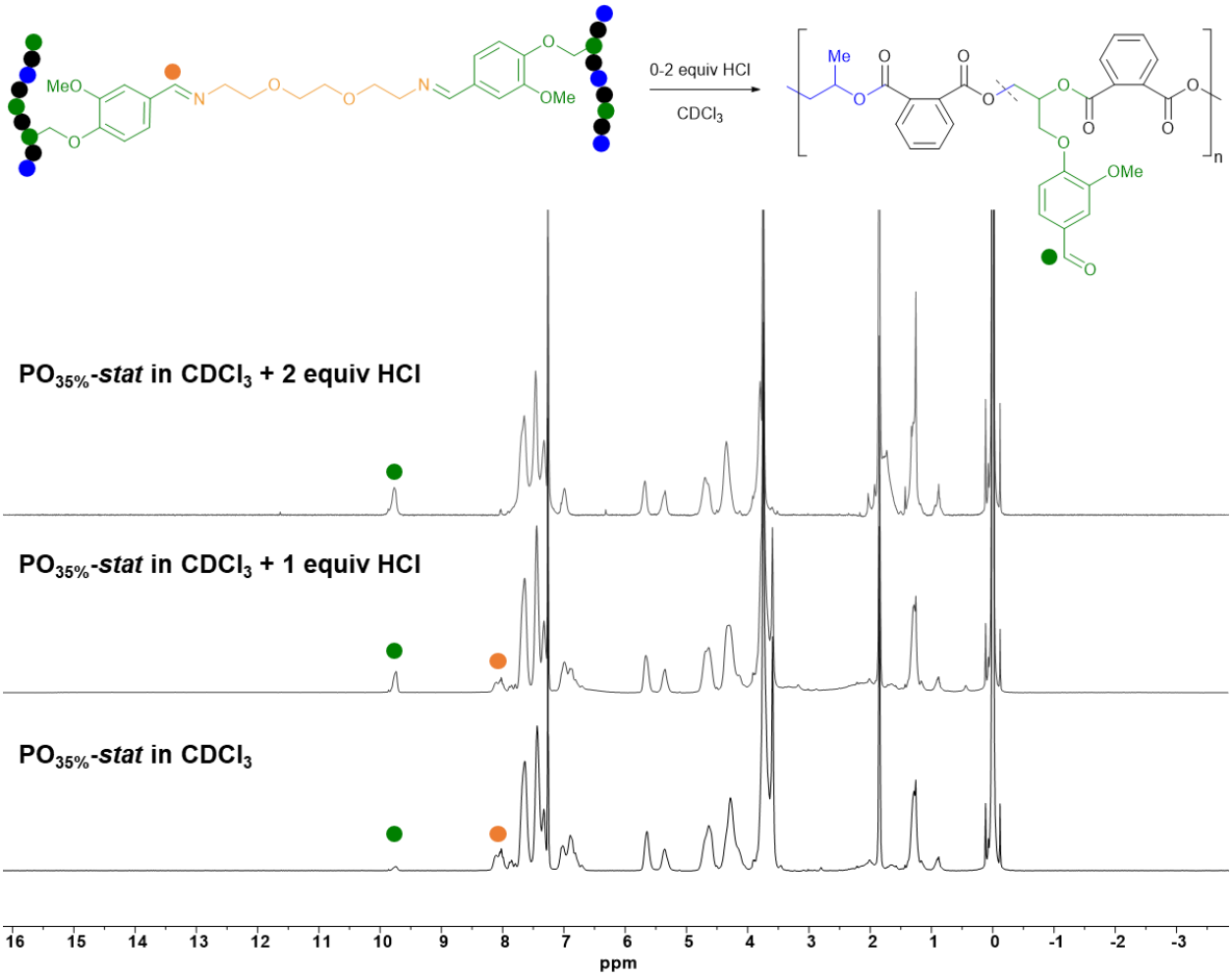

Figure S58. Acid-catalyzed imine dissociation to aldehyde and amine of the **PO$_{35\%}$-*stat*** network in $CDCl_3$.

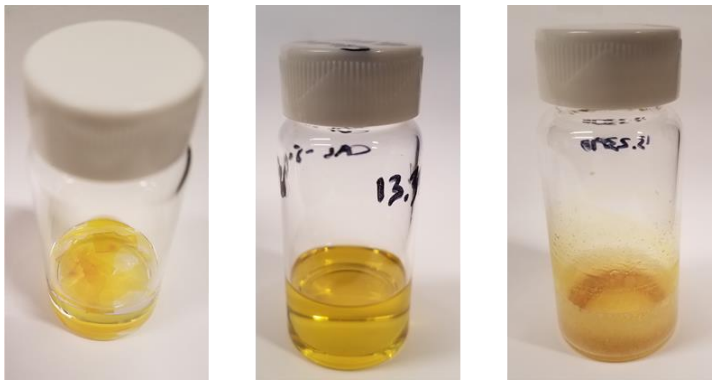

Figure S59. PO$_{35\%}$-*stat* network in $CHCl_3$ immediately after addition of HCl (left), dissolved network (center), and recovered pre-polymer (right).

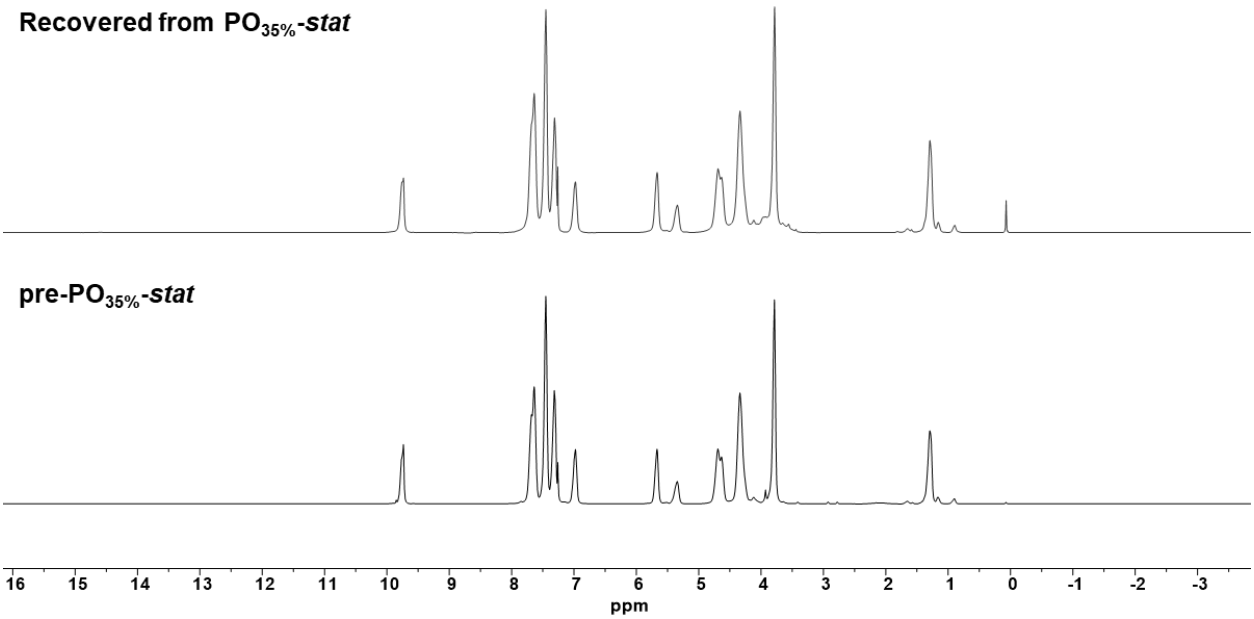

Figure S60. ^{1}H NMR spectra of **pre-PO$_{35\%}$-*stat*** (bottom) and recovered material from the acid-catalyzed dissolution of **PO$_{35\%}$-*stat*** in HCl and $CHCl_3$ (top).

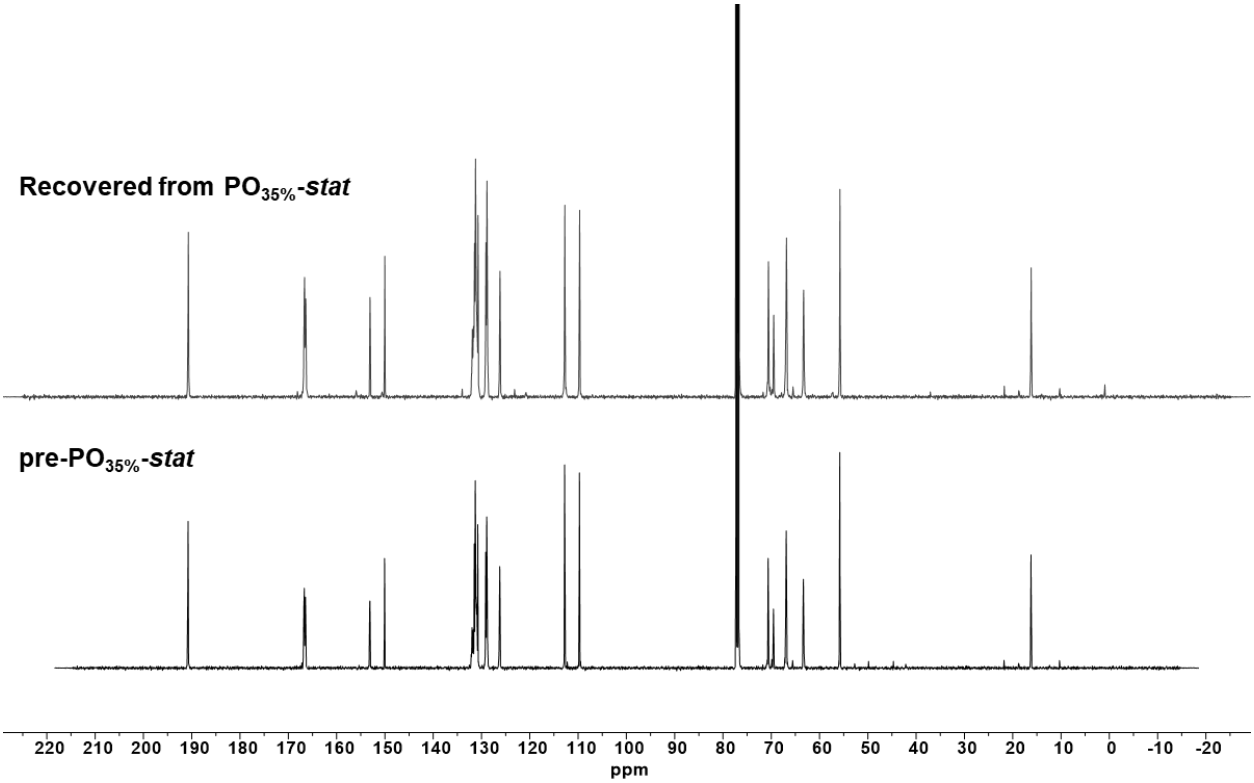

Figure S61. ^{13}C NMR spectra of **pre-PO$_{35\%}$-*stat*** (bottom) and recovered material from the acid-catalyzed dissolution of **PO$_{35\%}$-*stat*** in HCl and $CHCl_3$ (top).

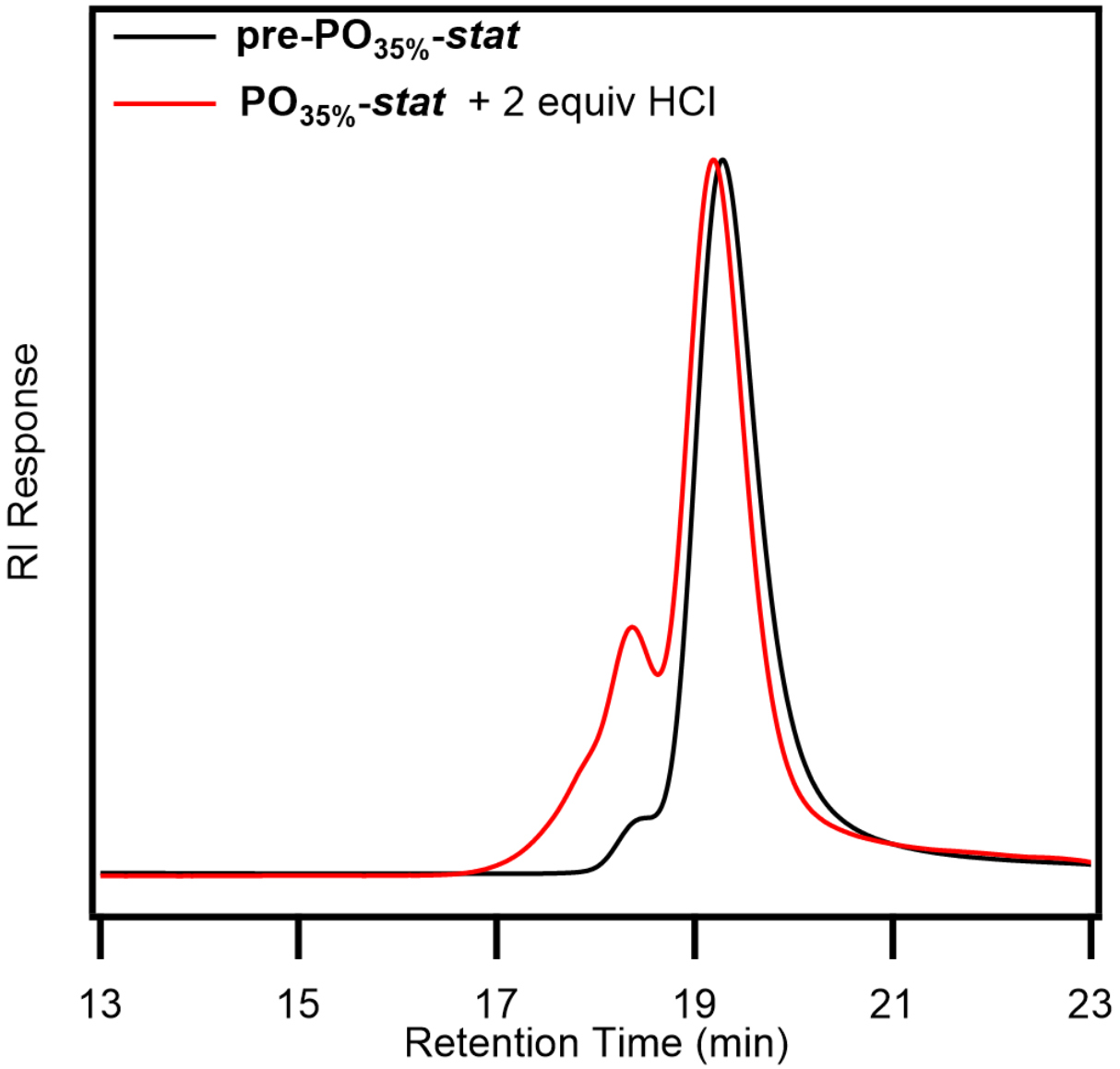

Figure S62. GPC traces of **pre-PO35%-*stat*** and recovered linear polymer after acid-catalyzed dissolution in $CHCl_3$ and precipitation into MeOH.

8. References

(1) J.P. Brutman, P.A. Delgado and M. A. Hillmyer, *ACS Macro Lett.*, 2014, **3**, 607–610.

(2) M. Capelot, M. M. Unterlass, F. Tournilhac and L. Leibler, *ACS Macro Lett.*, 2012, **7**, 789–792.

(3) J.-C. Liang, J.-L. Yeh, C.-S. Wang, S.-F. Liou, C.-H. Tsai and I.-J. Chen, *Bioorg. Med. Chem.*, 2002, **10**, 719–730.

(4) B. K. Pchelka, A. Loupy and A. Petit, *Tetrahedron*, 2006, **62**, 10968–10979.

(5) B. A. Abel, C. A. L. Lidston and G. W. Coates, *J. Am. Chem. Soc.*, 2019, **141**, 12760–12769.

(6) P. J. Flory, *Principles of Polymer Chemistry*, Cornell University Press, Ithaca, NY, 1953.

(7) N. Mungwe, A. J. Swarts, S. F. Mapolie and G. Westman, *J. Organomet. Chem.*, 2011, **696**, 3537–3535.